MODERN TECHNIQUES
IN MECHANICAL ENGINEERING

MODERN TECHNIQUES
IN MECHANICAL ENGINEERING

Editors:
Antoni Świć, Jerzy Lipski

LUBLIN 2009

REVIEWERS:
Prof. Eng. Oleg Draczow
Togliatti State University (Russia)
Prof. Eng. Bogusław Kuszta
Lublin University of Technology

Typeset by: M. Sc. Eng. Tomasz Kusz

The content-related, responsibility, style and presentation form falls on the authors of individual contributions.

Wydanie publikacji dofinansowane przez Ministra Nauki i Szkolnictwa Wyższego

ISBN 978-83-87833-92-3

Lubelskie Towarzystwo Naukowe
Plac Litewski 2, 20-080 Lublin
Nakład – 250 egz.

CONTENTS

JACEK DOMIŃCZUK

Using the gluing technology in assembly and regeneration

Introduction

The technology of gluing plays very important role in the development of modern constructions. In many cases it is used as an alternative for applied so far methods of joining, sealing up or the regeneration of the part of machines. Moreover gluing creates new possibilities in whole range of process of joining materials of various physical and geometrical characteristics and also allows reducing dimensions of connected elements thanks to reducing their construction [1, 2]. Glues are also wide used in repairs when using the process of regeneration of parts their costs of manufacturing are significantly decreased.

As research showed the endurance of glue connections is very complicated problem. Number of factors influences it, for example:

- the size of the glued surface described by length and the width of the adhesive-bonded joint,
- the thickness of adhesive-bonded joint,
- the stiffness of glued elements,
- the degree of the geometrical development of glued surfaces,
- the appearance of land effect,
- the change of connected materials shape in the glue-joint zone,
- the cleanness of connected surfaces,
- the symetricity of glued elements loading,
- the plastic strain of glued elements,
- the inhomogeneity of the energetic state of the top layer,
- the life time of the adhesive-bonded joint,
- the thermal impact fatigue,
- the inhomogeneity of the chemical constitution of glue,
- the inhomogeneity of the adhesive-bonded joint structure.

Thanks to application of set of methods for forecasting the endurance of glue connections more and more often gluing is used as the alternative technology of joining which creates new possibilities of developing products. This allows introducing changes in our surroundings.

Using of the gluing technology

1. Sealing up

Glues can be applied instead of solid seal everywhere where already existing tightening can be removed. They find wide use for sealing up combustion engines, transmission, collars, for strengthening the surface of the adhesion of thrust bearings, sealing up differential gear, etc. The examples of usage has been presented on fig. 1 and fig. 2.

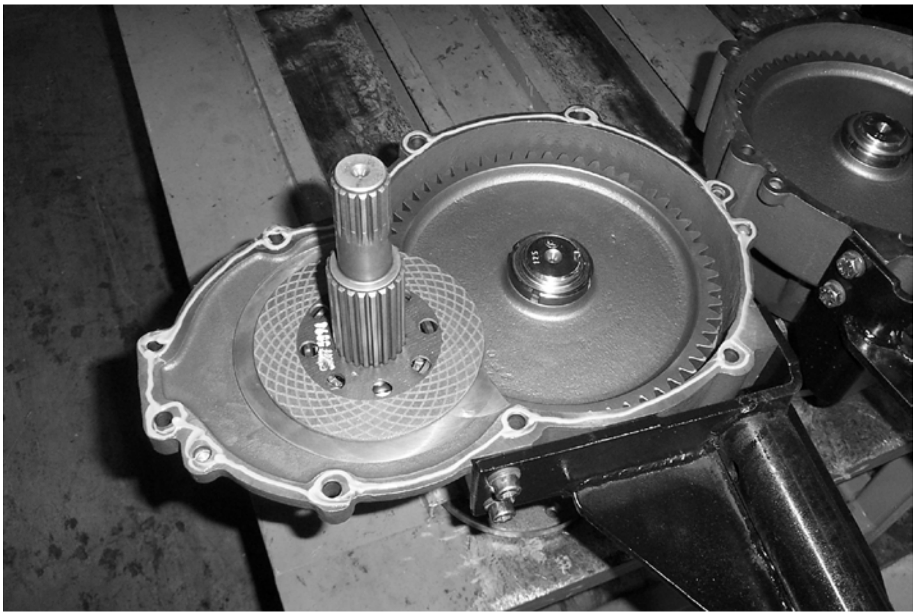

Fig. 1. Examples of usage the anaerobic gasketing material

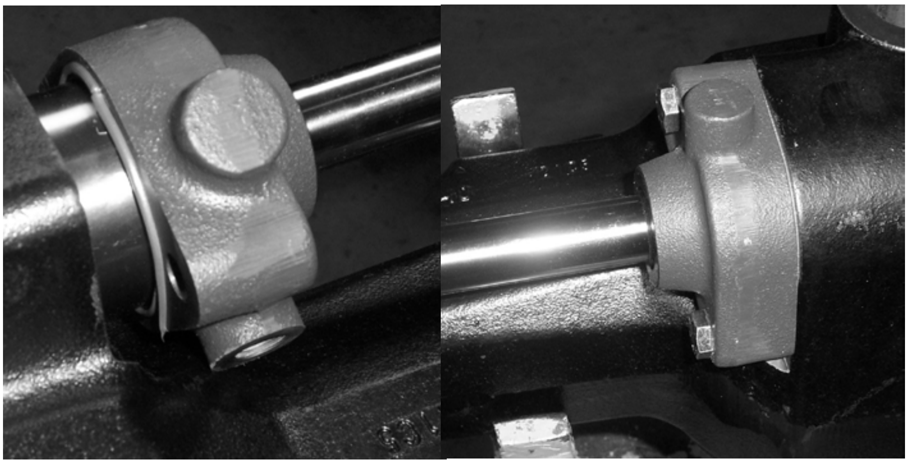

Fig. 2. Examples of usage the RTV silicone gasketing material

So far applied shape sealings required storing or inconvenient and time-consuming manufacturing in company. Unevennesses appearing on surfaces, machining traces, corrosion of the surface causing corrosion pits are real problems which traditional sealings does not correct.

The technology of gluing is not influenced by these failures. It assures among: the easiness of spreading the leak stopper, any time of spreading, any shape of the seal, easy disassembly, the correction of the surface depth up to 0.5 mm, surface protection against cold work (large bearing surface), transfer of large shearing loads. Glues are used also for sealing up screw joint what eliminates coated oakum and Teflon bands. They are also used as a protection against unscrewing screws, nuts, stud-bolts (fig.3), pins or other lock-nut.

Fig. 3. A lubricating nipple secured with an anaerobic threadlocking agent

2. Regeneration

Glues are also used to conducting repairs. Typical uses for repair:

- removing gas pipes leak;
- removing leaks in central heating systems;
- reconstruction of the knocked out bearings seatings;
- reconstruction of worn out bearing journals;
- removing leakages in reservoirs, cracked casings, e.g. engines, and leakages of all joint connections;
- reconstruction of truncate threads and knocked out splineways;
- tightening iron, steel and non-ferrous metals casts;
- reconstruction corroded bottoms of heat exchangers;
- embedding elements in metal, concrete.

3. Elements fixing

Glues, thanks to large shearing resistance up to 55MPa, are perfectly suitable for joining elements under such loading. Engineer should avoid connections working on tearing off, because resistance of glue on such burden is small. Gluing finds special usage when fixing cylindrical elements both in repairs and in manufacturing, during assembly of all fit connections e.g. immediate repairs of loose bearings, tooth wheels, sleeves, taper keys etc.[3] (fig.4).

Fig. 4. Assembling cylindrical parts with adhesives

High cost of the machining (most often in number of operations like polishing, finishing turning) before applying the fit connections technology of the assembly is main reason of choosing the gluing technology.

The main advantages of fixing using gluing:

- technological constructions, e.g. the facilitation of the assembly;
- shortening cycle of production, eliminating some operation;
- simplification of repairs – without expensive processing nor spare parts, e.g.:
- gluing keys;
- assembly of loose hubs in one place, without machining;
- shortening the time of repairs, no down-times;
- smaller warehouse of spare parts;
- possibility of the joining various material types, e.g. cast iron and aluminum, bronze and steel, etc.;

- ❑ strengthening of many constructional knots thanks using large bearing surface of part;
- ❑ possibility of using temporary fastenings instead of forced-in connections – nowadays produced glues are characterized by large producibility, they are simple in proportioning, moisten metals well. They allow reducing required tolerance of fitting and classes of processing quality. For example: instead of using fitting H6/k5, R_a 2.5, engineer can select R_a 10 with clearance 0.1 mm;
- ❑ the easiness of establishing the mutual position – in case of gluing hubs which weight by given relative position doesn't cause any disturbance of thin layer of glue between hub and pin, the automatic coaxialing of connected elements occurs.

Features of gluing technology

The endurance of every glued joint is qualified by adhesive and cohesive forces (fig.5). The cohesive force is measure of internal substances endurance. It depends from intermolecular strengths, their value and range of crosslinking. Adhesive force is measure of endurance of two substances bond, and spread of this force depends on the chemical structure of both substances and their physical properties. Adhesion is the bonding force at the contact surfaces of the materials. Physical forces of attraction and absorption, which together are described as "van der Waals forces," have the greatest significance in bonding. The range of these intermolecular forces is considerably lower if the adhesive material does not come in intimate contact with bonding sites due to the relative surface roughness of mechanically treated surfaces. This is why the adhesive must penetrate right into the surface roughness and wet the complete surface. The strength of the adhesive force thus depends on the penetration of the wetting (to adhesive the fullest intermolecular exchange) and, on the other hand, on the adhesive capacity of the surface. At a given surface tension of the adhesive, wetting depends on the surface energy of the substrate and the viscosity of the adhesive. Wetting can also be reduced if surface contaminants are present. This causes in fact that the preparation of the surface of materials is so very important [4]. Endurance of the joint depends on this factor in the large measure.

Cohesion is the force prevailing between the molecules within an adhesive which keeps the material together. These forces include:

- intermolecular forces of attraction (van der Waals forces) and
- Interlocking of the polymer molecules among themselves

In accordance with the rule that a chain is only as strong as its weakest link, the forces of adhesion and cohesion in a bonded joint should be about equal.

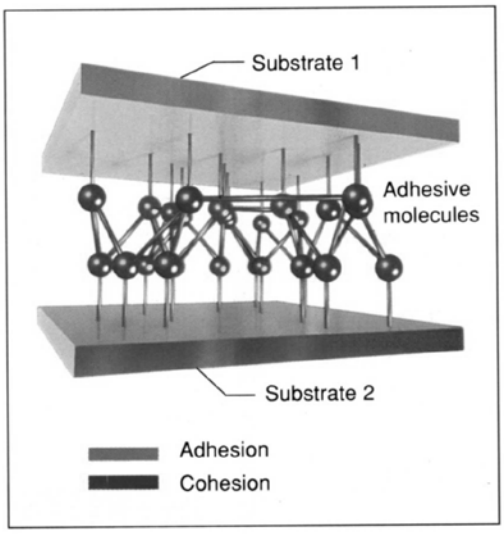

Fig. 5. The bonding forces in the adhesive joint

In glue connections the glue is hardened with the simultaneous creation of the adhesive bind and tightening the connection. Most adhesives are reactive polymers. They change from liquids to solids through various chemical polymerization reaction. Company has developed numerous adhesives with special curing properties for unique situations. It is possible to classify adhesives into the following groups on the basis of curing properties:

- anaerobic reaction,
- exposure to ultraviolet (UV) light (also secondary curing options),
- anionic reaction (cyanoacrylates),
- activation system (modified acrylics),
- moisture curing (silicones, urethanes).

Such connections operate well in the conditions of dynamic load as the vibration absorber, preventing corrosion, fretting and micro-displacements. The bearing part of the surface also grows up. It remains above the level of 80%, what influences the endurance of the connection fundamentally.

Correct surface pretreatment is necessary for optimum bonding. Bond strength is determined to a great extent by the adhesion between the joint surfaces and the adhesive. It is important to understand that adhesive joints are stronger the more thoroughly the surfaces are cleaned (fig.6) Adhesion is improved by:

- removing unwanted surface films by degreasing or mechanical abrasion, and, if needed,
- building up new, active surface by coating with primers.

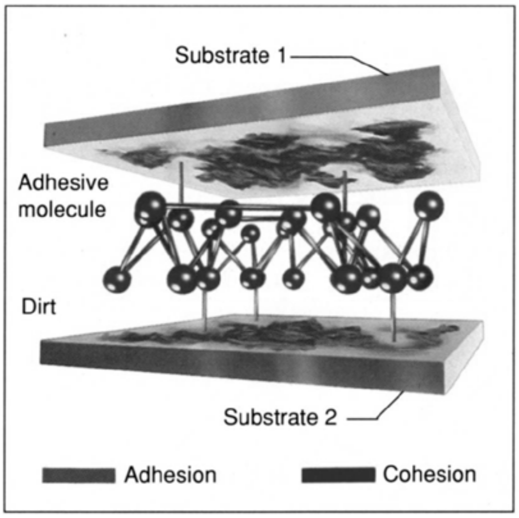

Fig. 6 Contamination on the surfaces of the substrates reduces adhesion

Cleaning processes can be evaluated with the “water break test.” Several drops of pure water are applied to the cleaned surfaces. On an inadequately cleaned surface, the spherical form of the drop is largely retained, and the surface must by cleaned once more. If the water runs on the treated surface, then wetting has been satisfactory; the bond face is sufficiently clean (fig.7).

This method is not suitable for anodic coatings on aluminium and magnesium. The advantage of the water break test is the easy availability of the “test fluid” – water. This advantage, however, is limited – the variation in water hardness which affects surface tension. In some cases even distilled water does not produce reliable results with the water break test. In such cases, comparable fluids, which are available with defined surface tensions, are recommended. Note that the test only covers wettability and not adhesive bonding capability.

Large influence on the endurance of the glue connection has the condition of surface. The proper cleanness of the surface gained after chemical or mechanical preparation, and the proper roughness of the surface have large meaning. From results of own investigations (fig.8) conducted for steel St3 conclusion can be drawn, that the highest endurance of the connection is after the processing using tool number P120 what fits R_a=6÷20 μm. Such roughness can be also gained through turning or sand blasting.

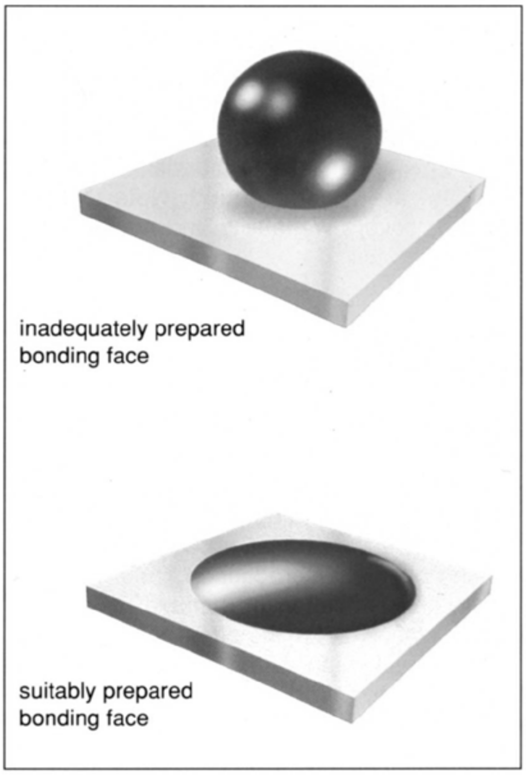

Fig. 7. Surface preparation can be tested with the “water break” test

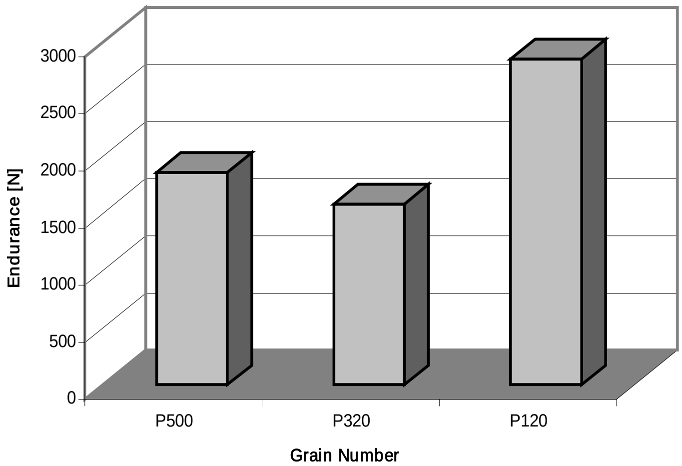

Fig. 8. Relationship between the endurance of glue connection and the condition of top layer

The measurements of endurance were taken on test samples according to Polish Norm PN 69/C-89300. The ripping force was measured using extensometrial converter connected to system allowing registration of load changes using of the computer software. The error in defining the destructive force did not exceed 0.3%. Connections were created under following conditions: glue - Araldit 2012 Rapid, the temperature - 20±2° C, humidity - 40±5%, pressure – 0,02 MPa, the seasoning period – 24 h.

The growth of connection endurance is connected with the „development” of the surface causing the growth of the active surface of the point contact of glue with the material. Surface energy (fig. 9), which characterizes work of the adhesion also increases. Mechanical bonds formed can also play the large role here as a result of catching the thin layer of hardened glue to ridges on the surface of the material.

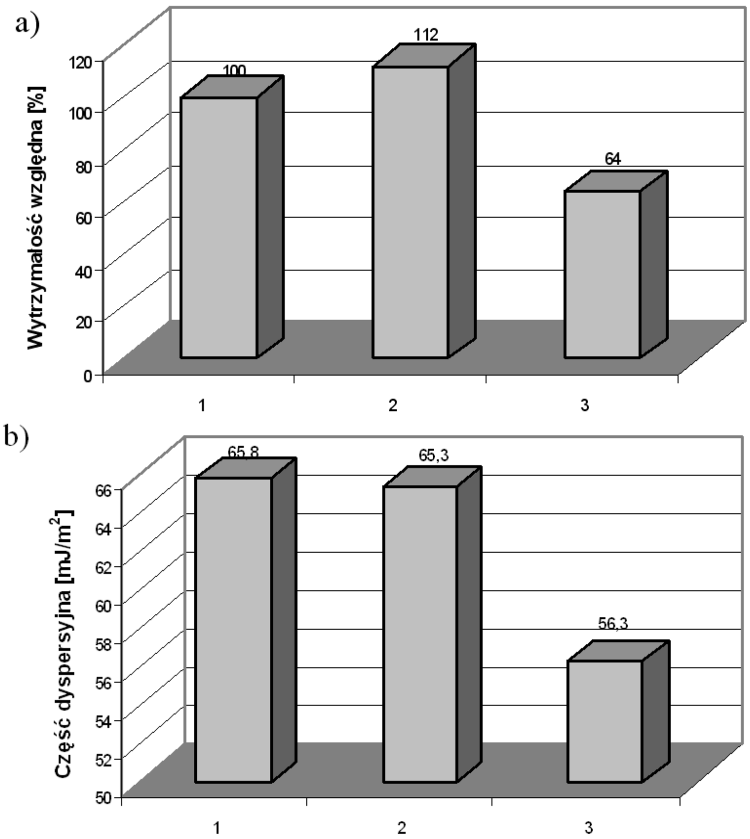

Fig. 9. Endurance of glue connections (a) for steel St3 and component value of dispersion of free energy (b): 1- after processing with abrasive tool P320, 2 - after processing with abrasive tool P320 and degreasing with Loctite 7061, 3 - after processing with abrasive tool P320 and rinsing with water

The transfer of force through the glue joint depends on surface (fig.10). This is not however linear dependence [5], and that is mainly result of the influence of land effects. The biggest part plays the length of the overlap, there is also the concept of the optimum length by which the highest tensions appears. The investigation conducted by [6] for pin-sleeve connections showed, that the most beneficial length of the overlap lays between 10 and 14 mm. Also the significant influence on the endurance of the connection has thickness of glue joint, which value e.g. for glue EPIDIAN 5 + PAC [6] should be 0,13 ÷ 0,15 mm. The size of the overlap, the roughness of the surface and the thickness of the glue joint should be chosen depending on conditions of the load (static, dynamic).

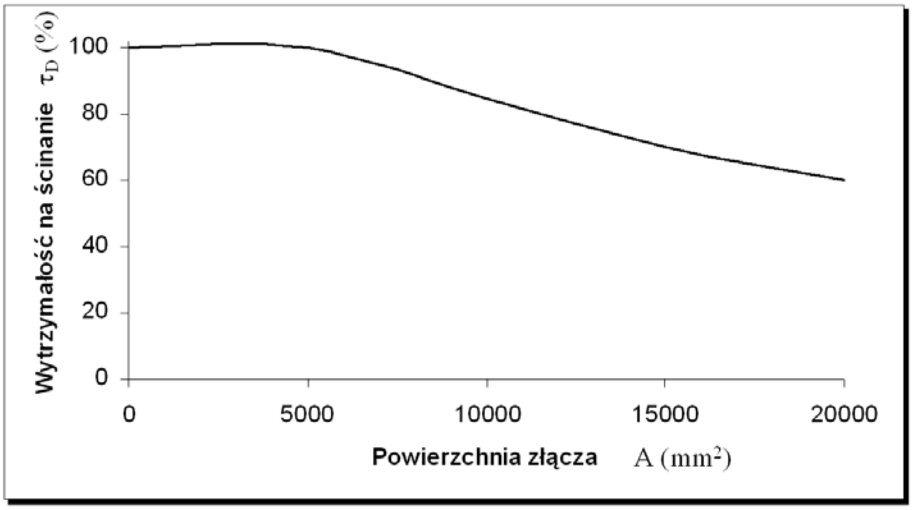

Fig. 10. Influence of the size of joins surface on endurance on cutting. The graph was prepared for the overlap L / D = 0,8÷1,2, where: L- shaft neck length, the D-diameter of the sleeve

Because glue connections can be subjected to various kinds of dynamic loads, acquaintance of long-lasting endurance of such connections is essential. In dependence from the kind of the load, the static endurance of glue needs to be multiplied by the suitable factor (smaller than 1) in order to get dynamic endurance.

As shown on graph (fig.11.) the dynamic durability of glue connections is 30-70% of the static endurance.

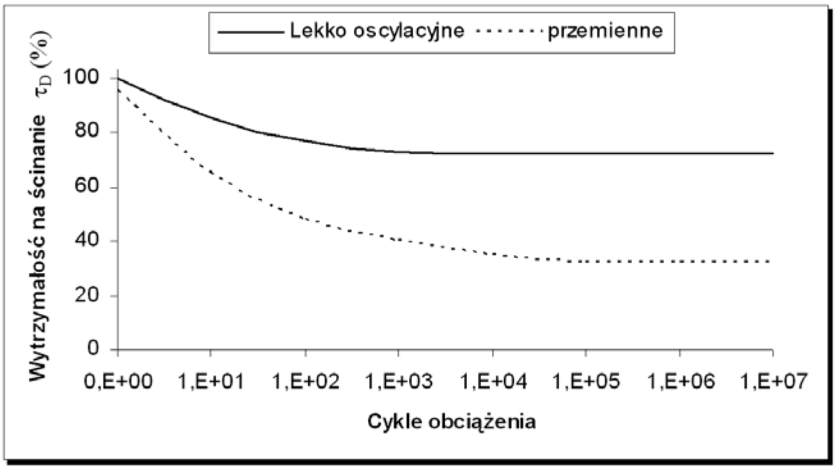

Fig.11. The dependence of endurance on cutting from the quantity of the cycles of load

Glues are also characterized by thermal shockability. The author of the work [5] dedicates more attention on this subject.

Glues produced at present show the significant chemical resistance. It depends not only from the layer of glue itself, but also from the surface of the material, the strength of adhesionand the time of putting out on the working of the chemicals. Chemical resistance of glues at the following factors: water, sewer water, saline solutions, low concentrated alkalines and acids, alcohols, aliphatic hydrocarbons (e.g.: mineral spirits, diesel oil, jet fuel), conventional cooling drips, oils used by cutting off processing, or oils and technical gas can be assumed. Glued connections are not resistant on acids and alkalies of higher concentrations.

Summary

The technology of gluing allows to receive connections characterized by high endurance and resistant on many external factors. This allows to replace the applied expensive methods of joining, by cheap and simple in realization - gluing. It is possible to join existing methods of the assembly with gluing what influences the technical values connections profitably.

The usage of glues during the repairs also allows lowering costs of repairs, shortening their time, and avoiding bearing additional costs connected with storing and replacing them on new.

Thanks to significant development in the chemistry of glues, the significant development of the glueing technology is expected. This is a result of opportunities and the advantages of gluing technology for example: receiving of stiff, resistant and light constructions, and the possibility of the joining of elements of difficult shapes, made from different materials and of various thickness.

REFERENCES

1. Kosiński K.: Montaż połączeń gwintowych, czopowych i kołnierzowych z zastosowaniem klejów Loctite. Kwartalnik Naukowo – Techniczny, Technologia i Automatyzacja Montażu nr 2/1994. – s. 41-43.
2. Kuczmaszewski J., Rudawska A.: Klejenie i uszczelnianie w technologii montażu. Kwartalnik Naukowo – Techniczny, Technologia i Automatyzacja Montażu nr 3/1997.
3. – s. 25-29.
4. Kuczmaszewski J., Domińczuk J.: Klejenie w montażu przekładni zębatych. Współczesne metody konstrukcji i technologii elementów uzębionych. IV Konferencja Naukowo-Techniczna. Łódż 1999. – s. 58-63.
5. Kuczmaszewski J., Domińczuk J.: Właściwości adhezyjne warstwy wierzchniej stali konstrukcyjnych. Przegląd Mechaniczny 3’01. – s. 5-8.
6. Kuczmaszewski J.: Fundamentals of metal-metal adhesive joint design. Polish Academy
7. of Sciences. Lublin Branch, Lublin 2006. – 205 st.
8. Harsan K.: Wpływ czynników konstrukcyjnych i technologicznych na wytrzymałość zmęczeniową klejonych połączeń czopowo – tulejowych. Rozprawa doktorska – Politechnika Rzeszowska.

Wykorzystanie technologii klejenia w montażu i regeneracji

Streszczenie

W pracy zamieszczono opis możliwości wykorzystania technologii klejenia w montażu i regeneracji. Przedstawiono przykłady praktycznego zastosowania. Zaprezentowano zespół czynników od których zależy jakość połączeń. Szczególną uwagę zwrócono na sposób przygotowania warstwy wierzchniej z uwzględnieniem stanu energetycznego jako wskaźnika prognostycznego wytrzymałości połączeń klejowych.

Słowa kluczowe: wytrzymałość, połączenia adhezyjne, montaż

Using the gluing technology in assembly and regeneration

Abstract

The description of the possibilities of using the gluing technology in assembly and regeneration was presented in the work. Examples of the practical use were introduced. Set of factors influencing the quality of connections was presented. The paper focuses on method of preparing the top layer with regard to the energetic state as the prognostic indicator of the endurance of glue joint.

Keywords: strength, adhesive joint, assembly

Using the gluing technology in assembly and regeneration

JACEK DOMIŃCZUK

Informacje o autorze

Dr inż. Jacek Domińczuk
Instytut Technologicznych Systemów Informacyjnych
Wydział Mechaniczny
Politechnika Lubelska
ul. Nadbystrzycka 36
20-618 Lublin
tel. 0815384585
e-mail: j.dominczuk@pollub.pl

KATARZYNA GUZ
JERZY WARMIŃSKI

Modelling of a Human Middle Ear System

Introduction

Mechanical models of a human ear system can deliver very important information about a sound transmitted from external environment to the inner ear. There are some ways to model behaviour of the ear system. One of them is to use Finite Element Method (FEM) that allows to see all stresses and strains, visualizes vibrations etc. Taking advantage of the FE method, number of engineers and doctors is engaged in finite element modelling on the basis of different histological sections, e. g. Gan, Sun, Chang et al [1, 2, 3].

In spite of the fact the FEM model is efficient and precise and allows for visualisation of many interesting phenomena, it does not allow for explanation of the received dynamics and the parameters influence. This disadvantage is caused by a lack of a strict mathematical model. Therefore, another approach for learning about how the ear works is to create mechanical model including masses, springs and dashpots. Although such models are less precise, different phenomena can be better described and understood. Some exemplary mechanical models were investigated and studied by Onchi [4, 5], Nakijama et al. [6], Feng and Gan [7], Ravicz et al. [8]. Authors of those studies proposed simple mechanical models of the human middle ear with different numbers of degrees of freedom: three [8], four [6], five [4, 5], six [7]. In [7] the lumped parametric model that consists of six masses suspended by ten dashpots and six springs is presented. The model is the most complicated one but it is also the most difficult because not all necessary coefficients' values can be found in by experimental tests. Many coefficients have to be determined by fitting procedure to get the model response similar to real one. Therefore, a four-mass model [6] and a three-mass model [8] are used by making assumption that an umbo mass is very small and a value of compliance of a joint that joins the umbo and the first ossicle – malleus can be neglected**,** so it does not change the model's behaviour in a significant way.

According to authors of a current study, the most helpful should be a model consisting of 3 masses presented in [8] and exactly that model, after tiny modifications, is studied here.

The aim of this study is to develop the simple linear model of the middle ear system and also to find influence of incus and stapes joint's stiffness on the behaviour of the middle ear. These characteristics are important in a case of otosclerosis, when during stapedotomy the stapes is substituted by the prosthesis.

3-Degree of Freedom Model of the Middle Ear

After Ravicz et al. [8], three-degree of freedom model of a middle ear is taken for investigations. The model is shown in Fig. 1, it consists of 3 masses (ossicles: malleus m_M, incus m_I and stapes m_S), 6 dampers *c* and 6 springs *k* (subscripts used in the notation have meaning: *TM* – tympanic membrane, *AML* – anterior malleal ligament, *IMJ* – incudomalleal joint, *PIL* – posterior incudal ligament, *ISJ* – incudostapedial joint, *AL* – annular ligament), V_U means an umbo velocity and V_S is a stapes velocity, l_M and l_S represent the length of the manubrium and the incus long process, respectively.

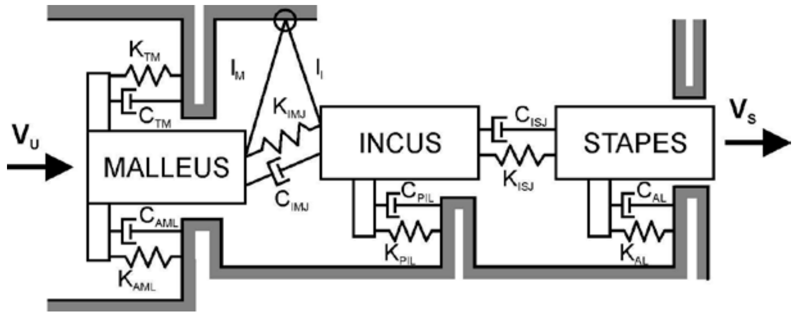

Fig. 1. 3-degree of freedom model of human middle ear ossicular chain (after [5], modified by authors)

In [8] the authors took several assumptions about flexibility and motion of ossiculars. They assumed compliances ratios and expressed velocities. Based on [6] when taking under consideration relationship between values of compliances and then stiffness of springs *k* following assumption are made:

1. $c_{MAN} \cong 0$
2. $k_{AML} = k_{PIL} = k_{TM} = 0$ (because $c_{AML}, c_{PIL}, k_{TM} \to \infty$);
3. from ratios of compliances it is assumed, that $c_{IMJ} = 1$ and other values are referred to this one:

$$k_{IMJ} = \frac{1}{c_{IMJ}} = 1,\ k_{ISJ} = \frac{1}{c_{ISJ}} = 0{,}481,\ k_{AL} = \frac{1}{c_{AL}} = 0{,}236$$

Values of damping are assumed arbitrary by authors as *1%* of stiffness:

$c_{IMJ} = 0{,}01,\ c_{ISJ} = 4{,}81 \cdot 10^{-3},\ k_{AL} = 2{,}36 \cdot 10^{-3}$

Masses of ossicles were taken as the mean value of those presented in the literature:

$m_M = 25mg,\ m_I = 28,5mg,\ m_S = 3,2mg$

To use the information presented above, dimensionless values of time, frequencies, displacements, masses, damping and stiffness are introduced in the current study.

The set of differential equations for the model in Fig. 1 takes the form:

$$\begin{cases} m_M \ddot{x}_M + k_{TM} x_M + c_{TM} \dot{x}_M + k_{IMJ}(x_M - x_I) + c_{IMJ}(\dot{x}_M - \dot{x}_I) + \\ + k_{AML} x_M + c_{AML} \dot{x}_M + F = 0 \\ m_I \ddot{x}_I - k_{IMJ}(x_M - x_I) - c_{IMJ}(\dot{x}_M - \dot{x}_I) + k_{PIL} x_I + c_{PIL} \dot{x}_I + \\ + k_{ISJ}(x_I - x_S) + c_{ISJ}(\dot{x}_I - \dot{x}_S) = 0 \\ m_S \ddot{x}_S - k_{ISJ}(x_I - x_S) - c_{ISJ}(\dot{x}_I - \dot{x}_S) + k_{AL} x_S + c_{AL} \dot{x}_S \end{cases} \tag{1}$$

After introducting dimensionless time

$\tau = \omega_M^* \cdot t$, where $\omega_M^* = \sqrt{\dfrac{k_{IMJ}}{m_M}}$,

dimensionless displacements

$X_M = \dfrac{x_M}{x_{st}^*},\ X_I = \dfrac{x_I}{x_{st}^*},\ X_S = \dfrac{x_S}{x_{st}^*}$, where x_{st}^* is a static displacement under a static input function and taking into account that

$$\frac{dx_M}{dt} = \frac{dx_M}{d\tau} \cdot \frac{d\tau}{dt} = \dot{x}_M \cdot \omega_M^* \text{ and } \frac{d^2 x_M}{dt^2} = \frac{d(\dot{x}_M \cdot \omega_M^*)}{d\tau} \cdot \frac{d\tau}{dt} = \ddot{x}_M \cdot \omega_M^{*\,2}$$

$$\frac{dx_I}{dt} = \frac{dx_I}{d\tau} \cdot \frac{d\tau}{dt} = \dot{x}_I \cdot \omega_M^* \text{ and } \frac{d^2 x_I}{dt^2} = \frac{d(\dot{x}_I \cdot \omega_M^*)}{d\tau} \cdot \frac{d\tau}{dt} = \ddot{x}_I \cdot \omega_M^{*\,2}$$

$$\frac{dx_S}{dt} = \frac{dx_S}{d\tau} \cdot \frac{d\tau}{dt} = \dot{x}_S \cdot \omega_M^* \text{ and } \frac{d^2 x_{SM}}{dt^2} = \frac{d(\dot{x}_S \cdot \omega_M^*)}{d\tau} \cdot \frac{d\tau}{dt} = \ddot{x}_S \cdot \omega_M^{*\,2}$$

we get

$$
\begin{cases}
\ddot{X}_M + \dfrac{k_{IMJ}}{m_M \omega_M^{*\,2}} X_M - \dfrac{k_{IMJ}}{m_M \omega_M^{*\,2}} X_I + \dfrac{c_{IMJ}}{m_M \omega_M^{*\,2}} \dot{X}_M - \dfrac{c_{IMJ}}{m_M \omega_M^{*\,2}} \dot{X}_I + F_1 = 0 \\
\dfrac{m_I}{m_M} \ddot{X}_I - \dfrac{k_{IMJ}}{m_M \omega_M^{*\,2}} X_M - \dfrac{k_{IMJ}}{m_M \omega_M^{*\,2}} X_I - \dfrac{c_{IMJ}}{m_M \omega_M^{*\,2}} \dot{X}_M - \dfrac{c_{IMJ}}{m_M \omega_M^{*\,2}} \dot{X}_I + \\
+ \dfrac{k_{ISJ}}{m_M \omega_M^{*\,2}} X_I - \dfrac{k_{ISJ}}{m_M \omega_M^{*\,2}} X_S + \dfrac{c_{ISJ}}{m_M \omega_M^{*\,2}} \dot{X}_I - \dfrac{c_{ISJ}}{m_M \omega_M^{*\,2}} \dot{X}_S = 0 \\
\dfrac{m_S}{m_M} \ddot{X}_S - \dfrac{k_{ISJ}}{m_M \omega_M^{*\,2}} X_I - \dfrac{k_{ISJ}}{m_M \omega_M^{*\,2}} X_S - \dfrac{c_{ISJ}}{m_M \omega_M^{*\,2}} (\dot{X}_I - \dot{X}_S) + \\
+ \dfrac{k_{AL}}{m_M \omega_M^{*\,2}} X_S + \dfrac{c_{AL}}{m_M \omega_M^{*\,2}} \dot{X}_S = 0
\end{cases}
\tag{2}
$$

Some ratios are substituted by the following coefficients:

$$\kappa_{IMJ} = \frac{k_{IMJ}}{m_M \omega_M^{*\,2}} = 1$$

$$\kappa_{ISJ} = \frac{k_{ISJ}}{m_M \omega_M^{*\,2}} = 0{,}481$$

$$\kappa_{Al} = \frac{k_{AL}}{m_M \omega_M^{*\,2}} = 0{,}236$$

$$\gamma_{IMJ} = \frac{c_{IMJ}}{m_M \omega_M^{*\,2}} = 1 \cdot 0{,}01$$

$$\gamma_{ISJ} = \frac{c_{ISJ}}{m_M \omega_M^{*\,2}} = 0{,}481 \cdot 0{,}01 = 4{,}81 \cdot 10^{-3}$$

$$\gamma_{AL} = \frac{c_{AL}}{m_M \omega_M^{*\,2}} = 0{,}236 \cdot 0{,}01 = 2{,}36 \cdot 10^{-3}$$

and also adequate coefficients for masses’ ratios:

$$M_M = 1,\ M_I = \frac{m_I}{m_M} = 1{,}14,\ M_S = \frac{m_S}{m_M} = 0{,}128$$

So the set of equations (2) can be presented in dimensionless form:

$$\begin{cases} M_M \ddot{X}_M + \kappa_{IMJ}(X_M - X_I) + \gamma_{IMJ}(\dot{X}_M - \dot{X}_I) - F_1 = 0 \\ M_I \ddot{X}_I - \kappa_{IMJ}(X_M + X_I) + +\kappa_{ISJ}(X_I - X_S) - \gamma_{IMJ}(\dot{X}_M + \dot{X}_I) \\ + \gamma_{ISJ}(\dot{X}_I - \dot{X}_S) = 0 \\ M_S \ddot{X}_S - \kappa_{ISJ}(X_I - X_S) + \kappa_{AL} X_S - \gamma_{ISJ}(\dot{X}_I - \dot{X}_S) + \gamma_{AL}\dot{X}_S = 0 \end{cases} \tag{3}$$

For the basic calculations it has been assumed that the exciting force equals zero. The set of equations (3) is homogeneous if $F_1 = 0$. For free and damped vibrations the displacements are sought as

$$\begin{array}{lllll} X_M = A_M \cdot e^{st} & & \dot{X}_M = s \cdot A_M \cdot e^{st} & & \ddot{X}_M = s^2 \cdot A_M \cdot e^{st} \\ X_I = A_I \cdot e^{st} & \Rightarrow & \dot{X}_I = s \cdot A_I \cdot e^{st} & \Rightarrow & \ddot{X}_I = s^2 \cdot A_I \cdot e^{st} \\ X_S = A_S \cdot e^{st} & & \dot{X}_S = s \cdot A_S \cdot e^{st} & & \ddot{X}_S = s^2 \cdot A_S \cdot e^{st} \end{array}$$

and after adequate arrangement, the following set of algebraic equations is obtained:

$$\begin{cases} A_M(M_M s^2 + \kappa_{IMJ} + \gamma_{IMJ} s) + A_I(-\kappa_{IMJ} - \gamma_{IMJ} s) + A_S \cdot 0 = 0 \\ A_M(-\kappa_{IMJ} - \gamma_{IMJ} s) + A_I(M_I s^2 + (\gamma_{IMJ} + \gamma_{ISJ})s + \kappa_{IMJ} + \kappa_{ISJ}) + \\ + A_S(-\kappa_{ISJ} - \gamma_{ISJ} s) = 0 \\ A_M \cdot 0 + A_I(-\kappa_{ISJ} - \gamma_{ISJ} s) + A_S(M_S s^2 + (\gamma_{ISJ} + \gamma_{AL})s + \kappa_{ISJ} + \kappa_{AL}) = 0 \end{cases} \tag{4}$$

To get nontrivial solutions for amplitudes, the main determinant of (4) has to equal zero, thus

$$\begin{vmatrix} (M_M s^2 + \gamma_{IMJ} s + \kappa_{IMJ}) & (-\kappa_{IMJ} - \gamma_{IMJ} s) & 0 \\ (-\kappa_{IMJ} - \gamma_{IMJ} s) & (M_I s^2 + (\gamma_{IMJ} + \gamma_{ISJ})s + \kappa_{IMJ} + \kappa_{ISJ}) & (-\kappa_{ISJ} - \gamma_{ISJ} s) \\ 0 & (-\kappa_{ISJ} - \gamma_{ISJ} s) & (M_S s^2 + (\gamma_{ISJ} + \gamma_{AL})s + \kappa_{ISJ} + \kappa_{AL}) \end{vmatrix} = 0 \tag{5}$$

After replacing coefficients M, γ, and κ by proper values, solutions of (5) are as follows:

$s_{1,2} = -0{,}000348235 \pm 0{,}263907 \cdot i$

$s_{3,4} = -0{,}00937757 \pm 1{,}36946 \cdot i$

$s_{5,6} = -0{,}0297776 \pm 2{,}44021 \cdot i$

where $i = \sqrt{-1}$.

Real parts of the complex numbers correspond to damping coefficients while imaginary parts are equal to damped natural frequencies. They are close to the natural frequencies values when in model from Fig. 1 there are no dampers.

The authors has also investigated the model with no dashpots, only springs and following values of natural frequencies have been obtained:

$\Omega_1 = 0,263949,\ \Omega_2 = 1,36943,\ \Omega_3 = 2,44049.$

Numerical calculation

In order to create a model in Matlab - Simulink the following substitutions are proposed:

$$
\begin{array}{lll}
\ddot{X}_M = y_M(t) & \dot{X}_M = \int y_M(t) & X_M = \iint y_M(t) \\
\ddot{X}_I = y_I(t) \quad \Rightarrow & \dot{X}_I = \int y_I(t) \quad \Rightarrow & X_I = \iint y_I(t) \\
\ddot{X}_S = y_S(t) & \dot{X}_S = \int y_S(t) & X_S = \iint y_S(t)
\end{array}
$$

After replacing the above values in (3) and adequate arranging, we obtain

$$
\begin{cases}
y_M(t) = F_1 - \iint y_M(t)dt + \iint y_I(t)dt - 0{,}01\int y_M(t)dt + \\
+ 0{,}01\int y_I(t)dt \\
y_I(t) = \dfrac{1}{1{,}14}\{\iint y_M(t)dt - 1{,}481 \cdot \iint y_I(t)dt + 0{,}481 \cdot \iint y_S(t)dt + \\
+ 0{,}01\int y_M(t)dt - 0{,}01481\int y_I(t)dt + 0{,}00481\int y_S(t)dt\} \\
y_S(t) = \dfrac{1}{0{,}128}\{0{,}481\iint y_I(t)dt - 0{,}717 \cdot \iint y_S(t)dt + \\
+ 0{,}00481\int y_I(t)dt - 0{,}00717\int y_S(t)dt\}
\end{cases}
\qquad (6)
$$

The diagram in Fig. 2 presents the model in Matlab - Simulink package. Displacements x_M, x_I and x_S have been calculated for different types of exciting force, when it is constant and equals one or when it is a harmonic function $F = A \cdot \sin \omega t$. The exemplary diagram for frequency that equals one and amplitude that also equals one is presented in Fig. 3. The time history was imposed for 2000 seconds in all three cases.

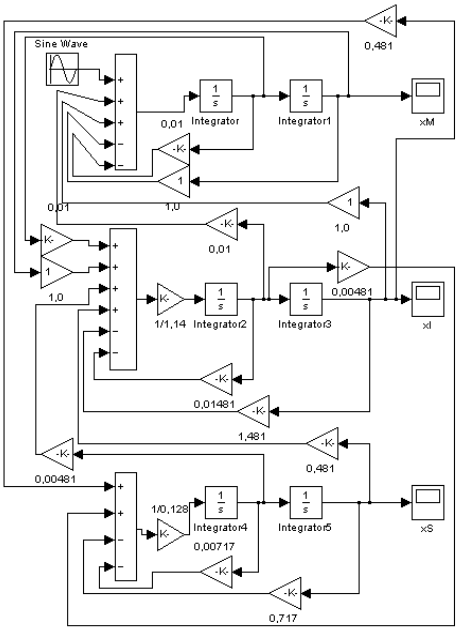

Fig. 2. Model in Matlab – Simulink package of the ossicular chain presented in Fig. 1

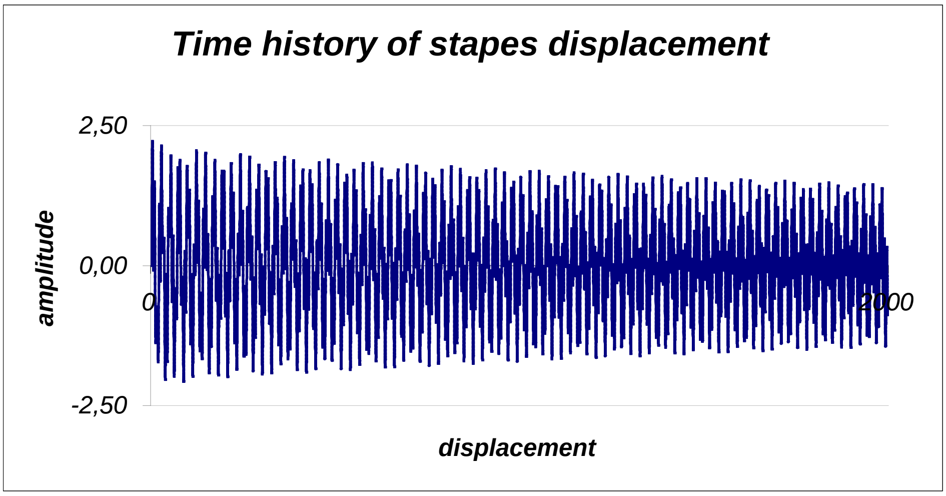

Fig. 3. Time history of x_S coordinate for both amplitude and frequency of the exciting force equalling one in time 2000 s

The solutions received in Matlab - Simulink package from direct numerical simulation have been compared with values of natural frequencies received analytically. By changing excitation frequency the amplitude-frequency curves are plotted (Table I. and Fig. 4). As a result, maxima of the three resonance curves arise around the normal frequencies determined analytically.

TABLE I. Data for the resonance curves

Ω	A_M^{M-S}	A_I^{M-S}	A_S^{M-S}	A_M^{A}	A_I^{A}	A_S^{A}
0,10	8,60	7,50	5,05	8,50	7,41	4,98
0,20	17,10	15,40	10,40	16,83	15,15	10,24
0,25	69,00	63,60	43,15	68,90	63,59	43,14
0,26	239,00	222,00	151,00	238,18	221,06	150,11
0,2639	***2670,00***	***2480,00***	***1685,00***	***1783,54***	***1659,27***	***1127,14***
0,27	151,00	141,00	96,00	150,05	140,12	95,24
0,30	24,50	23,30	15,90	23,82	22,68	15,46
0,50	2,60	2,95	2,10	2,41	2,81	1,97
1,00	0,12	1,06	0,85	0,05	1,00	0,82
1,30	2,40	2,65	2,55	2,41	2,65	2,55
1,35	7,75	7,80	7,75	8,41	7,83	7,78
1,36	13,74	12,38	12,40	13,92	12,55	12,56
1,3694	***19,80***	***17,30***	***17,40***	***20,25***	***17,74***	***17,89***
1,38	13,50	11,52	11,62	13,42	11,38	11,57
1,40	6,00	4,80	4,95	5,99	4,79	4,95
1,70	0,68	0,27	0,38	0,67	0,27	0,38
2,00	0,40	0,10	0,21	0,36	0,09	0,20

2,20	0,28	0,05	0,22	0,27	0,04	0,21
2,30	0,24	0,03	0,27	0,24	0,02	0,27
2,38	0,21	0,02	0,48	0,21	0,02	0,48
2,40	0,21	0,04	0,62	0,21	0,03	0,62
2,42	0,20	0,06	0,82	0,21	0,06	0,83
2,43	0,21	0,08	0,92	0,21	0,08	0,93
2,4402	***0,21***	***0,10***	***0,95***	***0,21***	***0,10***	***0,96***
2,45	0,21	0,10	0,88	0,21	0,10	0,89
2,50	0,20	0,07	0,37	0,20	0,07	0,37
3,00	0,14	0,03	0,03	0,13	0,02	0,02

Data in Table I. correspond to malleus, incus and stapes amplitudes. Fig. 4 presents exemplary curves for stapes only. Maximum for the first normal frequency is not visible in the diagram in order to enable showing values of the rest amplitudes.

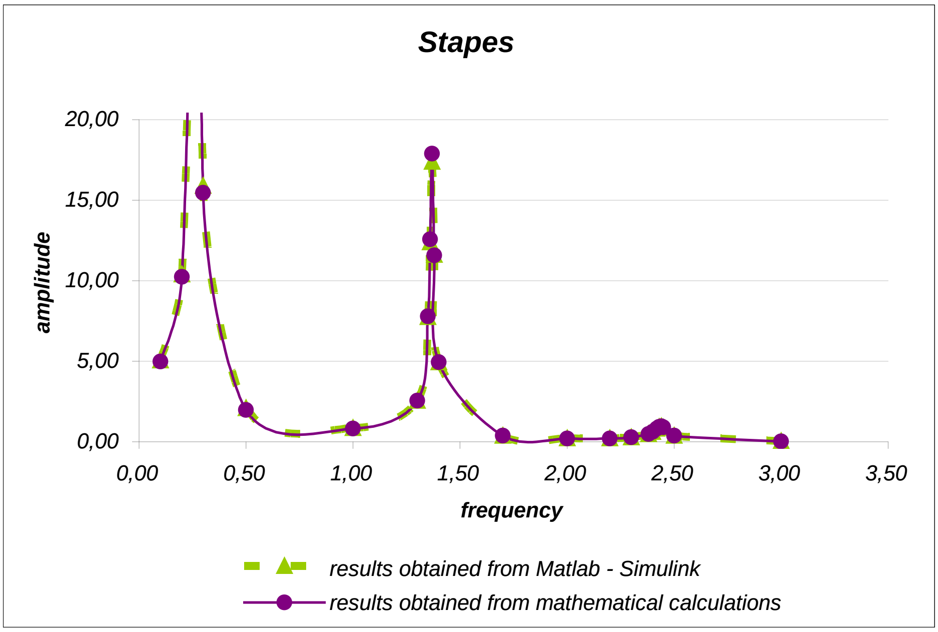

Fig. 4. Resonance curves for stapes

Effect of the influence of κ_{ISJ} on the ear's behaviour is also analyzed. The set of equations (3) for vibrations excited by harmonic force (harmonic acoustic pressure) versus κ_{ISJ} parameter and excitation frequency have been constructed and then the expressions for A_M, A_I and A_S have been found analytically.
For the range of κ_{ISJ} values from 0,2 to 10 and for Ω from 0,1 to 4,5, where κ_{ISJ} and Ω are dimensionless parameters the resonance curves have been obtained.

Exemplary curves for stapes for three values of κ_{ISJ} parameter (0,2; 0,481; 2,0) and fixed $\Omega=1,0$ are presented in Fig. 5 and the numerical values are placed in Table II. In Fig.5 we see that the resonance curves for three ossicles differ for different values of κ_{ISJ}. For $\kappa_{ISJ}=0,481$ maximum amplitudes appear near normal frequencies determined by Eq. (5), and this is the reference resonance curve. Varying κ_{ISJ} from 0,2 to about 1,0 the first pick moves towards higher frequencies and its values increase for frequencies from 0,2 to 0,481 (maximum) then they decrease to about 1,0 and increase to about 2,0 and after that they decrease steadily. The second pick appears around the second natural frequency and it stays in the same place in the whole range of κ_{ISJ} values for all ossicles. The maximum value changes slightly for κ_{ISJ} higher than 1,0. While in a case of the third pick, it moves towards higher frequencies steadily as κ_{ISJ} increases, and the amplitudes values rather decrease for the third natural frequency.

TABLE II. Data for the resonance curves for 3 values of κ_{ISJ}

$\kappa_{ISJ}\rightarrow$	0,2	0,481	2
$\Omega\downarrow$			
0,10	5,373	4,983	4,794
0,20	***24,294***	10,240	7,800
0,25	15,886	43,174	14,345
0,26	11,628	151,535	17,646
0,2639	10,506	***6090,922***	19,430
0,27	9,112	95,632	23,148
0,30	5,408	15,465	***3965,997***
0,50	1,276	1,971	2,793
1,00	0,649	0,816	0,949
1,30	2,417	2,549	2,626
1,35	7,581	7,735	7,807
1,36	11,973	12,359	12,514
1,3694	***16,281***	***17,277***	***17,667***
1,38	11,237	11,388	11,407
1,40	5,099	4,928	4,833
1,50	1,287	1,086	1,001
1,60	0,814	0,569	0,489
1,70	0,728	0,376	0,297
1,80	1,002	0,280	0,201
1,90	***1,613***	0,229	0,145
2,00	0,340	0,202	0,109
2,20	0,074	0,208	0,068
2,30	0,044	0,272	0,056
2,38	0,030	0,480	0,048
2,40	0,028	0,614	0,047
2,42	0,026	0,814	0,045

2,43	0,025	0,909	0,044
2,4402	0,024	***0,938***	0,043
2,45	0,023	0,873	0,043
2,50	0,019	0,369	0,039
4,00	0,000	0,001	0,019
4,30	0,000	0,001	0,065
4,40	0,000	0,001	***0,119***
4,50	0,000	0,001	0,032

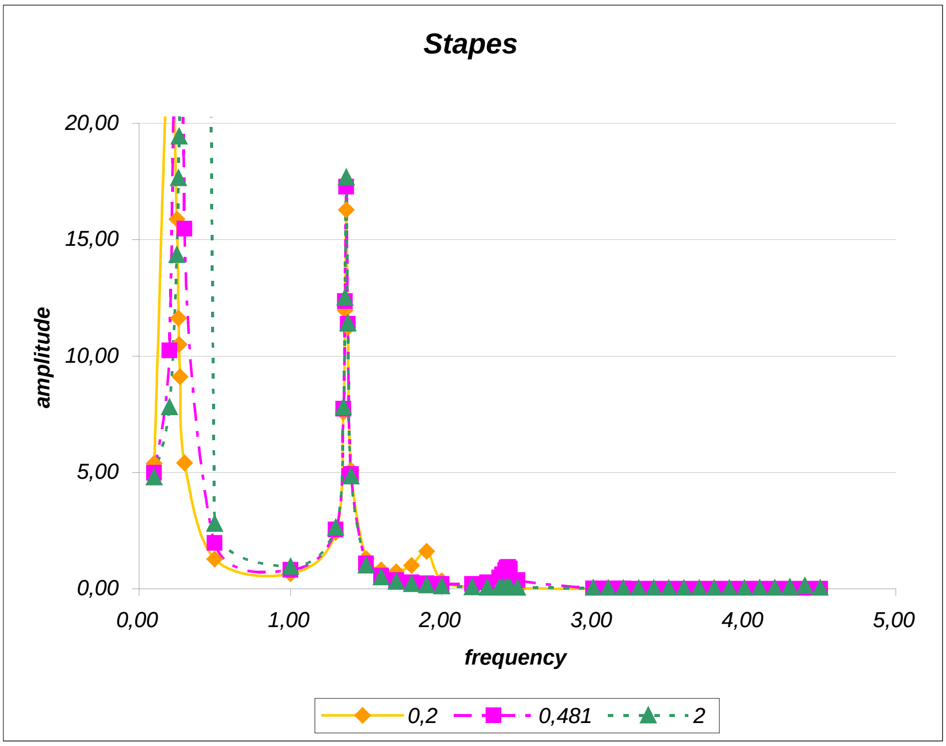

Fig. 5. Resonance curves for stapes for the following values of κ_{ISJ}: 0,2; 0,481; 2,0

Summary and conclusions

In the current study the authors took under consideration the three-masses linear mechanical model of a human middle ear. Dynamics of the system have been analysed by some reductions in coefficients of stiffness and damping values. The set of differential equations has been derived and solved for free and harmonically excited vibrations. The complex eigenvectors have been found and so-called damping coefficients (real parts) and damped frequencies values (imaginary parts) have been determined. To obtain time histories of coordinates x_M, x_I, x_S under different exciting forces, the model in Matlab - Simulink has been constructed. That model has been used to obtain the resonance curves for ossicles. For different values of exciting forces fixed values of amplitudes have been determined by the Matlab - Simulink model. The resonance curves have also been found by analytical approach and results have been compared with numerical simulations.

Influence of the stiffness parameter κ_{ISJ} of the joint between incus and stapes has been presented. Exemplary amplitudes values for various κ_{ISJ} that equals 0,2; 0,481 and 2,0 can be observed in the Fig.5. The middle pick stays in the same place while two other move towards higher frequencies when the stiffness κ_{ISJ} increases. This conclusion can be useful in the human middle ear diagnostics.

REFERENCES

1. *Gan R.Z., Sun Q., Feng B., Wood M.W.*: Acoustic-structural coupled finite element analysis for sound transmission in human ear – Pressure distribution. Medical Engineering & Physics 28 (2006) 395-404
2. *Sun Q., Gan R.Z., Chang K.-H., Dormer K.J.*: Computer-integrated finite element modeling of human middle ear . Biomechan. Model Mechanobiol. 1 (2002) 109-122
3. *Sun Q., Chang K.-H., Dormer K.J., Dyer R.K. Jr., Gan R.Z.*: An advanced computer-aided geometric modeling and fabrication method for human middle ear. Medical Engineering & Physics 24 (2002) 595-606
4. *Onchi Y.*: A Study of the Mechanism of the Middle Ear. The Journal of the Acoustical Society of America, July 1949 Vol. 21, Number 4, 404-411
5. *Onchi Y.*: Mechanism of the Middle Ear. The Journal of the Acoustical Society of America, June 1961 Vol. 33, Number 6, 794-803
6. *Nakajima H.H., Ravicz M.E., Merschant S.N., Peake W.T., Rosowski J.J.*: Experimental ossicular fixation and the middle ear's response to sound. Evidence for a flexible ossicular chain. Hearing Research 204 (2005) 60-70
7. Feng B., Gan R. Z.: Lumped parametric model of the human ear for sound transmission. Biomechan. Model Mechanobiol. (2004) 3: 33-47
8. *Ravicz M.E.., Peake W.T., Nakajima H.H., Merschant S.N., Rosowski J.J.,*: Modeling flexibility in the human ossicular chain: comparison to ossicular fixation data. Proceedings of the 3rd Symposium on Middle Ear Mechanics in Research and Otology, Matsuyama, Ehime, Japan 9-12 July, 2003

Modelling the human middle ear system

Abstract

In the paper different approaches to investigate behaviour of a human middle ear are presented. The three-degree of freedom model that consists of 3 masses, malleus, incus and stapes has been analysed. The set of differential equations has been solved in Matlab - Simulink package and by an analytical method. Natural frequencies and resonance curves for varied stiffness of the joint between incus and stapes κ_{ISJ} have been determined.

Keywords: middle ear, ossicular chain, mechanical model

Modelowanie ucha środkowego człowieka

Streszczenie
W artykule zaprezentowano różne podejścia do badania zachowań ucha środkowego człowieka. Oprócz analizy MES, możliwe jest również rozważenie modelowania mechanicznego. Rozpatrywany jest model o 3 stopniach swobody składający się z 3 mas (młoteczek, kowadełko, strzemiączko) połączonych tłumikami i sprężynami, został rozwiązany układ równań różniczkowych i zbudowany model fizyczny w programie Matlab - Simulink . Zostały przedstawione krzywe rezonansowe dla poszczególych kosteczek słuchowych.

Słowa kluczowe: ucho środkowe, łańcuch kosteczek słuchowych, model mechaniczny

Modeling the human middle ear system

KATARZYNA GUZ
JERZY WARMIŃSKI

Informacje o autorach

Mgr inż. Katarzyna Guz
Instytut Technologicznych Systemów Informacyjnych
Wydział Mechaniczny
Politechnika Lubelska
ul. Nadbystrzycka 36
20-618 Lublin
tel. (081)5384584
e-mail: k.guz@pollub.pl

dr hab. inż. Jerzy Warmiński, prof. PL
Katedra Mechaniki Stosowanej
Wydział Mechaniczny
Politechnika Lubelska
ul. Nadbystrzycka 36
20-618 Lublin
tel. (081)5384198
e-mail: j.warminski@pollub.pl

JERZY STAMIROWSKI
MARCIN RAK

An overview of the configuration selection methods in Reconfigurable Manufacturing Systems (RMS)

Introduction

Reconfigurable manufacturing system is based on a new manufacturing paradigm[1] introduced at the University of Michigan, which provides exactly the functionality and capacity needed exactly when needed. RMS combines general properties of DMLs (Dedicated manufacturing Lines) and FMS (Flexible Manufacturing System). The key characteristics of RMS are[1,2]: modularity, integrability, convertibility, customization, diagnosability.

RMS consists of modules (hardware and software), that can be easily added, removed or replaced to react to a change in market demand, government regulation, or introducing of new technologies. Modular structure of RMS empowers easy re-configuration and re-organization on each level: system, software, control, machine and process. There is a need for development of new theories and approaches or adopting existing ones for optimal selection of the best configuration for manufacturing system to produce desirable part families. This paper deals with methods for system configuration selection, and some of these theories are described in detail.

Survey of configuration selection technique

Different aspects of reconfiguration and system design have been extensively studied by many researchers. Abdi proposed a strategy for the selection of the most appropriate layout for each configuration stage using Analytical Hierarchical Process (AHP) model. In this work the emphasis is on the layout reconfigurability, cost, quality and reliability[3]. Xiaobo, Wang and Luo proposed a stochastic model of RMS that was divided into four parts: a framework, optimal configuration, optimal selection policy and performance measure. They classified all required products into a few product families (which consists of similar product) and stated that each product family corresponded with one system configuration[4,5,6,7]. Ren, Xu, Wang and Tan adapted Timed Event Graph (TEG) in order to model the cyclic reconfigurable flow shop. Using this method they tried to evaluate changes in system performances under different configurations (different combinations of modules and machines) and chose optimal configuration defined as the one with the minimum cycle time and the minimum number of pallets[8]. Youssef and ElMaraghy developed a metric to evaluate impact of the configuration on smoothness and easiness of reconfiguration process called Reconfiguration Smoothness (RS). This metric involves cost, time and effort indispensable to change system configuration from one to another. Authors utilized case study from literature to select the better of two demand scenarios for the manufacturing system using RS metric[9].

Galan developed a mathematical model for selection of the best set of product families and their production scheduling when the alternative routings for product exist in the manufacturing system [10]. The presented model has been tested with 35 instances from the literature (adapted from the Cellular Manufacturing Systems). To obtain the results within a reasonable computing time two heuristic procedures was proposed: Specific Heuristic and Tabu Search Metaheuristic. Ismail, Musharavati, Hamouda and Ramli implemented the genetic algorithm enhanced by specific heuristic for Manufacturing Process Planning Optimisation (MPPO)[11]. Their case study based on the system consisted of sixteen processing modules arranged in four stages. They utilized two algorithm in order to find optimal solution: modified genetic algorithm without a customized threshold operator (MGAWTO) and modified genetic algorithm with a customized threshold operator (MGATO). The obtained result showed that the MGATO is a better technique for modeling MPPO. Maier-Speredelozzi, Hu and co-authors described methodologies for evaluating the overall performance of different system configuration[12]. Three aspects of the performance evaluation methods were discussed: productivity, quality, scalability and convertibility. The case study based on system composed of six machines with four different configurations (one pure serial and one pure parallel, and two hybrid configurations).

Concept of the Reconfiguration Smoothness (RS)[9]

RS metric developed by Youssef and ElMaraghy takes into consideration three levels of reconfiguration, namely: market-level (TRS), system-level (SRS) and machine-level reconfiguration smoothness (MRS). The integrated RS representing smoothness and easiness of reconfiguration between two configuration is defined by equation:

$$RS = \alpha TRS + \beta SRS + \gamma MRS \tag{1}$$

where all coefficients lie in <0;1>, and:

$$\alpha + \beta + \gamma = 1 \tag{2}$$

All components representing different levels of configuration are defined as follows:

$$TRS = \varepsilon TRS_m + (1-\varepsilon) TRS_d \tag{3}$$

$$SRS = \phi SRS_s + \varphi SRS_m + \lambda SRS_f \tag{4}$$

$$MRS = \nu MRS_d + (1-\nu) MRS_o \tag{5}$$

where: all coefficient lie in <0;1>, and:

$$\phi + \varphi + \lambda = 1 \tag{6}$$

Components TRS_m and TRS_d representing changes related to use (add/remove) of machines and machine modules accordingly. Components SRS_s and SRS_m representing changes related to machines and stations accordingly, and SRS_f representing changes related to number of material flow paths. Components MRS_d and MRS_o representing changes related to utilization of machine modules and operation cluster assignments accordingly. It is recommended by authors that:

$$\beta > \gamma > \alpha \tag{7}$$

$$\varepsilon, \nu > 0.5 \tag{8}$$

To examine this methodology a case study from the literature was utilized. All calculation of RS metric for two consecutive configurations was provided, and sensitivity analysis for different metric parameters was performed.

AHP in a manufacturing systems[3]

Analytical Hierarchical Process (AHP) is one of the multi-criteria decision making methodologies that was developed by Thomas Saaty in 1980. By employing AHP, the complex problem can be decomposed to a hierarchical order. Abdi applied AHP in order to assess the objectives, criteria and layout configuration for selecting the most appropriate system layout configuration. Four objectives were determined: reconfigurability, cost, quality, reliability. Two of them (reconfigurability and cost) were decomposed into several criteria that must be strictly ranked with respect to system performance requirements (three levels of importance were proposed: low, medium, high). The alternative layouts were defined as shown on fig. 1.

In order to select the best configuration, the pair-wise comparative analysis of elements of built model (with respect to the element(s) at higher level(s) of the hierarchy) is performed and overall evaluation of the configuration layout possibilities is obtained.

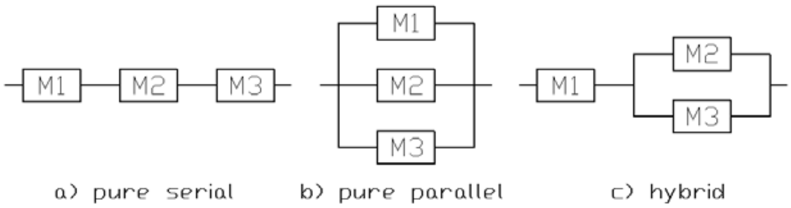

Fig. 1. The possible configuration for three machines.

Timed Event Graph for system configuration selection[8]

Ren, Xu, Wang and Tan have used timed event graph (4-tuple Petri Net) for modeling of reconfigurable flow shop (as shown on fig. 2). In order to find the optimal system configuration (configuration with minimum cycle time and minimum number of pallets), two mixed-integer programs (MIP1 – the minimum cycle time, and MP2 – minimum number of pallets) based on TEG properties were proposed. Reconfigurable flow shop described in [8] was modeled using 4-tuple Petri Net :

$$TEG = (P, T, F, K_0) \tag{9}$$

where:

P – is the set of places, and:

$$P = P^b \cup P^r \cup P^{c_1} \cup P^{c_2} \tag{10}$$

where:

$P^b, P^r, P^{c_1}, P^{c_2}$ – are the sets of buffer, resource, unmarked command and marked command places accordingly,

T – is the set of transitions (transition $t_{k,j}$ denotes the operation of job J_k on machine M_j),

F – is the set of directed arcs, and:

$$F = F^b \cup F^r \cup F^{c_1} \cup F^{c_2} \tag{11}$$

where:

$F^b, F^r, F^{c_1}, F^{c_2}$ – are the sets of directed arcs that go from or to buffer, resource, initially unmarked command and initially marked command places accordingly,

K_0 – is the initial marking.

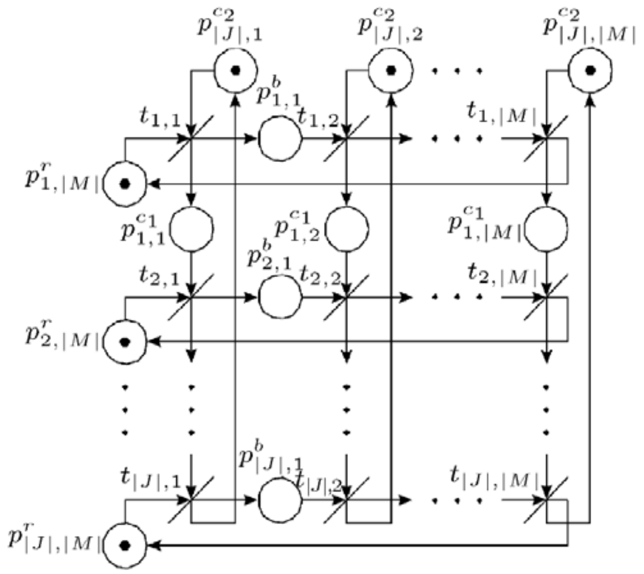

Fig. 2. The TEG model of reconfigurable flow shop[8].

Conclusion

The selection of the best system configuration in order to fulfill new market requirements is a cornerstone issue for manufacturing systems designers and plant managers. This paper deal with system configuration selection methods studied by many researchers. There is a need for improving the existing methodologies or development of new strategies that will take into consideration all costs and efforts related to change of system configuration, for instance in adjusting the above-mentioned methodology to microfabrication (micromachining, microassembly) system configuration..

REFERENCES

[1] Mehrabi, M. G., Ulsoy, A. G., Koren, Y. *Reconfigurable manufacturing systems: keys to future manufacturing.* J. of Intelligent Manufacturing Systems, Vol. 11, No. 4, pp. 403-419, 2000.

[2] Koren, Y., Heisel, U., Jovane, F., Moriwaki, T., Pritschow, G., Ulsoy, G., Van Brussel, H. *Reconfigurable manufacturing systems.* Annals of the CIRP Vol. 48/2/1999.

[3] Abdi, M. R. *Selection of layout configuration for reconfigurable manufacturing systems using the AHP*. ISAHP, Honolulu, 2005.

[4] Xiaobo, Z., Wang, J., Luo, Z. *A stochastic model of a reconfigurable manufacturing system. Part 1: A framework.* International Journal of Production Research Vol. 38, No. 10, pp 2273-2285, 2000.

[5] Xiaobo, Z., Wang, J., Luo, Z. *A stochastic model of a reconfigurable manufacturing system. Part 2: Optimal configurations.* International Journal of Production Research Vol. 38, No. 12, pp 2829-2842, 2000.

[6] Xiaobo, Z., Wang, J., Luo, Z. *A stochastic model of a reconfigurable manufacturing system. Part 3: Optimal selection policy.* International Journal of Production Research Vol. 39, No. 4, pp 747-758, 2001.

[7] Xiaobo, Z., Wang, J., Luo, Z. *A stochastic model of a reconfigurable manufacturing system. Part 4: Performance measure.* International Journal of Production Research Vol. 39, No. 6, pp 1113-1126, 2001.

[8] Ren, S. CH., Xu, D., Wang, F., Tan, M. *Cyclic reconfigurable flow shop under different configurations modelling and optimization based on timed event graph.* Acta Automatica Sinica Vol. 32, No. 1, 2006.

[9] Youssef, A. M. A., ElMaraghy, H. A. *Assessment of manufacturing systems reconfiguration smoothness.* International Journal of Advanced Manufacturing Technology Vol. 30, No. 1-2, 2006.

[10] Galan, R. *Model and heuristics for scheduling in reconfigurable manufacturing environments.* IPROMS, Submitted in 2007.

[11] Ismail, N., Musharavati, F., Hamouda, A. S. M., Ramli, A. R. *Manufacturing process planning optimisation in reconfigurable multiple parts flow lines.* Journal of Achievements in Materials and Manufacturing Engineering Vol. 31 Issue 2, 2008.

[12] Zhong, W., Maier-Speredelozzi, V., Bratzel, A., Yang, S., Chick, S. E., Hu, J. *Performance analysis of machining systems with different configurations.* Proceedings of the Japan USA Flexible Automotion Conference, Ann Arbor, MI, 2000.

Abstract

Rapid changes in market demand brought about the need for manufacturing systems that are more adaptive. The Reconfigurable Manufacturing Systems were developed to stay competitive in new markets conditions. In order to fulfill all requirements for new products and changes in system capacity, the best system configuration must be chosen. This paper presents a brief survey of system configuration selection methods for the new generation manufacturing systems. The most important properties of this methods were outlined.

Keywords: Reconfigurable Manufacturing System, System Configuration, Reconfiguration Smoothness, AHP.

An overview of the configuration selection methods in Reconfigurable Manufacturing Systems (RMS)

JERZY STAMIROWSKI
MARCIN RAK

Informacje o autorach

Dr hab. inż. Jerzy Stamirowski, prof. PŚK
Katedra: Automatyka i Robotyka
Wydział: Mechatronika i Budowa Maszyn
Politechnika Świętokrzyska
Al. Tysiąclecia Państwa Polskiego 7
25-314 Kielce
e-mail: jerzy.stamirowski@neostrada.pl

Mgr inż. Marcin Rak, doktorant
Katedra: Automatyka i Robotyka
Wydział: Mechatronika i Budowa Maszyn
Politechnika Świętokrzyska
Al. Tysiąclecia Państwa Polskiego 7
25-314 Kielce
E-mail: rakmarcin@vp.pl

PIOTR BORAL

Machining of cone worms using CAD/CAM systems

Introduction

Progress in the construction of double-worm counterrotating extruding presses is associated with the increased importance of the technology of processing non-softened PVC in the form of a dry mix. The cause of the development of this technology is aiming to reduce the processing costs by excluding the process of granulation [1]. The most important assembly of an extruding press is the plasticizing system consisting of one or several worms and a cylinder [1, 2, 3, 4].

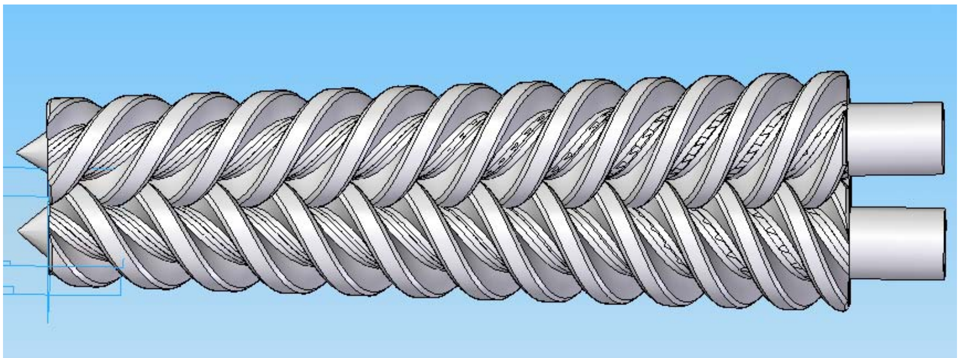

Fig. 1. A system of two variable-pitch cone worms in the batching zone

The execution of the plasticizing system, and particularly the cone worms of double-worm systems, poses a lot of difficulties. The greatest problem is to obtain the appropriate magnitudes of lateral inter-thread clearance. The characteristic feature of the variable-pitch cone worm is the variation of all geometric parameters in the axial section along the worm length and the lack of possibility of verifying their accuracy [1, 5]. An added difficulty in the execution of worms to be used in the plasticizing systems of double-worm extruding presses is their length, which can reach 5 m.

For functional reasons, this worm is divided into several zones differing in geometric parameters, which enables each of them to be considered separately (Fig. 1).

Machining of variable-pitch cone worms on a special machine tool

A special numerically controlled milling machine manufactured by Waldruch Coburg is presently used in Poland for cutting cone worms, where finger-type conical milling cutter is employed for machining [5, 6, 7, 8, 9, 10]. Setting up the machine tool requires the prior analysis of variation in the worm axial profile, as dependent on the geometric parameters of the tool and its positioning during operation. During machining of a cone worm with a finger-type cutter with a rectilinear profile in the axial section of the action surface, the cutter axis is positioned perpendicularly to the worm cut bottom at a specific distance from the worm axis. The distance of the cutter from the worm axis can be decomposed into two components:

- vertical shift, and
- cutter offset from the axial plane in the direction perpendicular to the cutter axis and the worm axis by the value of Δy.

The value of Δy is determined from the condition of assuring the minimum deviation of worm axial profile rectilinearity, and can be generally expressed by the following relationship (1) [6].

$$\Delta y = f\left(\gamma_f,\ d_f,\ s_{11},\ s_{21},\ b_1,\ b_2,\ x_l,\ k,\ h_1,\ h_2,\ d_1,\ d_2,\ l\right) \quad (1)$$

where:

γ_f - angle of mill axial profile,
d_f - minor mill diameter,
s_{11} - worm pitch at the beginning of the zone,
s_{21} - worm pitch at the end of the zone,
b_1 - cut width at the beginning of the zone,
b_2 - cut with at the end of the zone,
x_l - position of the profile examined on the zone length,
k - multiplicity of the profile examined (left-hand or right-hand),
h_1 - height of the axial profile and the beginning of the zone,
h_2 - height of the axial profile and the end of the zone,
d_1 - worm outer diameter at the beginning of the zone,
d_2 - worm outer diameter at the end of the zone,
l - worm (zone) length.

To satisfy the assumed rectilinearity, the value of Δy is varied along the worm axis during machining. A computation program for geometric analysis and the optimization of worm construction and specific technology with the theoretical determination of clearances has been developed [6].

However, a constant value of the shift Δy is used in practice in Poland when cutting a given worm zone, which is a simplification in the case of cone worms, both variable- and fixed-pitch ones.

Due to the absence of the detailed geometric analysis of worms and, as a consequence, their accuracy that influences the magnitude and distribution of clearances between mating worms, such extruding presses are not competitive to foreign extruders.

Machining of variable-pitch cone worms on a CNC machining centre using CAD/CAM systems

Special-purpose machine tools are built to order, being tailored for a specific technology of similar parts. They are very expensive, and therefore they should be exploited to the maximum. For this reason, when designing technological processes, we use them only in the case of having no possibility of using general-purpose machine tools.

I propose to use a general-purpose machining centre numerically controlled in at least 5 axes for machining the cuts of a fixed- and variable-pitch cone worms for pre-machining.

Software applications designed for computer-aided engineering work enable presently the control of design activities, from the design, through strength calculation, kinematic simulation, to the generation of the NC machine tool code and the simulation of execution of finished parts. Systems available now allow these processes to be carried out either within a single program that includes integrated modules, or within separate programs, which are usually specialized in one of those parts of the finished product manufacturing process [11].

Before proceeding with the planning of machining, the worm needs to be space modelled in the CAD program. Then, it should be exported in a format readable to the CAM program.

The worm was modelled in the SolidEdge program. The worm model was stored in the form of a solid body in a format readable to the EdgeCAM program (Parasolid Text Transmit Document).

Next, it was red out in the EdgeCAM program and, after the identification of specific model features, its machining was performed using functions available in the application.

Due to the high degree of complexity of the part, a machine tool with 5 numerically controlled axes was set up for machining.

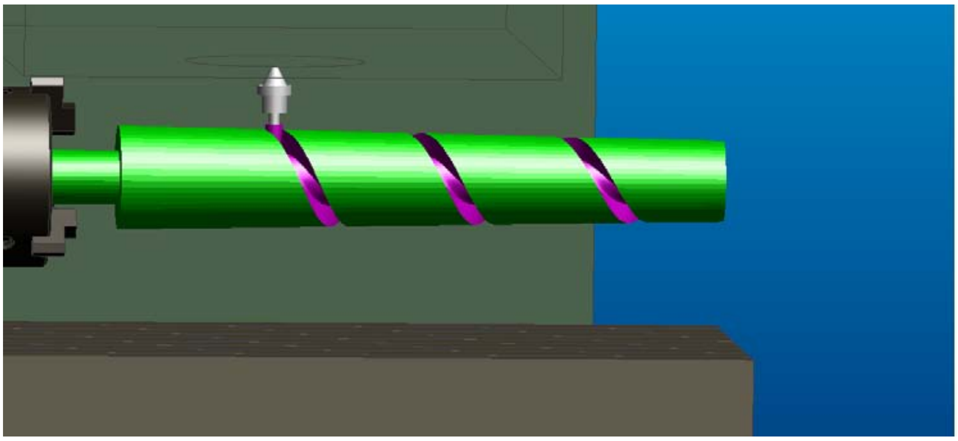

Fig. 2. Machining of the right-hand side of the cut profile of a right-thread worm of the following parameters, using a finger-type cone cutter with a diameter of d_f = 14 mm and a cutter profile angle of γ_f = 11°: pitches at the beginnung and end of the zone $s_{11} = 180$mm, $s_{21} = 144$; worm multiplicity $z = 3$; zone length $l = 675$mm; outer diameters At the beginning and end of the zone $d_1 = 90{,}5$mm, $d_2 = 115{,}408$mm; axial profile heights at the beginning and end of the zone $h_1 = 22$mm, $h_2 = 24{,}499$mm; cut widths on the outer diameter At the beginnung and end of the zone $b_1 = 35{,}2$mm, $b_2 = 29{,}7$mm

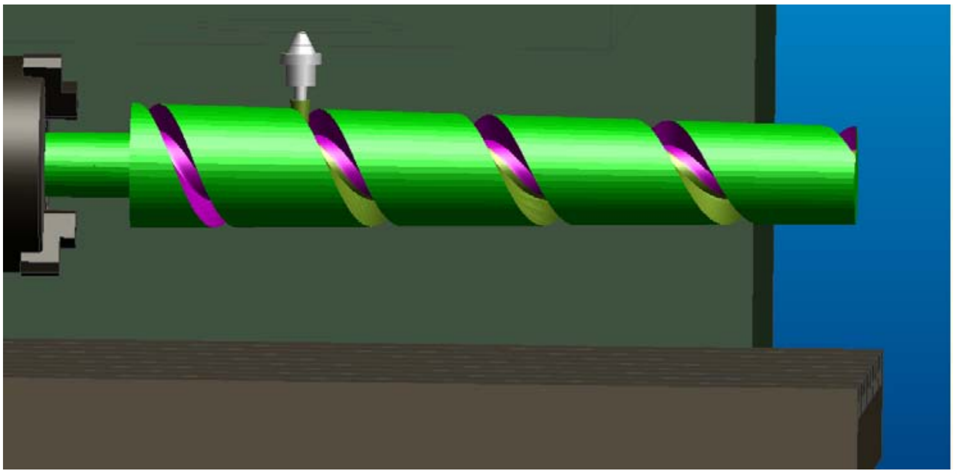

Fig. 3. Machining of the left-hand side of the cut profile of a right-thread worm of the parameters, as given above, using a finger-type cone cutter with a diameter of d_f = 19 mm and a cutter profile angle of γ_f = 9°

The worm cut axial profile is rectilinear, and the angle of inclination of the profile sides is approx. 10° in relation to the worm cut bottom profile. Owing to the fact that the configured control system has no capability to incline the tool spindle, the cutter of a taper angle of 11° was used for machining the right-hand side of the worm profile (Fig. 2), and 9° for the left-hand side (Fig. 3).

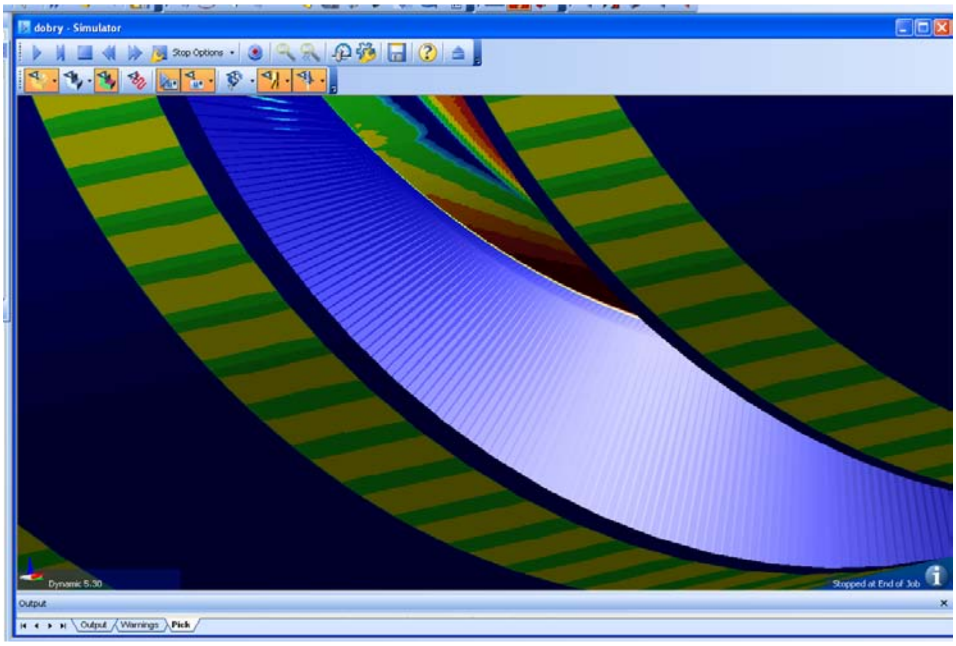

Fig. 4. Comparison of the theoretical model with the part generated on the simulator

The prepared technological process can be subjected to detailed analysis. We can view the simulation of the machining process and determine the machine time and the actual appearance of the part machined, along with the theoretical traces formed after the passage of the tool (with great simplifications, such as ideal material homogeneity, no vibrations, no tool wear, etc., assumed).
The CAM system provides the capability to make comparison of the model generated by the system based on the assumed machining with the theoretical model input from the CAD system. Figure 4 shows that some deviations occur. In the upper part of the profile, the material remains unmachined (positive deviations), while in the lower part the cutter cuts into the model and an undercut results (a negative deviation). In addition, the cutter axis is positioned perpendicularly to the worm axis, and not perpendicularly to the cut bottom cone surface. This causes the formation of a trace at the boundary between the first cutter milling and the second cutter milling.

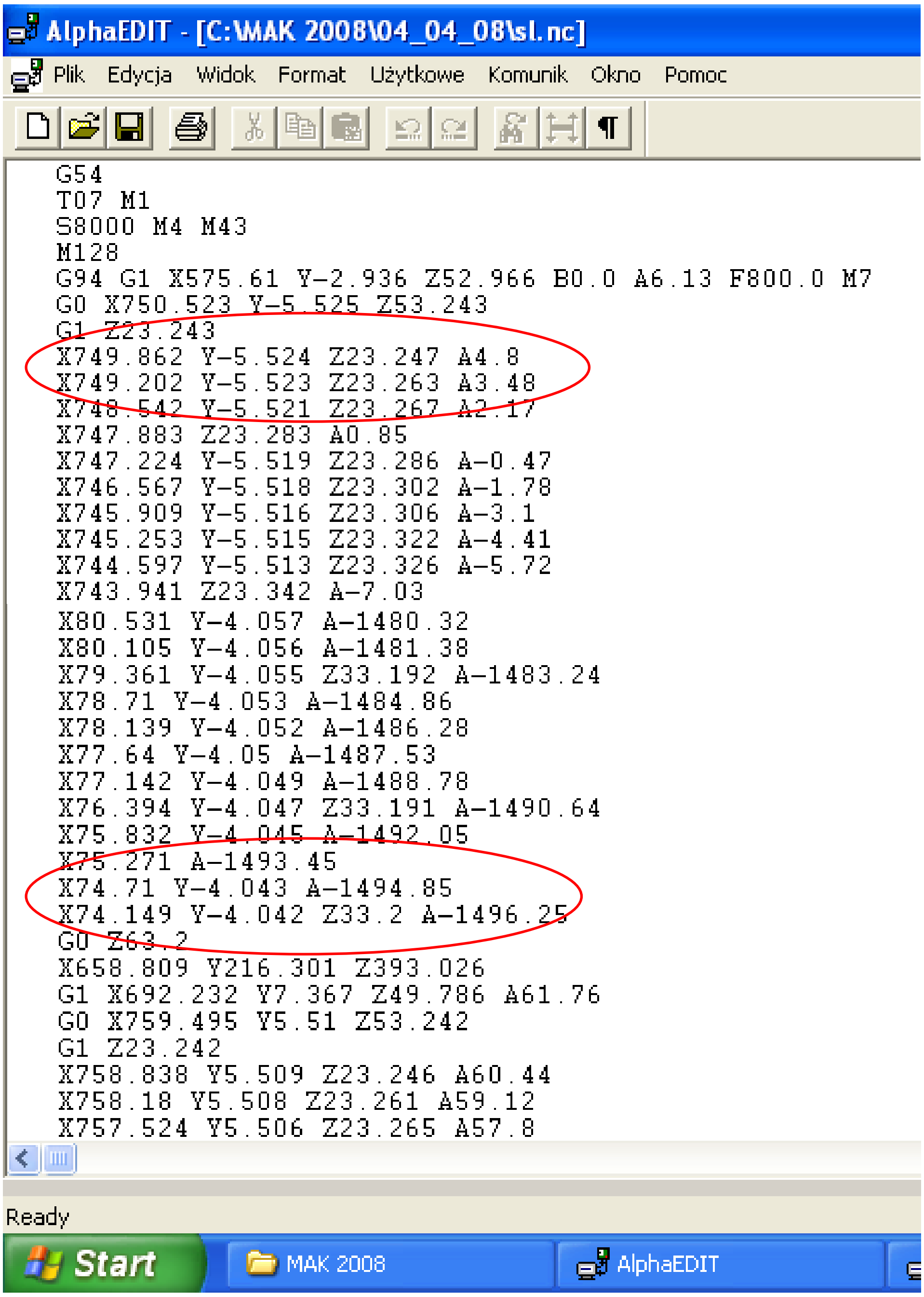


```
G54
T07 M1
S8000 M4 M43
M128
G94 G1 X575.61 Y-2.936 Z52.966 B0.0 A6.13 F800.0 M7
G0 X750.523 Y-5.525 Z53.243
G1 Z23.243
X749.862 Y-5.524 Z23.247 A4.8
X749.202 Y-5.523 Z23.263 A3.48
X748.542 Y-5.521 Z23.267 A2.17
X747.883 Z23.283 A0.85
X747.224 Y-5.519 Z23.286 A-0.47
X746.567 Y-5.518 Z23.302 A-1.78
X745.909 Y-5.516 Z23.306 A-3.1
X745.253 Y-5.515 Z23.322 A-4.41
X744.597 Y-5.513 Z23.326 A-5.72
X743.941 Z23.342 A-7.03
X80.531 Y-4.057 A-1480.32
X80.105 Y-4.056 A-1481.38
X79.361 Y-4.055 Z33.192 A-1483.24
X78.71 Y-4.053 A-1484.86
X78.139 Y-4.052 A-1486.28
X77.64 Y-4.05 A-1487.53
X77.142 Y-4.049 A-1488.78
X76.394 Y-4.047 Z33.191 A-1490.64
X75.832 Y-4.045 A-1492.05
X75.271 A-1493.45
X74.71 Y-4.043 A-1494.85
X74.149 Y-4.042 Z33.2 A-1496.25
G0 Z63.2
X658.809 Y216.301 Z393.026
G1 X692.232 Y7.367 Z49.786 A61.76
G0 X759.495 Y5.51 Z53.242
G1 Z23.242
X758.838 Y5.509 Z23.246 A60.44
X758.18 Y5.508 Z23.261 A59.12
X757.524 Y5.506 Z23.265 A57.8
```

Fig. 5. Fragments of the EdgeCam-generated CNC machine-tool program for the machining of the right-thread cone worm with parameters, as given above

From the generated program (Fig. 5) it can be noticed that in objects of the type, where a curve in the form of a helical line occurs, the tool motion trajectory is defined by very small segments. The program uses the preparatory function G1 with the parameters of the coordinates X, Y, Z and A. In line with the previous analyses using the author's own program (Fig. 6), the coordinate Y (Δy, the cutter offset from the axial plane during machining) is variable along the worm length.

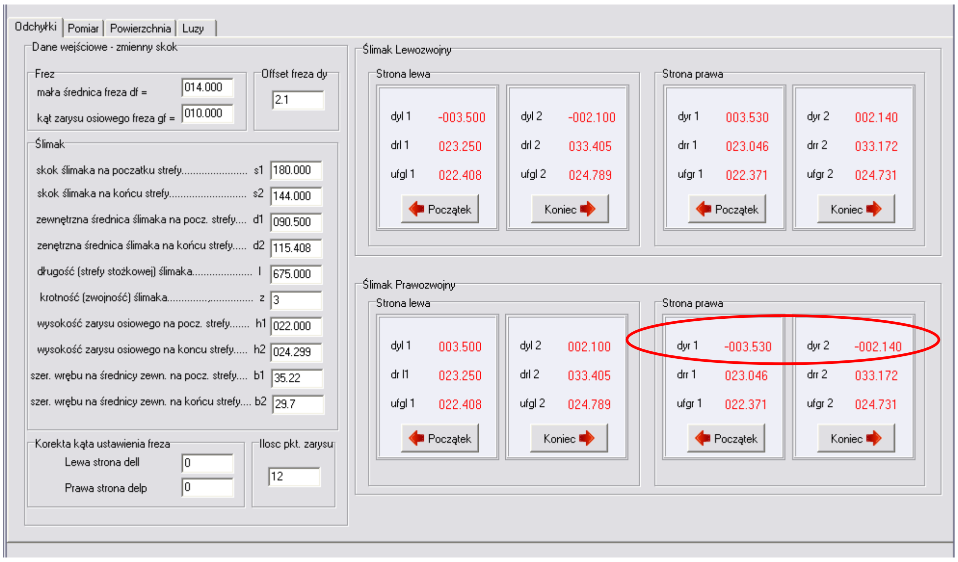

Fig. 6. The optimal parameters of worm and cutter relative positioning during machining

Summary

CAM system are used for generating the G code in the case, where the model is complex and is not possible to be programmed manually. Various operations (such as planning, coarse machining, profiling, rowing, etc.) and cycles (a curve-wise projection cycle, a concentric cycle, a circular projection cycle, etc.) are used. Five-axis machining involves additionally machining functions between two curves, between two surfaces, projecting along a curve, etc. Programs of this type are used for typical objects, such as the classes of sleeves, shafts, bodies, forms, etc. Objects, such as the variable-pitch cone worm under analysis, can also be made using specific 5-axis machining functions. The accuracy of execution of the worm is not satisfactory; therefore, software of this type can be used for the generation of the G code, but for coarse machining only.

So, for untypical objects, which the worms under analysis are, special software needs to be developed, which would generate the trajectories of tool motion on general-purpose machine tools controlled in 5 axes.

REFERENCES

1. *Stasiek J.*: Wytłaczanie tworzyw polimerowych, wybrane zagadnienia, Wydawnictwo Uczelniane Uniwersytetu Technologiczno-Przyrodniczego w Bydgoszczy, Bydgoszcz 2007.
2. *Sikora R.*.: Przetwórstwo tworzyw wielkocząsteczkowych, WE, Warszawa 1993.
3. *Stasiek J., Nieszporek T.*: Problemy projektowania i wykonywania ślimaków dwuślimakowych wytłaczarek przeciwbieżnych, Polimery 2002, 47, nr 6, pp. 441.449.
4. *Stasiek J.*: Effect of Screw Geometry and Conditions of Extrusion on the Course of PVC Plastifikation in a Twin-Screw Extruder. The Polymer Processing Society. Stuttgart 1995.
5. *Nieszporek T., Boral P.*: Bases of the design and technology of variable-pitch cone worms, The 4-th International Conference on Advanced Manufacturing Technologies "ICAMaT 2005" Bucharest, Romania, pp. 73.78
6. *Boral P.*: Analiza geometryczna układu dwóch ślimaków stożkowych o stałym i zmiennym skoku stosowanych w wytłaczarkach dwuślimakowych do transportu tworzywa, Praca doktorska, Politechnika Częstochowska, Częstochowa 2001.
7. *Boral P.*: The determination of inter-thread clearance in the screw plasticizing system. 6-th European Conference of Young Research and Science Workers in Transport and Telecommunications "TRANSCOM 2005", University of Žilina, Slovak Republic, 2005, pp. 285.288.
8. *Nieszporek T., Boral P.*: The design and technology of cone worms, The Third International Scientific Conference MECHANICS 2002, Rzeszów 2002, pp. 259.264.
9. *Нешпорек Т., Боряль П.*: Основы профилирования конических червяков с изменяющимся и постоянным шагом. V Международый Конгрес 2005 „Конструкторско-технологическая информатика". Московский Государствен-ный Технологический Университет СТАНКИН. pp. 58.61
10. *Boral P.*: Obróbka ślimaków stożkowych, Koła zębate, wytwarzanie, pomiar, KBM PAN, Poznań 2004, pp. 55.59.
11. *Augustyn K.*: EdgeCAM, Komputerowe wspomaganie wytwarzania, Wydawnictwo HELION, Gliwice 2007.

Obróbka ślimaków stożkowych z zastosowaniem systemów CAD/CAM

Streszczenie

Zmienność wszystkich parametrów geometrycznych ślimaków stożkowych o zmiennym skoku stosowanych w układach uplastyczniających wytłaczarek dwuślimakowych przeciwbieżnych powoduje, że obrabia się je na specjalnych obrabiarkach wyposażonych w sterowanie numeryczne. Proponuję zastosowanie systemów CAD/CAM do przygotowania programu do obróbki tego typu ślimaków na uniwersalną obrabiarkę sterowaną CNC w co najmniej 5-osiach.

Słowa kluczowe: ślimak stożkowy, systemy CAD/CAM

Machining of cone worms using CAD/CAM systems

Abstract
The variability of all geometric parameters of variable-pitch cone worms used in the plasticizing systems of counterrotating double-worm extruding presses causes these worms to be machined on special-purpose machine tools provided with numerical control. I propose the application of CAD/CAM systems for the preparation of a program for machining of this type of worm on a general-purpose CNC machine tool controlled in at least 5 axes.

Keywords: cone worm, CAD/CAM systems

Machining of cone worms using CAD/CAM systems

PIOTR BORAL

Informacje o autorze

Dr inż. Piotr Boral
Instytut Technologii Maszyn I Automatyzacji Produkcji
Wydział Inżynierii Mechanicznej i Informatyki
Politechnika Częstochowska
Al. Armii Krajowej 21
42-200 Częstochowa
tel. 034 3250588, 034 3250509
e-mail: piotrek@itm.pcz.pl

HENRYK CZARNECKI

The use of computer techniques for the analysis of material effort in the irregularity contact region in the dry friction process

Introduction

The development of computer techniques creates new possibilities for modelling and simulation with the use of numerical techniques for conducting experiments on virtual models describing tribological nodes. Instead, or rather along with carrying out difficult and time-consuming studies on, e.g., correlation between the geometric structure of the tribological layer and its tribological properties in actual objects, or model objects, analyses using computer simulations can be conducted. With the present development of both hardware and software, simulation modelling creates new possibilities for examining even hypothetical situations. There are many software applications enabling the examination of real objects with the use of the finite-element theory that enables the determination of the components of states, i.e. stress and strain, or the components of displacements. The application of CAD systems with a finite-element method (FEM)-based computation module to the analysis of tribological phenomena on the contact between the elements of irregularities in a micro-scale can facilitate the understanding of phenomena accompanying the friction process and the selection of the geometric surface structure at the stage of designing the construction and technology for making the top layer.

Stress in the technological top layer and its importance

During constituting the technological top layer changes in the dimensions of individual material structure elements take place under the influence of physical and chemical phenomena occurring at the tool-workpiece contact. As the result of exceeding the elastic strain in the top layer, stress forms also after removing the agents that induce it. A particular role is played by internal stress located in the top layer being exposed to the highest stress deriving from external forces, which, either alone or summed with the stress produced by working loads, can reduce or enhance top layer durability under the conditions of mechanical or corrosive influences. It can be said that it influences the effort which is the measure of a dangerous state manifesting itself in the appearance of local plastic strain, or a crack at any point of the element concerned [1, 7]. By simplification, it is assumed that the effort is dependent exclusively on the stress state components and the mechanical properties of material, such as the tensile yield stress, R_e, or the ultimate tensile strength, R_m, etc. [1,6,7]. For the evaluation of the effort of the whole body, the weakest link principle is applied, whereby the effort of the entire body is decided upon by that single point, at which the reduced stress is the highest. In view of the above, the general form of the strength criterion can be written as [1]

$$\sigma_{red} \leq \sigma_{dop} \tag{1}$$

Due to the fact that the contact between the surface elements of the tribological pair occurs at the tops of irregularities, and this is where their wear takes place, it is justifiable to believe that the knowledge of the state of effort could be helpful in the selection of a technology that will provide the surface roughness necessary to assure the transfer of stress induced in operation processes.

Investigation and experience show that such a stress distribution is the most advantageous to machine part operation, where the top layer has compressive stress at the surface. In that case, cyclic external influences superpose on the internal stress and, as a consequence, cause the resultant stress to be shifted deep into the material. This phenomenon causes the fatigue centre to form not on the surface of the material being weakened by various notches, but inside it. This if of great practical importance, since at that case the material surface defects do not play the key role in the fatigue failure process.

It should be stressed, though, that the thickness of the strengthened layer with compressive stress may not exceed a limiting value, since should this happen, the fatigue centre would form again at the part surface.

When considering the effect of internal stress on the change in the effort of the top layer loaded with operational stress, the rule of superposition of stress fields generated by internal and external forces can be used.

The problem of the influence of internal stress on the change in the effort of top layer material with the simultaneous action of external loads can be reduced to the examination of one or more main stresses (σ_x, σ_y, σ_z), on the assumption that the resultant stress is equal to

$$\sigma_w = f\left(\sigma_x, \sigma_y, \sigma_z\right) \tag{2}$$

As the vast majority of hypotheses of the fatigue failure of metals are based on the hypotheses of dislocation-initiated crack propagation, making tangential stress primarily responsible for the incubation of cracks, their growth into critical slip bands that, through the nucleation of microcracks and their combination, lead to the fracture of the specimen, it seems the most justified to analyze the effect of internal stress on material effort, as expressed by one of the plastic strain hypotheses. A hypothesis combining the state of stress with plastic strain is the Huber-Mizes-Hencky hypothesis. Its part related to the mean tangential stress can be used for considering the problem of the effect of internal stress on the surface and bulk strength, as it clearly indicates a relationship to exist between dislocation-starting internal stress and the plastic deformation phenomenon.

According to this hypothesis, the material effort at the yield point, σ_w, as a function of main stress is expressed by the equation:

$$\sigma_w = \sqrt{\sigma_x^2 + \sigma_y^2 + \sigma_z^2 - \sigma_x\sigma_y - \sigma_y\sigma_z - \sigma_z\sigma_x} \tag{3}$$

If we assume that the internal stress acts in a direction consistent with the main stress direction, its effect on the change in top layer effort can be written as follows:

$$\sigma_w = \sigma_y + \sigma = f\left(\sigma_y^{'}\right) \tag{4}$$

Where σ is the resultant internal stress (assuming a uniaxial stress state).

The effect of the modified stress, i.e. that increased by the internal stress, can be considered for two cases:

$$1.\ \text{when}\quad \sigma_x + \sigma_z > 0 \tag{5}$$

$$2.\ \text{when}\quad \sigma_x + \sigma_z < 0 \tag{6}$$

For both cases, an advantageous range of values of the stress $\sigma_y^{'}$, reducing the material effort, can be distinguished. In those ranges, there is a specific optimal internal stress value with the corresponding minimum of effort. It is characteristic that for the operational stress, where $\sigma_x + \sigma_z < 0$, the optimal total stress value is also negative (less than zero), while for instances, where $\sigma_x + \sigma_z > 0$, the optimum should be searched for among positive values, as well.

The presented relationships and their interpretation show a possibility for carrying out simulations for models using the method of superposition, or the separation of influences on the model adopted. Allowing for the increase in the strength of the top layer due to its strengthening and the change in the state of stress in simulation studies is possible by taking increased strength indices (R_e, R_m). Variations in their magnitude with increasing hardness are shown in work [1].

To enable the transferring of model study results onto the real object, the appropriate consistency of that object based on the theory of probability is essential. One of the principal similarities between models and reality is the geometric analogy, which always occurs as the prerequisite for determining the physical consistency. Most generally, geometric similarity, understood as the transformation of the metric space X on the spaces X and Y varying at a constant ratio (the similarity of scale), and the similarity of the ratios of homogeneous quantities, should be retained in this case.

Determination of the effort of the material of irregularities by the finite element method (FEM) for dry friction

The contact between irregularities in a tribological pair occurs during dry, borderline and mixed friction. Only in those cases do the micro-irregularities of rough surfaces come into contact with each other and transfer loads resulting from operational conditions and the physical chemistry of the process. Contacting irregularities of a tribological system surface can be modelled as single elementary solids, on the assumption that the contact is discrete and the irregularities come into contact at incidental points of time and have a random intensity. Moreover, irregularities have the shape of an ellipsoid or pyramid with a spherical vertex. As the result of wear in the initial period of grinding in, the vertices are truncated down to 0.01 of the height, and the heights and their distribution on the surface have either a random or determined character. The mechanical, physical and chemical properties of the coupled materials of a tribological pair have a crucial influence on the wear. During friction, as the result of complex mechanical, physical, chemical and thermal processes occurring in the friction zone, the properties of the technological top layer vary and can significantly differ from the initial ones. The elementary physicochemical processes accompanying the interaction between the irregularities of surfaces sliding over each other, including in particular local deformations, occur within thin regions of the surface layer. In view of the above, it is the properties of this layer, and not the properties of the material core, that have a decisive effect on the type and character of deformations and wear. Therefore, in tribology, the parameters characterizing the physico-mechanical properties of material and the technological top layer determine the top layer resistance to the actions of external and internal loads accompanying the friction process. For the dry friction process these are:

- the normal force perpendicular to the friction surface, deriving from the load of the tribological pair and the actual friction elements contact surface,
- the friction force tangential to the contacting elements surface, being dependent on the normal force and the friction coefficient for the mating bodies,
- heat micro-sources on the actual micro-contacts surface.

Moreover, the interaction of contacting micro-surfaces in the tribological process can be either static, when there is no motion or the motion takes place at low relative speeds, or dynamic, when the pair is in motion.

An irregularity model with the following variable parameters was subjected to analysis: the height parameter, *Rm*, and the horizontal parameter, *RSm*. For these parameters, the dimensions of irregularities being modelled were computed. The values of these parameters were taken from the author’s own studies [1, 3].

Spatial finite elements of tetrahedral type based on 10-14 nodes and having three degrees of freedom were used in computation. For such models, the finite element dimension was defined, which determined their resultant number. This guarantees results to be obtained for the identical finite elements, despite the different dimensions of the model itself. A sample finite-element grid is shown in Figure 1.

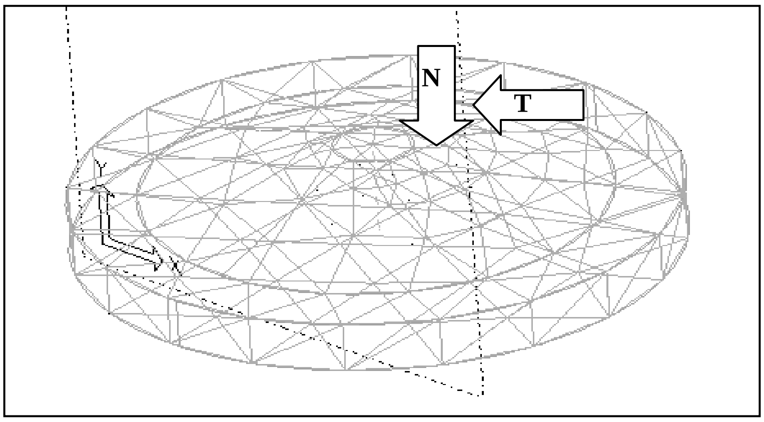

Fig. 1. The discrete irregularity model with the generated grid taken for analysis

For solving the problem, the following assumptions were made: the deformations of protrusions take place in a spatial strain state and do not influence one another, the material is ideally rigid-plastic and isotropic in respect of deformation directions, and also has a constant density.

The irregularities were loaded with the following forces: the normal force, *N*, and the friction force, *T*, both acting statically and dynamically (variable in time). Considering the fact that heat is generated during the friction process, the model that had its vertex loaded with a heat flux deriving from so called "flash temperature" was also analyzed. The values of the normal load were taken at the level of the permissible pressures for the slide bearing, and were increased as high as up to the material yield point, R_e. This procedure results from the fact that the share of the relative contact surface, defined as the ratio of the actual surface to the nominal surface, is very small, ranging from several to a dozen or so percent [1,5]. The friction force was computed taking into account the friction coefficient for typical slide bearings within the limits determined (by a tabular method) for material couples in sliding bearings. While the thermal loads producing temperatures of 100, 450 and 500°C in the place of contact was taken from the studies reported in literature [8].

The present study gives sample results of simulation carried out for **micro-irregularity protrusion models for surfaces** obtained from finishing treatment by grinding, turning or burnishing.

An example of reduced stress distribution on the cross-section in the force action direction for the irregularity model loaded with the normal and tangential forces is shown in Fig. 2. The figure indicates that the location of the greatest effort (so called "Belayev's zone) is shifted along the friction force action direction.

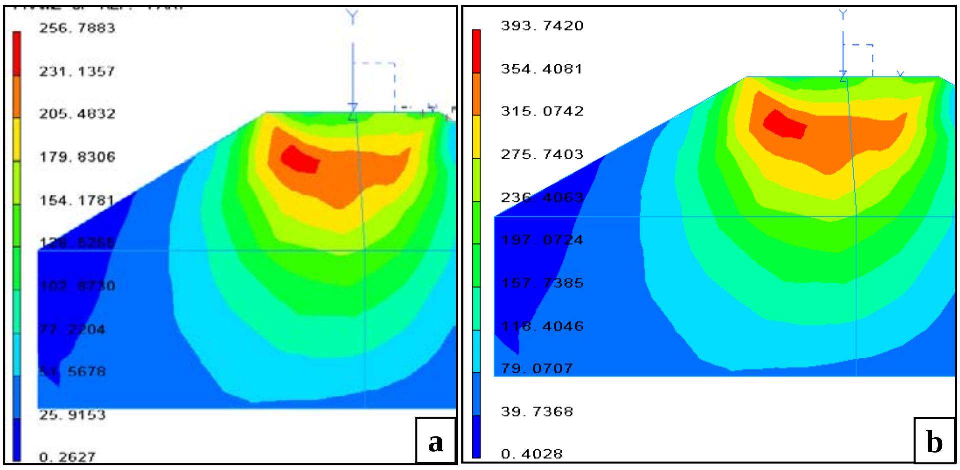

Fig. 2. Distribution of reduced stress σ_{red} on the irregularity cross-section in the force action direction at different loading of irregularities with the force resultant from the normal force [MPa]: a – 300, b - 460 and the friction force with μ = 0.1

The reduced stress distributions allow the determination of the location of the greatest material effort region, where extreme tangential stress occurs. It can be seen from the results shown in Figure 2 that the maximal stress occurs predominantly under the contact surface. Computer simulation enables this region to be readily determined around Belayev's point. Figure 3. illustrates the effect of loading an irregularity with the normal force and the tangential friction force with a friction coefficient of μ=0.1 on the change in the distance of the maximum stress region from the surface for the micro-irregularity obtained from grinding.

It can be noticed that with increasing irregularity loading, the distance from the greatest stress location surface initially increases, and then with the further increase in loading a shortening of this distance follows. Whereas, the increase in the friction force causes the maximum stress to move from the irregularity axis of symmetry towards the side of the irregularity being modelled.

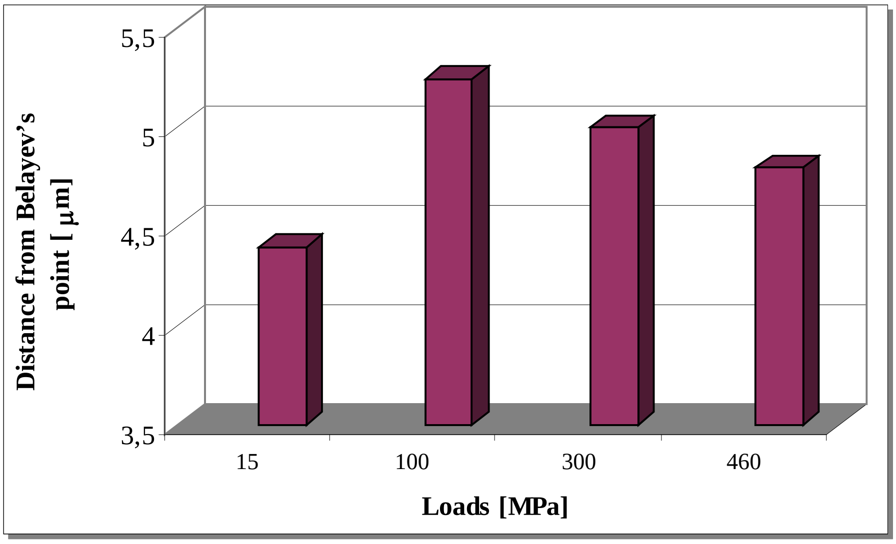

Fig. 3. Distance from the location of the greatest shearing stress point, as dependent on the loading of the irregularity model with Ra = 1.195 μm and RSm = 399.5 μm

The displacement of the surfaces of the tribological pair elements is a common phenomena which determines the occurrence of wear. During motion, individual irregularities of the mating surfaces interact with each other. The frequency and duration of interaction between irregularities depends on the friction process rate and the surface topography. For a rotary tribological pair, the same irregularities come into contact with each other either after one rotation, or, in the case of their determined distribution, more often. It is assumed that the time of a repeated contact occurring is less than 0.002 seconds. Obviously, this depends on the material of the tribological pair and the type and purpose of the bearing [6,7]. For these reasons, it was decided to perform the simulation of the effect of the duration of loading micro-irregularities with external and internal forces on the material effort. Sample results for a micro-irregularity with Ra = 1.195 μm and RSm = 399.5 μm with a unit external load of q = 8 [MPa] and the friction force with a friction coefficient of μ = 0.1, are illustrated in Fig. 4. It can be observed that the maximum stress varies with varying duration of loading. These variations are not regular. The simulation studies confirm the thesis put forward in many studies that the analysis of the friction process should take into account the product of load times the velocity of motion, ***qv.***

An important role in the processes of friction and machine part wear is played by the temperature of the nominal contact surface, which can rise only slightly, despite the very high temperature increments in the neighbourhood of real micro-contacts. The elementary heat micro-sources form as the result of the change in the mechanical energy absorbed for making and breaking a micro-contact, transforming itself into the heat, Q.

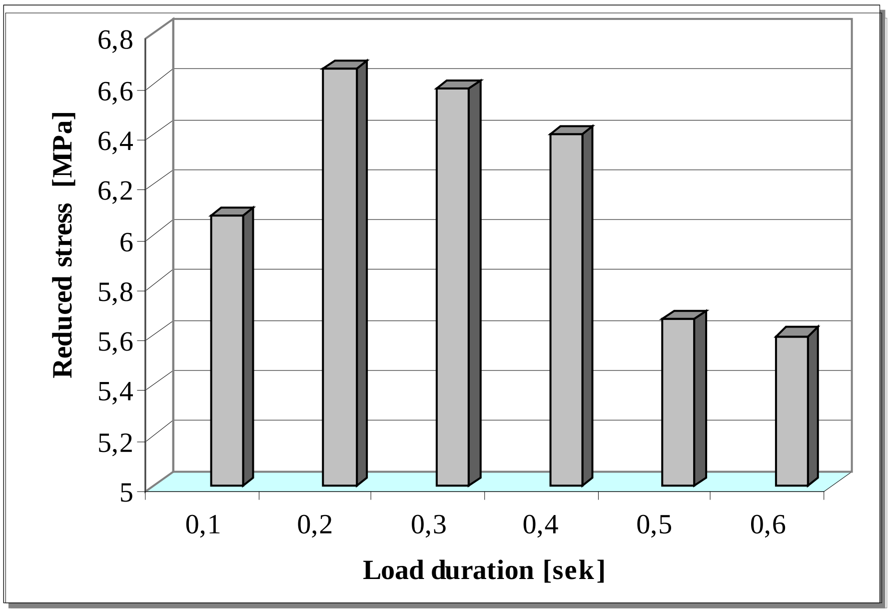

Fig. 4. Variation of reduced stress for an irregularity loaded with the normal and tangential forces with variable force action time, with a unit load of q = 8 [MPa] and the friction force with μ = 0.1

The quantity of heat released in the elementary contact surface zone is dependent on the amount of work input and the type and progress of friction. As the result of removing the heat from the momentary contact surfaces, the sub-surface layers of the bodies in friction heat up, with the temperature distribution showing a steep decline with increasing distance from the surface. The determination of the temperature at the heat source location is difficult and requires further studies. Hence, the temperature for the present analysis was taken based on the studies reported in literature [8]. The simulation was performed on the assumption that the heat generated during friction is released on the surface of contact between the mating bodies and heats it up to a specific temperature. Considering the fact that the irregularity protrusion moves at a specific velocity, the problem should be treated also as the problem of a moving heat source. In the case under consideration it was assumed that, in addition to the surface forces, also heat acts on the irregularity vertex. Sample results illustrating the distribution of stress for the adopted model are shown in Fig. 5, and the distribution of displacements in Fig. 6.

While the heat flux producing a surface temperature of 100°C results in an increase in the magnitude of reduced stress, its distribution within the irregularity is similar to that for the irregularity loaded without a thermal impulse, Fig. 5.a. However, when the thermal impulse cause a temperature increase of up to 450°C, the maximal stress moves from the bulk of the material to its surface, Fig. 5.b.

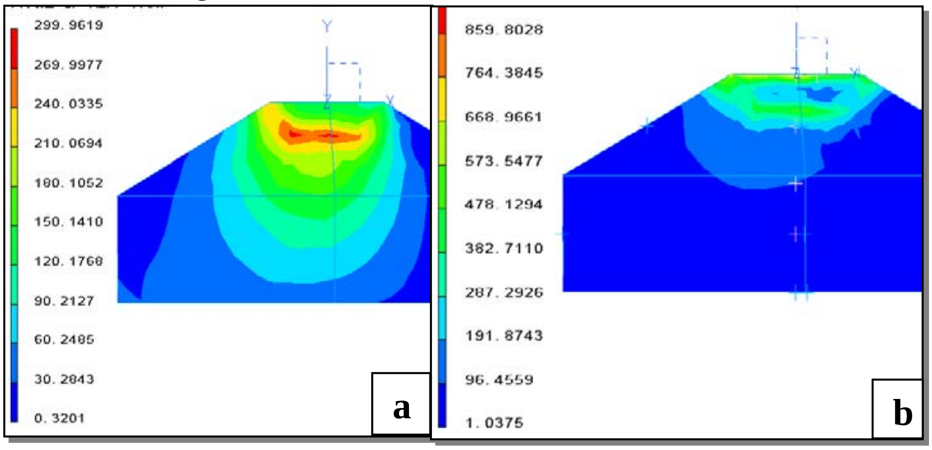

Fig. 5. Distribution of reduced stress within the irregularity loaded with the normal and friction forces and with a heat flux at a temperature of: a – 100°C; b – 450°C

Moreover, we observe intensive deformation of the material of the irregularity at its very top, which is confirmed by Fig. 6.

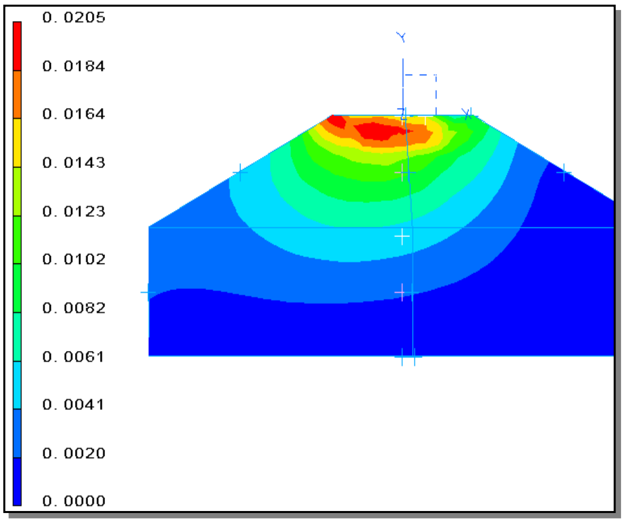

Fig. 6.
Resultant displacement (section in the plane XY) for the model loaded with forces and heat (a temperature of 450°C) simultaneously

These studies enable the evaluation of the effect of heat on the friction-zone phenomena to be made. A further analysis of the phenomenon might help infer on the possibility of bonding (welding) irregularities together.

The effect of loading duration on the magnitude of reduced and tangential stresses is discussed in work [1] which shows that with increasing loading duration, the stress magnitude increases linearly, which means that when the duration of load action on the micro-irregularity decreases, lower stress magnitudes occur in the micro-irregularity. The increased duration of heat action on the irregularity surface causes the heating of deeper-laid layers to a higher temperature, which results from the principles of the propagation of heat with its source moving. A higher temperature of the layers causes the formation of higher magnitudes of temperature change-induced stress. Hence, with increasing micro-irregularity loading duration, the reduced and tangential stresses increase.

In view of the fact that the value of temperature change with material depth depends on the body volume, among other factors, an analysis of the distribution of reduced stress occurring in micro-irregularities was made. The change in the irregularity volume takes place along with the change in the spacing between irregularities, *RSm*. Figure 7 shows the effect of changes in the irregularity volume on the stress.

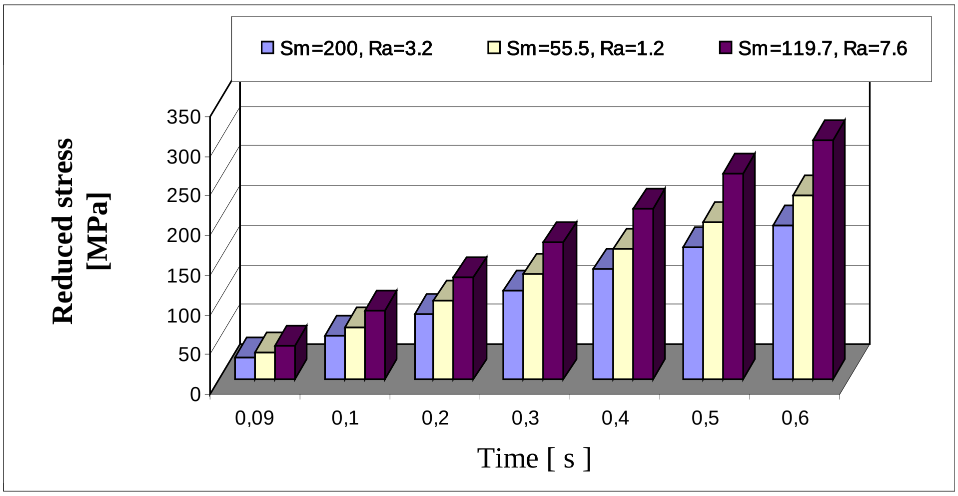

Fig. 7. Change in the magnitude of reduced stress for the variable time of action on the irregularity and the variable RSm and Ra, with a unit load of q = 15 [MPa] and a temperature of 500°C

The results illustrated in the figure confirm the thesis that the volume of the micro-irregularity influences the temperature gradient, and thus the magnitude of thermal load-induced stress within the irregularity.

The possibility of making the analysis of the effect of friction heat is important, insomuch as it enables the determination of the magnitude of thermal stress formed, which is quite difficult to be done by experimental methods. We can only infer from the permanent changes occurred in the top layer after the friction process, being considered, however, in a macro scale. The computer analysis allows the changes to be considered in a micro scale, or in the volumes, where this phenomenon comes into being. This is particularly important, since when the magnitude of thermal impulse-induced thermal stress exceeds the fracture toughness of the material, micro-cracks may appear. This is especially true for brittle materials.

Summary

On the basis of performed animations it can be stated that computer simulation enables the analysis of the state of effort of the tribological pair irregularity model to be made. The capability to take into account external loads, such as the load-derived action force, friction forces, and internal loads, such as heat, can help explain many phenomena occurring in micro-regions, without having to carry out quite burdensome and costly studies. This enables the determination of the phenomena occurring in the tribological system and their analysis, which can be used for preparing testing-stand experimental and operational studies with a precisely defined scope and oriented towards more detailed explanations of the occurring phenomena.

Computer simulation based on the finite element theory makes it possible to observe changes occurring in the tribological system. It can be said that it substitutes for macro-scale photo-elastic examination for the determination of the stress distribution in the analyzed pair in a micro-scale. Moreover, this analysis can be carried out for spatial (3D) models, and enables the optimization of the geometric surface structure in the phase of designing a tribological pair.

REFERENCES

1. *Czarnecki H.:* Udział warstwy wierzchniej w kształtowaniu odporności na zużycie tribologiczne, seria Monografei nr 139, Wydawnictwo Politechniki Częstochowskiej, Częstochowa 2008.
2. Czarnecki H.: Możliwości wykorzystania programu I-DEAS w badaniach symulacyjnych procesów tribologicznych. Przegląd Mechaniczny 2007, 5, Suplement, 40-43.
3. *Czarnecki H*.: Analiza właściwości warstwy wierzchniej w procesie tarcia suchego, Tribologia R.35 nr 3, s. 45-53, ISSN 0208-7774.
4. *Czarnecki H*.: Soprotivlenie poverchnostej, obrabotannych metodom osciljacionnoj PPD iznosu v uslovijach trenija, W: Progressivnye technologii i sistemy masinostroenija. Mezdunarodnyj sbornik naucnych trudov. Vyp.28, Doneck 2004, s. 184-187, ISBN 966-7907-16-3.
5. *Czarnecki H*.: Wpływ struktury geometrycznej powierzchni na zmęczenie stykowe mikronierówności. Tribologia na progu trzeciego tysiąclecia, Oficyna wydawnicza Politechniki Wrocławskiej Wrocław 2002, str. 61-66

6. *Czerniec M.*: Wytrzymałość stykowo-tarciowa oraz trwałość systemów tribotechnicznych ślizgowych, Wydawnictwo Politechniki Lubelskiej, Lublin 2000.
7. *Pytko S*. Problemy wytrzymałości kontaktowej. PWN, Warszawa 1982
8. *Sadowisk J.*: Temperatura styku powierzchni chropowatych podlegających zużyciu wskutek tarcia. Zagadnienia Eksploatacji Maszyn Zeszyt 2-1980. s 133-144.

The use of computer techniques for the analysis of material effort in the irregularity contact region in the dry friction process

Abstract

The paper discusses the problem related to the effort of material at the contact between the elements of irregularities of the tribological pair in the dry friction process. It is proposed to use of the finite element method for the simulation of this contact and the determination of the effect of external and internal loads on the system under consideration. The effect of these loads deriving from the action of irregularities on the model, separately and in combination, and in a stationary and time-variable manner, is illustrated. The results indicate a possibility for carrying out model studies either jointly with testing-stand studies, or instead of them. The simulations may also be helpful in the determination of the optimal geometric surface structure already in the design phase.

Keywords: computer techniques, material effort

Wykorzystanie technik komputerowych do analizy wytężenia materiału w obszarze styku nierówności w procesie tarcia suchego

Streszczenie

W opracowaniu omówiono zagadnienia związane z wytężeniem materiału w styku nierówności elementów pary tribologicznej w procesie tarcia suchego. Zaproponowano wykorzystanie metody elementów skończonych do symulacji tego styku i określenia wpływu na system oddziaływań zewnętrznych i wewnętrznych. Zobrazowano wpływ tych obciążeń działających na model nierówności pojedynczo oraz w połączeniu stacjonarnie i dynamicznie. Wyniki wykazują możliwość realizacji badań modelowych w połączeniu lub zamiast badań stanowiskowych. Symulacje mogą być również pomocne przy określeniu optymalnej struktury geometrycznej powierzchni już w fazie projektowania.

Słowa kluczowe: techniki komputerowe, wytężenie materiału

The use of computer techniques for the analysis of material effort in the irregularity contact region in the dry friction process

HENRYK CZARNECKI

Informacja o autorze

Dr hab. inż. Henryk Czarnecki, Prof. P.Cz.
Politechnika Częstochowska
Wydział Inżynierii Mechanicznej i Informatyki
Instytut technologii Maszyn i Automatyzacji Produkcji, al. Armii Krajowej 21
Al. Armii Krajowej 21
42-200 Częstochowa, e-mail:
tel. (0-34) 32 50 536, lub sekretariat (0-34) 32 50 509
czarneck@itm.pcz.czest.pl lub itm@itm.pcz.czest.pl

JERZY MONTUSIEWICZ

Computer-aided reduction of the nondominated solution set using optimality in the sense of an undifferentiation interval

1. Introduction

The question of multicriterial decision aid in technological problems has become extremely important because of application of computer tools in designing and producing machine elements. Computational methods with built-in optimalisation procedure, such as the total review, intentional programming, Monte Carlo, gradient and gradientless methods, discrete optimalisation methods, genetic algorithms, evolutionary algorithms, as well as methods without built-in optimalisation procedures, e.g. finite element method or boundary element method, allow the generation of very numerous solution sets for different constructional parameters. [1, 2, 3, 4, 5, 6, 7, 8, 9, 10]. Using a vector quality index, the constructor faces the problem of making a choice: at the introductory stage – of a subset of optimal solutions together with determining of a subset of decisional variables interesting for him, and at the final stage – of one solution. A literature analysis shows a considerable disproportion between the state of research on the development and application of methods serving the calculation of construction design indices and those serving the aid of the choice process.

An often encountered problem in technological questions is that of the choice of solution from a catalogue or tender offer. An offer is understood here as a set of already existing solutions, applied by a number of users, or as a set of new, only just worked-out, designed and produced constructions which are being examined in order to establish their actual utility parameters [11, 12, 13, 14, 15, 16].

2. Selected fundamental concepts

Presented below are selected concepts from the area of multicriterial analysis, necessary to understand the structure and operation of the algorithms applied in the nondominated solution reduction method, using the idea of optimality in the sense of an undifferentiation interval.

The task of multicriterial optimalisation

Generally speaking, the problem of multicriterial optimalisation can be formulated as follows:
find a vector of decision variables:

$$x^* = [\mathbf{x}^*_1, \mathbf{x}^*_2, \ldots, \mathbf{x}^*_i]^T \quad (1)$$

which optimalises the vector function:

$$F(x) = [F_1(x), F_2(x), \ldots, F_j(x)]^T \quad (2)$$

and fulfils the imposed limitations, where:

$i = \{1, 2, \ldots, I\}$ – a set of variable decision indices,
$j = \{1, 2, \ldots, J\}$ – a set of criteria indices.

The object analysed is described by decision variables which are subject to variances in the optimalisation process, as well as by parameters – quantities established earlier (adopted design assumptions) remaining constant during the whole optimalisation process. The decision variables are determined in an i-dimentional space of decision variables $A \subset R^I$. The area of acceptable solutions X is delineated by the limitations imposed on the decision variables and constituting part of the decision variable space.

The limitations occurring in the multicriterial optimalisation task can be divided into boundary and conservative ones. Boundary limitations occur in an overt form and are superimposed on the elements of the decision variable vector

$$\underline{x}_i \le x_i \le \overline{x}_i \quad (3)$$

Conservative limitations are relationships between decision variables and parameters, and can accept the form of equations or inequalities:

$$h_l(x) = 0, \ l = 1, 2, \ldots, s; \ \ g_l(x) \le 0, \ l = s + 1, \ldots, S \quad (4)$$

The component of the vector function $F_j(x)$, often called the purpose function, quality index or criterion, is usually a mathematical expression describing a chosen property of the optimalised object.

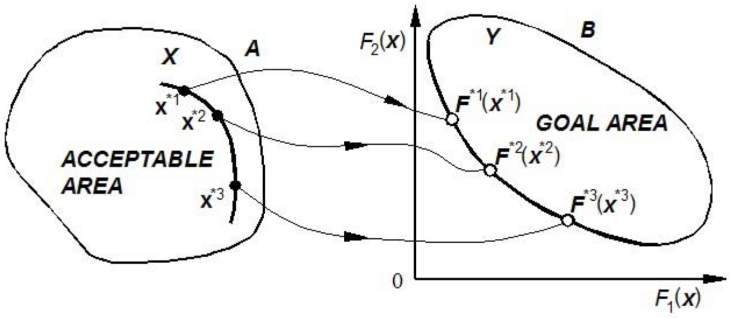

Fig. 1. Mapping of the acceptable area X into the goal area Y, ● – nondominated solution, ○ – evaluation of the nondominated solution

Pareto optimum

Pareto optimal solutions, often called nondominated solutions, are explicitly defined mathematically. A solution is Pareto optimal if none of the criteria $F_1(x)$, $F_2(x)$, ..., $F_j(x)$ can be improved without a simultaneous deterioration of at least one of them. Element $x^* \in X$ is called Pareto optimal if and only if in set X there is no element x^-, such that for every $j \in J$:

$$F_j(\boldsymbol{x}^-) \leq F_j(\boldsymbol{x}^*) \tag{5}$$

and there exists $m \in J$, such that

$$F_m(\boldsymbol{x}^-) < F_m(\boldsymbol{x}^*) \tag{6}$$

Partial order relations

To determine Pareto optimal solutions we use partial order relations described by a cone. A positive cone with the vertex at zero, belonging to j-dimentional Euclidean goal space is defined as follows:

$$C_0 = \{F = [F_1, ..., F_j]^T \colon F_j \geq 0 \; (j = 1, ..., J)\} \tag{7}$$

and a positive cone with the vertex at point $F^s = [F^s_1, ..., F^s_j]^T$

$$C_F s = \{F = [F_1, ..., F_j]^T \colon (F_j - F^s_j) \geq 0 \;\; (j = 1, ..., J)\} \tag{8}$$

Definition of a partial order relation described by a positive cone is as follows: element $F^a = [F^a_1, ..., F^a_j]^T$ is smaller, according to a partial order relation ($^c<$) described by a positive cone, than element $F^b = [F^b_1, ..., F^b_j]^T$, if element F^b belongs to a positive cone with the vertex at point F^a:

$$F^a \, {}^c\!< F^b, \text{ if } F^b \in C_F a \tag{9}$$

Figure 2 shows a situation described by relation (9) and a situation in which element F^c, compared to element F^a, is neither larger nor smaller according to a partial order relation described by a positive cone. Elements F^a and F^c belong to a set of nondominated estimations.

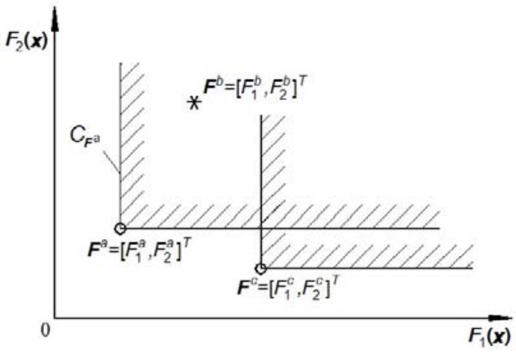

Fig. 2. Illustration at bicriterial minimalisation – minority relation described by a positive cone according to a partial order relation, O – nondominated estimations, ✱ – dominated estimation

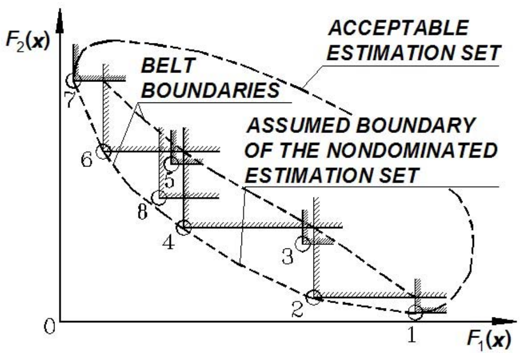

Fig. 3. Illustration at bicriterial minimalisation – distributions of dispersed nondominated estimations; O – nondominated estimations, ✱ – dominated estimation

Figure 3 shows the so-called dispersed distribution of nondominated elements, occurring practically the most often. Nondominated estimations lie in a belt, whose width depends on the size of the analysed set and the position of its elements. It can be seen that not all nondominated solutions are of equal status. If a solution appeared whose estimation lay closer to the assumed boundary, e.g. solution number *8*, it would eliminate the so-far nondominated solution number *5*, which lies well inside the belt.

Optimality in the sense of an undifferentiation interval

A multicriterial analysis of nondominated solutions is carried out in criterial space and aims at determining whether a solution mutated (‘*deteriorated’*) by the adopted undifferentiation interval *UI* still remains a nondominated solution and will be added to the currently created subset of nondominated solutions. In the case of criteria minimalisation, element $x\wedge \in \Omega$ will be optimal (or nondominated) in the sense of an undifferentiation interval if and only if when the set Ω has no element x^+ such that for every $l \in N$:

$$\begin{aligned} &\text{if } F_l(\boldsymbol{x}\wedge) \geq 0\text{: } F_l(\boldsymbol{x}\wedge) < F_l(\boldsymbol{x}^+) \text{ then } \left(1+\tfrac{UI_l}{100}\right)F_l(\boldsymbol{x}\wedge) > F_l(\boldsymbol{x}^+) \text{ is true,} \\ &\text{if } F_l(\boldsymbol{x}\wedge) < 0\text{: } F_l(\boldsymbol{x}\wedge) < F_l(\boldsymbol{x}^+) \text{ then } \left(1-\tfrac{UI_l}{100}\right)F_l(\boldsymbol{x}\wedge) > F_l(\boldsymbol{x}^+) \text{ is true,} \end{aligned} \tag{10}$$

where Ω is a non-empty set of Pareto optimal solutions.

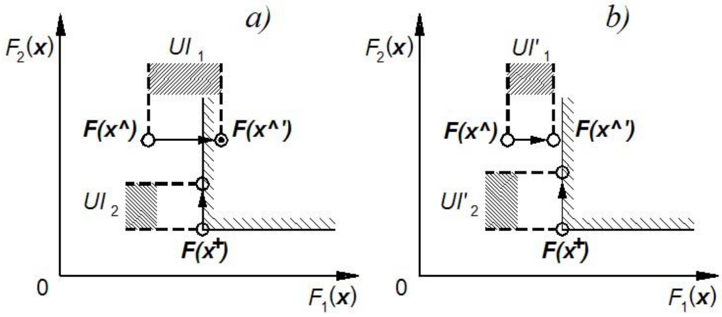

Fig. 4. Operation of condition (10) at bicriterial minimalisation,
○ – solution outside the domination cone, ⊙ – solution within the domination cone

Figure 4 graphically shows the idea of optimality in the sense of an undifferentiation interval described by conditions (10) with minimalisation of two criteria. Solutions $\boldsymbol{x}^+$ and $\boldsymbol{x}\wedge$ are nondominated because solution $\mathbf{x}\wedge$ has a smaller value of criterion F_1 and a greater value of criterion F_2 than solution $\mathbf{x}^+$. By introducing a modified mutation we temporarily ‘*deteriorate*’, by the value calculated from the adopted undifferentiation interval, the components of the criteria which had smaller values for the compared solutions. Figure 3a shows a situation when condition (10), for the introduced undifferentiation intervals UI_1 and UI_2, is fulfilled, i.e. solution $\boldsymbol{x}\wedge$ is not a nondominated solution in the sense of an undifferentiation interval and is eliminated. Figure 3b shows a case when condition (10), for new values of UI_1' and UI_2', is not fulfilled and none of the solutions is eliminated, i.e. both solutions are nondominated in the sense of an undifferentiation interval for the adopted values of the undifferentiation interval.

3. The operation principle and the structure of the reduction algorithm

The presented reduction of nondominated solutions by using optimality in the sense of an undifferentiation interval resorts to the idea of a modified mutation [11]. The value of the mutation is given by the designer as the percentage of the value of the analysed criterion and called the undifferentiation interval. The mutation has come to be described as the percentage of the analysed solution, this being a recognised and often used way in technology (intuitively understandable for a potential user), e.g. a percentage value describes the measurement precision of an instrument, or an increase in load or strength. It should be noted that the selection task concerns a finite set of existing solutions (for instance a catalogue offer, a set of solutions generated by using (FEM), therefore the mutation proposed here differs significantly from the one used in classical genetic and evolutionary algorithms [5, 6, 7]. In the selection task the modified mutation concerns a criteria vector and is introduced only during the operation of the selection.

The presented principle of algorithm operation is used for a set of nondominated solutions. In a single course of the reduction process at an unchanged mutation value each solution after mutation is compared in pairs with the remaining solutions. Each analysed solution is subject to mutation according to a given algorithm. For the minimalisation task it is as follows:

- **step 1:** Determine the values of the undifferentiation intervals for all the components of the criteria vector (the values may be the same or different, some may accept the value zero – which means no mutation of a component).
- **step 2:** Compare the components of the criteria vector of two nondominated solutions in order to establish which components are smaller and to which solutions they belong.
- **step 3:** Components with smaller values are subject to mutation – enlarge them by the value resulting from the product of a component and the adopted undifferentiation set. Mutation of the analysed solutions leads to the generation of mutated solutions.
- **step 4:** Compare the estimations of the mutated solutions. A solution with dominated estimations is rejected, and a solution with nondominated estimations passes to the generated subset. When both the compared solutions are nondominated, they pass to the generated subset. In the subset thus created the solutions are recorded in the primary, and not the mutated, form.

The end effect of the operation of the procedure is the generation of a subset of solutions with nondominated estimations, whose size, at the right selection of the undifferentiation interval values, will be considerably smaller than the size of the primary set.

On the basis of the above assumptions and the presented principle of operation a one-phase algorithm was built which carries out a single examination of the criterial space area, with condition (10) being checked twice, both with regard to the solution from the Pareto optimal set and the solutions already in the set of solutions nondominated in the sense of an undifferentiation interval (SNSUI), Figure 5.

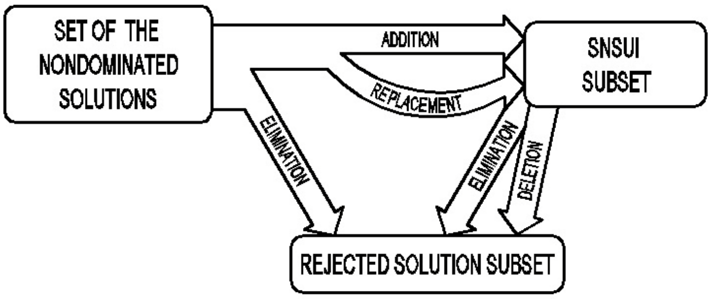

Fig. 5. Idea of the operation of a one-phase algorithm

The application of a one-phase algorithm, depending on the resulting situation, leads to the performance of different operations. The comparison of a currently selected solution from the nondominated set with successive solutions already in the SNSUI subset may lead to:

- addition of the solution to the created SNSUI subset,
- elimination of the solution by the solution already in the SNSUI subset; in this case the eliminated solution is added to the subset of rejected solutions,
- replacement of an existing element of the SNSUI subset by the solution analysed,
- deletion of the elements of the SNSUI subset by the solution which earlier replaced the existing elements of the subset; in this case the deleted solution goes to the subset of rejected solutions.

Addition of solutions contributes to the enlargement of the size of the SNSUI subset (in an extreme case when the undifferentiation interval is too small, the sizes of the nondominated solution set and the SNSUI subset are identical). Elimination of solutions selected from the nondominated solution set causes that at this stage of algorithm operation the size of the SNSUI subset is the same. Likewise replacing a solution from the SNSUI subset by the currently analysed solution from the nondominated solution set does not affect the size of the SNSUI subset. The solution which earlier replaced the existing element of the SNSUI subset may in the further analysis lead to the deletion of one or more elements of the SNSUI subset, which causes a further reduction of its size.

Algorithm with a correction of the undifferentiation interval

In the case of reduction of a nondominated solution set by using a one-phase algorithm the so-called phenomenon of the mutual exclusion of the compared solution estimates may occur. This is a situation where both the compared solutions eliminate each other during the analysis of particular components of the criteria vector. Such a situation is shown in Figure 6a. Solution 1, via the analysis of the component of the criteria vector $F_2(x)$, eliminates solutions 2 and 3, and solution 2 eliminates solution 3. While analysing the component of the criteria vector $F_1(x)$ it turns out that solution 3 eliminates solutions 1 and 2, and moreover solution 2 eliminates solution 1. Thus there occurs a classical phenomenon of mutual exclusion. It is assumed that if the phenomenon occurs when the analysed solutions are compared in pairs, none of the solutions is eliminated and both become elements of the generated SNSUI subset.

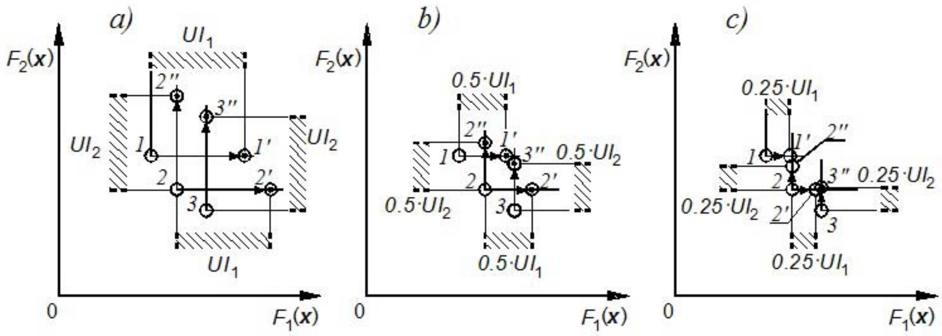

Fig. 6. Elimination of a solution from the SNSUI subset by using a double correction of the undifferentiation interval during the phenomenon of mutual exclusion

Examination of the one-phase algorithm in test examples has shown that with the growing value of the undifferentiation interval for the same nondominated solution set analysed there is a growth in the size of the generated SNSUI subset. A growth in the value of the undifferentiation interval causes a greater frequency of the occurrence of the mutual exclusion phenomenon, which results in the passage of the analysed solutions to the SNSUI subset.

Algorithm with a correction of the undifferentiation interval is based on the idea of a one-phase algorithm. In this algorithm, in the case of the mutual exclusion phenomenon, there occurs another analysis of the mutually exclusive solutions, or a check of condition (10) against the corrected value of UI. If, given the diminished value of UI, the analysed solutions do not exclude one another, it is the one which excluded the analysed solution that passes to the SNSUI subset. The operation of the algorithm is illustrated in Figure 5. The values of the undifferentiation interval adopted for the original analysis: UI_1 and UI_2 are so large that the mutual exclusion phenomenon occurs, Figure 5a. The first correction of their values ($UI_1' = 0.5\ UI_1$ and $UI_2' = 0.5\ UI_2$) caused no exclusion of the obtaining phenomenon – Figure 5b. Only the second correction ($UI_1'' = 0.25\ UI_1$ and $UI_2'' = 0.25\ UI_2$) allows to exclude solution number 3 by solution number 2 – Figure 5c.

The operation of the presented algorithm of the reduction of the nondominated solution set is to some extent dependent on the order of data introduction. In such situations in evolutionary strategies an approach is used consisting in a multiple use of the prepared algorithm. It is assumed in the study that the algorithm will be used repeatedly, and the order of solutions selected for analysis will be random. The end result of the performed reduction of the nondominated solution set is the result of the analysis of the rejected solution subset. Ultimately the SNSUI subset does not include those solutions rejected in all the analyses carried out.

4. A numerical example

In order to check the operation of the algorithm created for the reduction of nondominated solutions, using the notion of optimality in the sense of an undifferentiation interval, calculations of results were performed in example [12]. The example concerned the optimalisation of impulse electrochemical processing. The analysed set of acceptable solutions had 30 elements, numbered from 1 to 30. The ranking of the best variants of the processing, generated by the weight-correlation method in the acceptable solution set is as follows: 23, 5, 20, 11, 17, 27, 26, 4, 1, 10, 16, 13, 24, 19, 8, 22, 29, 9, 28, 30, 2, 12, 21, 15, 7, 18, 14, 6, 3. Solution number 25 was not classified.

In study [12] four optimalisation criteria were distinguished:

- criterion 1. – average increase of the width of the gap between the electrodes during the processing,
- criterion 2. – average roughness of the processed surface,
- criterion 3. – angle of inclination of the processed surface,
- criterion 4. – rectilinearity error of the processed surface.

The first criterion was maximalised and the remaining three were minimalised. The nondominated solution set had 20 elements numbered as follows: 1, 2, 3, 4, 5, 8, 10, 11, 12, 13, 16, 17, 19, 20, 22, 23, 24, 26, 28, 30. The determination of the SNSUI subset was done for seven different orders of data introduction. Because of this a possibility existed of checking whether a change in the order of entering the data into the analysis influences the size and contents of the final subset generated. The results of the analysis obtained by using an algorithm taking into account the phenomenon of mutual exclusion and applying a correction of the undifferentiation interval are shown in Table 1.

Table 1. Calculation results according to the algorithms presented

1	2	3	4	5	6	7
№	***UI* %**	**Algorithm ignoring PME***		**Algorithm from CUI****		
		Number of elements	Solutions always eliminated	Number of elements	Solutions always eliminated	Solutions sometimes eliminated
1.	1.5	18	2, 30	18	2, 30	-
2.	2.5	15	1, 2, 3, 8, 30	16	1, 2, 3, 30	-
3.	3.5	14	1, 2, 3, 8, 12, 30	15	1, 2, 3, 8, 30	-
4.	4.5	13	1, 2, 3, 8, 12, 13, 30	14	2, 3, 8, 12, 13, 30	1
5.	5.0	12	1, 2, 3, 8, 10, 12, 13, 30	14	2, 3, 8, 12, 13, 30	1
6.	6.0	11	1, 2, 3, 8, 10, 12, 13, 16, 30	15	2, 3, 8, 12, 30	1

* phenomenon of mutual exclusion
** correction of the undifferentiation interval

A single application of algorithms realising optimality in the sense of the undifferentiation interval allows a division of the analysed set of nondominated solutions into 2 subsets:

- The SNSUI subset – its size depends on the range of values of the elements of the analysed set and the *UI* values (columns 3 and 5),
- subset of solutions which are eliminated (columns 4 and 6).

In the case of multiple use of the reduction algorithm and a randomly generated order of the selection of solutions for analysis there usually occur:

- a subset of solutions which are always eliminated (columns 4 and 6),
- a subset of solutions which are eliminated sporadically (column 7)
- a temporary subset SNSUI (column 5).

In this situation the final SNSUI subset is determined by deleting from the set of nondominated solutions only those that always occur in the subset of eliminated solutions.

Generation of the SNSUI subset by using an algorithm with a correction of the undifferentiation interval contributes to a considerable reduction of the size of the set of nondominated solutions (at *UI*=1,5% reduction by 10%; at *UI*=2,5% reduction by 20%; at *UI*=3,5% reduction by 25%), which allows easier scanning of results and making the right decision.

5. Conclusions

Following through the results obtained by testing the analysed algorithms allows to form the following detailed conclusions.

1. An algorithm with a correction of the undifferentiation interval yields stable results of the reduction of the set of nondominated solutions, which is confirmed by the decreasing number of the element of the subset while the values of *UI* (column 5) are being increased. An exception are only the results for *UI*=6% (a tiny increase of the size of the SNSUI subset, which proves the occurrence of the phenomenon of mutual exclusion, which was not eliminated through the use of the correction mechanism of the undifferentiated interval.
2. An algorithm ignoring the phenomenon of mutual exclusion generates SNSUI subsets smaller in number (column 3), but their contents to a large extent depends on the order of entering data.
3. Comparing the solution ranking from study [12], obtained by the weight-correlation method with the SNSUI subsets obtained for different *UI* values it can be seen that the algorithm worked out does not eliminate solutions which took the highest positions in the ranking. Of the eleven first positions in the ranking 9 elements are included in all the generated SNSUI subsets (at *UI*=1,5 even 10 elements). These results show that the reduction of elements from the nondominated solution set by using optimality in the sense of the undifferentiation interval leads to elimination of solutions less significant in multicriterial sense.
4. The reduction show in the study, using optimality in the sense of the undifferentiation interval can successfully be included in the support systems of multicriterial decisions as well as in the elimination of solutions generated at different stages of the calculation procedure, e.g. in random methods or methods using genetic algorithms.

REFERENCES

1. Bauer J.: A survey of methods for discrete optimum structural design. Comp. Assisted Mech. and Engineering Sciences, vol. 1, 1994, s. 27–38.
2. Burczyński T.: Metoda elementów brzegowych w mechanice, WNT, Warszawa 1995.
3. Gutkowski W., Bauer J.: Discrete Structural Optimization. Springer, Berlin – New York, 1993.
4. Kaliszewski I.: Soft Computing for Complex Multiple Criteria Decision Making. Springer, New York 2006.
5. Michalewicz Z.: Genetic Algorithms + Data Structures = Evolution Programs. Springer, Berlin – New York 1992.
6. Osyczka A.: Evolutionary Algorithms for Single and Multicriterial Design Optimization. Springer. Heidelberg – New York 2002.
7. Parmee I.C.: Evolutionary and Adaptive Computing in Engineering Design. Springer, Heidelberg – New York 2007.
8. Romero C.: Extended lexicographic goal programming: a unifying approach. Omega, vol. 29, 2007, s. 63–71.
9. Teghem J., Tuyttens D., Ulungu E.L.: An interactive heuristic method for multiobjective combinatorial optimization. Comp. and Oper. Res., vol. 27, 2006, s. 671–681.
10. Zhang W.H.: Pareto optimum sensitivity analysis in multicriteria optimization. Finite Elements in Analysis and Design, vol. 39, 2003, s. 505–520.

11. Montusiewicz J.: Reducing the Pareto optimal set by means of the undifferentiation interval method. [in:] Gutkowski W., Mróz Z. (red.): Structural and Multidisciplinary Optimization. Proceedings of WCSMO–2, vol. 1, 26–30 May, Zakopane 1997, pp. 97-102.
12. Łubkowski K., Pogorzelski W.: Ranking wariantów impulsowej obróbki elektrochemicznej. [w:] Tarnowski W., ZN WM nr 19, WSInż. w Koszalinie 1995, s. 135–138.
13. Montusiewicz J., Osyczka A.: A Decomposition strategy for multicriteria optimization with application to machine tool design. Engineering Costs and Production Economics, vol. 20, 1990, s. 191–202.
14. Montusiewicz J., Tarkowski P.: O aplikacjach metody analizy wielokryterialnej w wybranych badaniach rozpylaczy paliwa silników o zapłonie samoczynnych. PAN Oddział w Krakowie, Zeszyt 23 Monografia 3, Kraków 2002.
15. Rosenman M.A., Gero J.S.: Reducing the Pareto optimal set in multicriteria optimization. Eng. Opt., vol. 8, 1985, s. 189–206.
16. Vincke P., Gassner M., Roy B.: Multicriteria decision-aid. John Wiley & Sons, Chichester – New York – Brisbane – Toronto – Singapore, 1992.

Abstract
The study shows the idea of optimality in the sense of the undifferentiated interval with regard to the problem of multicriterial choice. The idea discussed was used in construction of algorithms allowing to reduce the size of the nondominated solution set. Moreover the paper describes the phenomenon of mutual exclusion and the way of its elimination by introducing a correction of the undifferentiation interval. The study includes tests of the algorithms discussed, using data found in the literature. The obtained results are compared with one another and with those received by using the weight-correlation method.

Keywords: Computer-aided decision, multicriterial analysis

Komputerowo wspomagana redukcja zbioru rozwiązań niezdominowanych przy wykorzystaniu optymalności w sensie przedziału nierozróżnialności

Streszczenie
W pracy przedstawiono koncepcję optymalności w sensie przedziału nierozróżnialności w odniesieniu do zagadnień problemu wielokryterialnego wyboru. Przedstawioną koncepcję wykorzystano do budowy algorytmów, które umożliwiały redukcję liczebności zbioru rozwiązań niezdominowanych. Ponadto opisano zjawisko wzajemnego wykluczania oraz sposób jego eliminacji poprzez wprowadzenie korekcji przedziału nierozróżnialności. W pracy przeprowadzono testy opracowanych algorytmów wykorzystując dane zamieszczone w literaturze. Otrzymane wyniki porównano między sobą oraz z rezultatami uzyskanymi poprzez metodę korelacyjno - wagową.

Słowa kluczowe: Komputerowe wspomaganie decyzji, analiza wielokryterialna

Informacje o autorze

DR INŻ. JERZY MONTUSIEWICZ
Lublin University of Technology
Faculty of Fundamentals of Technology
Departament of Fundamentals of Technology

Stanislaw Staszic University of Arts and Sciences in Kielce
Department of Computer Science

Adres do korespondencji:
Lublin University of Technology
ul. Nadbystrzycka 38
20-618 Lublin,
tel. 0815384489
e-mail: a.montusiewicz@wis.pol.lublin.pl

ALEKSANDER NIEOCZYM

Robotized working cell

1. Critical area of co-operation robots

One from among the problems associated with structure and functioning of assembling unit has been analysed in the present study, viz. minimizing of functioning areas overlapping for the robots performing manipulation functions.
Assembling unit is defined herein as isolated space incorporating robots performing manipulation functions and work station including equipment The spaces occupied by individual robots are limited by the length of arm, its rotation and lift angle as well as by rotation angle of robot base in relation to vertical axis. Such space called “manipulation area” encompasses technological area being characterized by assembling operation processes being carried out and consisting of the following parts:

1. Critical area being the common part of technological area for two cooperating robots
2. Non-critical area.

The objective of designer of robotized work station is to minimize manipulation area and to maximize its utilization being characterized by means of overlapping factor Kp:

$$K_p = \frac{S_T}{S_M}, \qquad (1)$$

Where: ST - technological area,
SK - critical area.
The factor Kp is also considered in course of creation of alternative variants for robotized system designing as well as in case of industrial robot selection. The system with lower value of factor Kp shall be selected in course of graphical animation phase on work station. In order to complete such phase the following data are required: arrangement of facilities and equipment on work station as well as robot kinetics. The analysis for collisions of robot, peripheral equipment and tooling is carried out and determined by means of technological area and work time of work station.

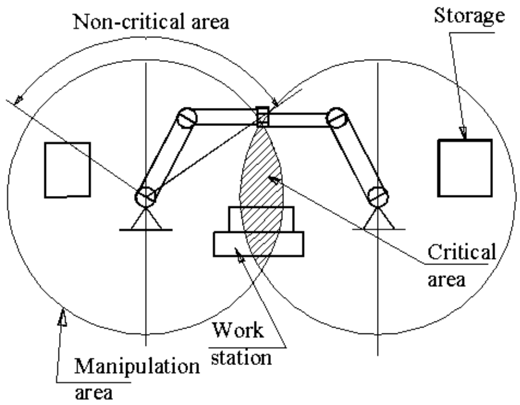

Figure 1. Diagram illustrating critical area of co-operation for two robots

Possibility of robots collision in specific critical area (Figure 1) is minimized by determination of time spent by robots in that area.

$$T_i = T_{i1} + T_{i2}, \tag{2}$$

Where: Ti - total assembling time for assembly i,
Ti1 – time spent out of critical area,
Ti2 – time spent in critical area.
Robots situated on work station will be indicated by symbols Ra and Rb. Work times for individual robots:

$$T_i^a = T_{i,1}{}^a + T_{i,2}{}^a \tag{3}$$

$$T_i^b = T_{i,1}{}^b + T_{i,2}{}^b \tag{4}$$

Activity out of critical area encompasses gripping of workpiece, its transport towards work station and approach to critical area to be used for further assembling actions viz.: workpiece positioning, fixing, assembling etc.
Assuming two assembling robots provided on work station i.e. Ra and Rb two following types of work sequences can be specified [1]:

1. serial operation (serial action) – assembling actions are performed by the robots in determined order. The robot Rb will start to work when assembling actions are completed by robot Ra.
2. parallel operation – assembling actions can be performed by the robots simultaneously in order to complete assembling operation. The robots are independent from each other.

Depending on robot specialization level, three following task units can be specified:

1. Specialized robot: tasks assigned for robot Ra time of the tasks Ti1,Ti2
2. General purpose robot: tasks assigned for robot Ra or Rb time of the tasks $T_{i,1}^{a}, T_{i,2}^{a}, T_{i,1}^{b}, T_{i,2}^{b}$
3. Co-operating robots: tasks assigned for robots Ra and Rb time of the tasks T(i,1)eq, T(i,2)eq

Considering the phases of assembling plan, the following definition of equivalent time of activity out of T(i,1)eq and within T(i,2)eq of equivalent area is possible [2]:

$$T_{(i,1)eq} = \min[ETO(R_a), ETO(R_b)] - \min[STO(R_a), STO(R_b)] \tag{5}$$

$$T_{(i,2)eq} = \max[ETI(R_a), ETI(R_b)] - \min[STO(R_a), STO(R_b)] - T_{(i,1)eq} \tag{6}$$

Where: STO – start of time period spent out of critical area,
ETO - end of time period spent out of critical area,
STI - start of time period spent in critical area,
ETI - end of time period spent in critical area.

The order of tasks being carried out in critical area is determined in course of creation of collision free assembling plan. That action consists of four steps:
K1: preliminary assumption of priority for works being carried out.
K2: Priority modification, introduction of new relations. Collisions number will be limited in order to ensure introduction of parallel works
K3: definition of tasks and arranging in order to adapt critical area size by adaptation of hypothesis saying that each non-specialized task is assigned to the robot with lower value Ti, 2.
K4: Tasks commencement time testing in chronological order. Modification of robot designed for non-specialized tasks or tasks commencement time delaying is often necessary. Critical area is reduced in result of such delay, but remaining work times of robots shall be arranged repeatedly.

Sequences assembling planning for the unit consisting of two robots and analysis of factors limiting potential collision have been presented below.

Under the assumption that the both elements eia and eib are installed by the robots Ra and Rb correspondingly; with element eia placed on work station as the first one (Figure 2). Interval of time Δ has been defined in [4] as time elapsing between the ends of Ti-1a, Ti-1b and characterizing the event: commencement of operation OPia by the robot Ra takes place during time Δ parallel to assembling operation OPi-1b performed by the robot Rb (a new part is gripped in course of OPia by robot Ra, but assembling operation OPi-1b is still performed by the robot Rb). All analyses of assembling selections time are carried out in respect of assumed definition of Δ value.

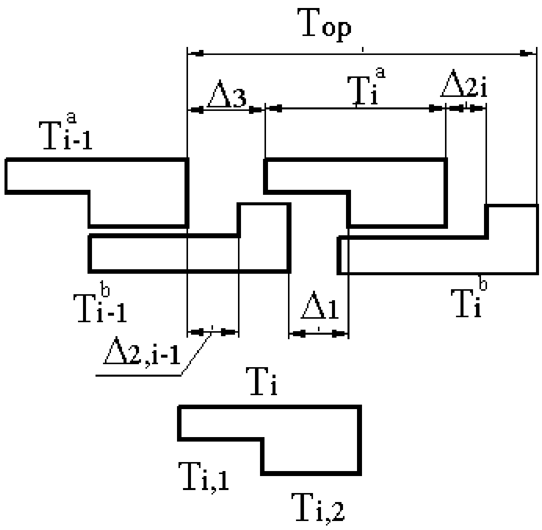

Figure 2. Gantt chart illustrating assembling sequences for the unit consisting of two elements. Top – time including all actions performed by the robot i.e. elapsed between gripping of the element in storage and completion of assembling operation. Remaining symbols specified in text

Another definition of time interval has been presented in the study of the author and in [4, 5]. Interval of time Δ has been defined as time elapsing between the end of assembling operation OPi-1 by robot Rb and commencement of operation OPib performed by the robot Ra. The interval has been provided with symbol Δ1.

The time elapsed between the end of activity of robot Ra and commencement of activity by robot Rb in course of assembling operation OPi is the next time (interval) to be considered. The interval has been provided with symbol Δ2.

According to [2] and [5], spare time i.e. unproductive time shall be provided in course of assembling line operation between assembling operations of successive units in order to introduce required changes associated with tools and components as well as with revisions of assembling procedures. The interval has been provided with symbol Δ3. The last change can be introduced in on-line mode.

On the basis of Figure 2, assembling process time can be expressed as:

$$T_{op} = T_i^a + T_{i2}^b + \Delta_{2,i} + \Delta_3$$
$$\Delta_3 + \Delta_{2,i-1} + T_{2,i-1}^b + \Delta_1 + T_{i,2}^a + \Delta_{2,i} + T_{i,2}^b \quad (7)$$

Optimization of operation time Top is carried out for conditions characterized by minimum values of Δ1, Δ2, i-1, Δ2-i.

From equation (1) it appears that completion time of operation OP1 is also affected by lag time elapsing between leaving of critical zone by robot Ra and entering by robot Rb. Assuming that performed operations OP1 and OPi-1 will be not changed (i.e. without any change of program and procedures in course of unproductive time Δ3), we obtain

$$\Delta_{2,i-1} = \Delta_{2,i} \tag{8}$$

Work time is also affected by lag time Δ1 elapsing in course of operation OPi-1 between leaving of critical zone by robot Rb and entering by robot Ra in order to perform operation OPi.

The time Δ1 being significantly dependent on time spent by robot Ra out of critical zone mainly consists of arm travel to the magazine, part gripping and return to critical zone. The refore reduction of time Δ1 is possible in case of change of storage bin position or application of different gripping device.

The reduction of time Δ2 can be achieved in case of different planes for robot arms movements in critical zone.

2. Determining the movement trajectory of the industrial robot arm

2.1.Number of degrees of freedom

During initial stage of designing it is necessary to identify the requirements to be fulfilled by the robot at the work stand. Next, the kinematics of the arm movement and the number of degrees of freedom are specified. The number of degrees of freedom of the robot's actuator is defined as the sum of all possible movements with regard to a stationary element of the robot structure (bracket with guides, body or base). Depending on its purpose, the industrial robot can have from one to seven degrees of freedom of the actuator. In order to relocate workpieces to any point within the robot's working area, it is enough for the working unit to have 6 degrees of freedom: three linear displacements along the three reciprocally perpendicular axes (movements for the purpose of workpiece transfer only) and three angular displacements with regard to these axes (movements for the purpose of orientation only). Movement of the gripper jaws provides one more degree of freedom which is however not taken into account in the characteristic of the manipulator mobility due to the fact that this movement is not related neither to the group of movements connected with transfer of workpieces nor to the movements connected with orientation of workpieces.

Complete set of all degrees of freedom is very rarely necessary to be used. Rejection of the optimisation principles concerning degrees of freedom results in the increase of overall dimensions, weight and costs of the robot as well as causes reduction of assembling accuracy and reliability of the robot, which

finally leads to violent decrease of technical and economic efficiency of the robot utilization. Functional parameters of the robot should be formulated after prior analysis concerning all necessary assembling movements which the robot is designed to perform.
The problem connected with determination of the assembling movements is solved in parallel with optimisation or modification of the technological process of assembling. This is achieved by performing, among others, the following activities [8]:

– developing alternative variants of the technological process of the product assembling,
– dividing variants of the technological process of assembling into separate operations and next, into elementary operations and individual transfers in order to determine the possibility of their automation,
– improving producibility of design in order to increase the degree of the assembling process automation,
– choosing typical auxiliary equipment, tooling and tools required to achieve automated performance of operations and, at the same time, the fulfilment of the parts assembleability condition.

2.2. Robot operation parameters

Three groups of the robot parameters have been defined which describe accuracy of the manipulator movement and which refer to:

- description of positioning in a given point,
- achieving of speed parameters,
- achieving of a preset trajectory.

Selection of the parameters which are subject to description and assessment is dependant on specific requirements determined for the machine. Most frequently these are the tasks defined by the technological process comprised in the production cycle.

2.2.1. Parameters concerning the accuracy of the trajectory

Accuracy and repeatability of AT trajectory [10,11] characterize the ability of the robot to move the end effector along a preset trajectory during repeated movements in opposite directions. In a physical sense this is a maximum difference between the preset trajectory and the path which is the mean trajectory. Repeatability of a trajectory is expressed by a degree of conformity between trajectories achieved during their repeated realization. Deviations concerning changes of direction of CR and DR movements [10,11] describe the changes of the actual trajectory with regard to the preset trajectory. The parameters of the trajectory accuracy are the basis for assessing the robot with regard to performance of the technological tasks connected with guiding of the end effector along a preset path.

2.2.2. Speed parameters

This group of parameters includes:
accuracy of speed i.e. the difference between the speed programmed and the average value of speed achieved during repeated movements along a preset trajectory,
repeatability and fluctuation of speed (i.e. maximum amplitude of speed changes during one working cycle).
These parameters play an important role in assessing the results of the robot operation when the robot is used for active inspection of dimensions or assembling of parts which move along the production line.

2.2.3.Assessment of the robot's coordinates and the movement trajectory

The assessment is carried out on the basis of the following measurements:

- Measurement of the positioning accuracy of a point belonging to the robot. The positioning accuracy is the algebraic difference between the result of the measurement concerning the position of the robot's point in its working area and the result of the measurement concerning the position of the point assumed to be a basic point (measurement point).
- Measurement concerning the accuracy of the spatial trajectory which consists in measuring the position of a point during movement of the robot on a trajectory being realized, at any moment in time.

Testing the robot which is continuously moving, so-called flaying start finish.

Trajectory planning methods

The literature of the subject has very frequently presented the solution to his problem in which a constant speed of the robot arm movement was assumed. Currently, the task of the trajectory designing is performed by optimisation or quasi-optimisation with the use of the below-described criteria.

2.3.1. Designing the optimum trajectory with regard to the speed of movement

The parametric method [9] is frequently used for planning of the path. This method makes it possible to obtain a preliminary trajectory of the actuator movement along a closed contour (Continous Path Control). Assuming that

$$q_i = f_i(\lambda) \quad i = 1,2..m \tag{9}$$

where: λ – path,

i – measuring points on the trajectory and assuming that $\dot{q}_i$ takes the maximum value of $\dot{q}_{i\max}$

Consequently:

$$|v|_{i\max} = \frac{\dot{q}_{i\max}}{\frac{df_i}{d\lambda}} \quad i = 1,2..m \tag{10}$$

In the extreme ranges $\Delta\lambda$:

$$|v|_{i\max} = \frac{\dot{q}_{i\max}}{\frac{f_i(\lambda + \Delta\lambda) - f_i(\lambda)}{d\lambda}} \tag{11}$$

2.3.2. Movement with a constant kinetic energy

The problem consists in defining such movements of the manipulator along the set contour during which the kinetic energy of the movement of the mechanic components of the manipulator has a constant value between two preset points of the path. The trajectory which meets such a requirement fulfils also the condition necessary to achieve maximum external forces and speeds of drive units [7].

Another input data concerns maximizing technological influences within a limited working area. Two main problems are solved in this case:

- method of arranging the loading-feeding positions, working positions and tooling positions in a limited area in order to achieve minimum sum of paths in a time necessary to complete a technological process of movement.
- criteria of choosing the trajectory and technological speeds of movement at a preset wide range of values of forces and moments created, anisotropy of a working area with regard to elastic deformations and high accuracy of movement. Both tasks can be solved with the condition assumed that refers to minimizing of loss of energy during the assembling process.

We assume that the specified ranges comprising the technological process of assembling will be written in the form of a graph:

$$\Gamma = ((\,)_{ji}, U_{ji}) \tag{12}$$

Where:

0ji – vertexes of the graph defining different possibilities of transfers,
Uji – arcs corresponding to the components of the movement trajectory according to the time-related and the spatial area from one transfer to another.

An important characteristic of the graph Γ is the time vector $T = \{t_{ji}\}$.

With the use of the graph models one of the optimisation criteria will be specified [6]: minimum time of movement:

$$T_{\min} = \sum_{k=1}^{R} t_{op,jk} + \sum_{t=1}^{n} t_{tr,ji} \tag{13}$$

One of the constraints should be used for a given function, i.e.: utilization coefficient of the tooling of j-unit:

$$k_{ij} = [(\sum_{k=1}^{R} \frac{t_{op,jk}}{T_{\min}} + \sum_{i=1}^{n} \frac{t_{tr,ji}}{T_{\min}}) + \frac{t_{st}}{T_{\min}}]^{-1} \tag{14}$$

Where:

$\sum_{k=1}^{R} t_{op,jk}$ - time of the main technological transfers, operations,

$\sum_{i=1}^{n} t_{tr,ji}$ - sum of the times of the transport and setting operations,

t_{st} - standstill time,

R – number of working positions which are serviced.

Geometric planning of the trajectory is aided by numeric programs, e.g. LabVIEV or SEMORS.

SEMORS system enables performance of the following activities:

1. preliminary specification of design (number of degrees of freedom (DOF), number of connections – articulated joints)
2. kinematic and dynamic analysis of the robot model,
3. graphic generation of a desired movement trajectory,
4. defining the sequence of the technological process,
5. selecting the control method with regard to the functioning and collision-free operation of the equipment,
6. arrangement of the sensors controlling correctness of operation, measurement method and data collection,
7. simulation.

The system is divided into two areas:

1. the first area – contains tools and means grouped for the purpose of designing and off – line programming,
2. the second area presents graphic results of designing.

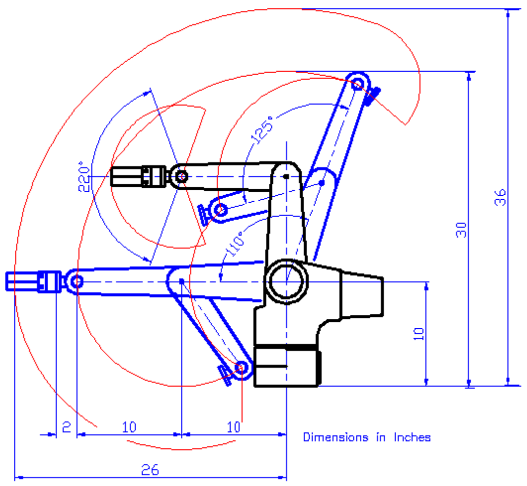

Figure 3. The movement trajectory of A250-ARM industrial robot arm [12]

Calculation, visualization and checking of the correctness of the robot arm movement trajectory are carried out in SEMORS program. This scope of this task includes three optional subgroups:

- Point to point – assigning two extreme points of the working end movement. The path between these points is monitored by the controller of the robot.

- Straight – a preset trajectory of movement between two specific points in the form of a straight line,

- Via points – the option designed for assigning specific points on the path of the working end during its operation.

Visualization of the robot movement trajectory (AMTEC - Automation, Measurement and Test Technologies) by means of SEMORS program is shown on figure 3, 4.

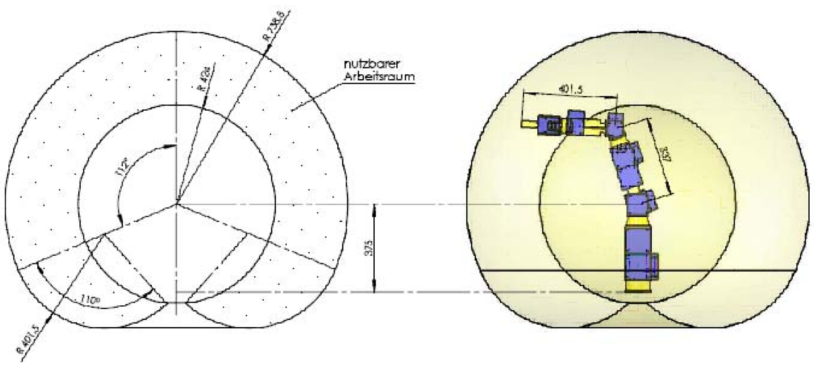

Figure 4. The movement trajectory of SCARA robot with 5 degrees of freedom

LITERATURE

1. 1 Jiang K., Senevirate L., Earles S. Assembly scheduling for an integrated two robot workcell. - Robotics and Computer Integrated Manufacturing, 1997, vol 13, n.2, pp131 – 143.
2. Mohamed S., Petty D., Harrison D. A cell managment system to support robotics assembly. - International Journal of Advancated Manufacturing Technology, 2001, n. 18, pp 598 – 604.
3. Nieoczym A. Zagadnienia projektowania hierarchicznie zorganizowanych systemów montażowych. - Lubelskie Towarzystwo Naukowe, Lublin 2002.
4. Nieoczym A. Some criteria used for reducing the working time of a robotized assembly cell. - 6th International Conference on Automatization / Robotics in Theory and Practice, Kosyce, Słowacja 2002, pp 267 – 273.
5. 5.Nieoczym A.: Badania teoretyczne pracy komórki montażowej w aspekcie produktywności jej elementów. Politechnika Lubelska, 2004.
6. 6 Nieoczym A. Badania teoretyczne pracy komórki montażowej w aspekcie produktywności jej elementów. Wydawnictwo Uczelniane Politechniki Lubelskiej,. ISBN 83-89246-08-2. 2004
7. 7 Podurajev D., Samlo J.: A view approach to the contour following problems in robot control. Mechatronics, vol. 3, #2 1993.
8. 8.Shin K., Epstein M. Intertask communications in in an integrated multirobot system. - IEEE Journal Robots and Automation, 1987 n. 3, pp90 – 100.
9. 9 Shin K., McKay N.: Minimum time control of robotics manipulators with geometric path constraints. IEEF of Automatic Control, pp 531-541, 1985.
10. 10 ISO 9283. Industrial Robots Performance criteria and related testing methods.
11. ISO 9946. Industrial Robots Presentation of characteristics.
12. www. adept.com
13. www. epson.de

Robotized working cell

Abstract

Manipulation area of working cell encompasses technological area being characterized by assembling operation processes being carried out and consisting of the following parts: critical area being the common part of technological area for two cooperating robots and non-critical area. The spaces occupied by individual robots are limited by the length of arm, its rotation and lift angle as well as by rotation angle of robot base in relation to vertical axis. During initial stage of designing it is necessary to identify the requirements to be fulfilled by the robot. Next, the kinematics of the arm movement and the number of degrees of freedom are specified. Depending on its purpose, the industrial robot can have from one to seven degrees of freedom of the actuator. Rejection of the optimisation principles concerning degrees of freedom results in the increase of overall dimensions, weight and costs of the robot as well as causes reduction of assembling accuracy and reliability of the robot, which finally leads to violent decrease of technical and economic efficiency of the robot utilization.

Keywords: technological area, critical area, assembling sequences, degree of Freudom

Zrobotyzowane stanowisko robocze

Streszczenie

Przestrzeń manipulacyjna ograniczona jest długością ramienia, jego kątem obrotu i wzniosu oraz kątem obrotu podstawy robota względem osi pionowej. Wyróżniamy tu obszar krytyczny będący częścią wspólną obszaru technologicznego dwu robotów oraz obszar pozakrytyczny. Dąży się do minimalizacji obszaru manipulacyjnego, który powinien być w maksymalnym stopniu wykorzystany. Kolejną czynnością podczas projektowania jest identyfikacja wymagań stawianych robotowi. Określana jest kinematyka ruchu ramienia oraz liczba stopni swobody. W zależności od przeznaczenia manipulator może posiadać od jednego do siedmiu stopni swobody urządzenia wykonawczego. Odrzucenie zasad optymalizacji liczby stopni swobody powoduje zwiększenie gabarytów, masy i kosztów robota, zmniejszenie dokładności montażu, niezawodności robota co ostatecznie prowadzi do gwałtownego spadku techniczno – ekonomicznej efektywności jego wykorzystania.

Słowa kluczowe: obszar technologiczny, obszar krytyczny, sekwencje montażowe, stopień swobody

Robotized working cell

ALEKSANDER NIEOCZYM

Informacja o autorze

Dr inż. Aleksander Nieoczym
Katedra Podstaw Konstrukcji Maszyn
Wydział Mechaniczny
Politechnika Lubelska
ul. Nadbystrzycka 36
20-618 Lublin
e-mail: a.nieoczym@pollub.pl

TADEUSZ NIESZPOREK

Identification of the rake surface of hobs

Introduction

Hobs are designed chiefly for machining involute cylindrical gears by the hobbing method. In the machining process, the tool action surface and the gear wheel being machined form a technological gear [1]. The accuracy of machining is substantially influenced by the accuracy of the hob action surface, which is the geometric locus of blade cutting edges. A cutting edge forms as the result of the intersection of the rake surface and the hob blade flank face. The accuracy of the hob cutting edge profile is therefore determined by the form of the blade surface. The blades of a solid hob are executed as backed-off, so the hob is ground on its rake surface only, as it wears. The design and technology of hobs are very complex [2, 3], and in the case of highest-accuracy hobs, their appropriate geometric analysis needs to be made. Special measuring machines are used for the verification of the execution accuracy of hobs by their manufacturers. The hob accuracy class is determined for a new tool.
The user of a hob must grind it from time to time in the course of its operation. An incorrectly performed grinding may result in a reduction of hob accuracy. Therefore, the identification of the rake surface of a hob is essential for its proper operation.

The measurement of the rake surface profile

Normally, the user does not have a special measuring machine available for testing the accuracy of the hob profile after grinding. In addition to the value of the module, profile angle, accuracy class and the hob thread lead angle, the rake surface helical line pitch is also indicated on the hob flanks. The rake surface is ground with a unilaterally tapered disc-type grinding wheel. In the process of geometrical analysis of hobs it is often assumed that the hob rake surface is a ruled helical surface. This is technologically difficult to achieve, as it requires the formation of a grinding wheel axial profile for grinding the hob rake surface along a special curve [4, 5]. In the case of forming the rake surface with a grinding wheel with an axial rectilinear profile, this will specifically be a cone-derivative surface. This is technologically simpler, which is of key importance from the user's point of view [3, 5]. While the measurement of the pitch and profile of the rake surface can be carried out on a coordinate measuring machine – Fig. 1.

Fig. 1. The measurement of the hob rake surface on a coordinate measuring machine

In the simplest case without the use of a turntable, the measurement is performed in the system of rectangular coordinates with the fixed hob. The hob is so positioned on the turntable that its axis is rectangular to the turntable. With the constant value of the coordinate Z, the gauging point is moved over the hob rake surface to record the coordinates X and Y for successive measurement points. The measurement of the diameter of the hob mounting hole needs also to be made to identify the coordinates of its centre as the origin of the coordinate system for the description of the hob rake surface profile. The measurement of the coordinates of a point on the same rake surface on one of the consecutive blades, so for a different value of the coordinate Z, enables the determination of the rake surface helical line pitch. The point of a given radius on the rake surface profile should be determined by the approximation method. Having two points on the same helical surface with the same radii rotated by a certain angle relative to each other and knowing their distance in the axial direction, the helical rake surface pitch can be determined from the relationship:

$$S_r = 2\pi \frac{\Delta Z}{\Delta \varphi} \tag{1}$$

where:

S_r	- hob helical rake surface pitch,
ΔZ	- distance between two measurement points, as measured in parallel to the hob axis,
$\Delta\varphi$	- angle of the angles of radial position of the measuring points, as defined in the plane perpendicular to the hob axis.

Determination of the grinding parameters

A rectilinear grinding wheel axial profile is assumed – Fig. 2a

$$\bar{\boldsymbol{r}}_s(u_n) = [-r_n + u_n\cos\alpha_n, \quad r_n tg\alpha_n - u_n\sin\alpha_n, \quad 0]^T \tag{2}$$

where:

r_n	- analytical grinding wheel radius,
α_n	- grinding wheel axial profile angle,
u_n	- grinding wheel axial profile parameter.

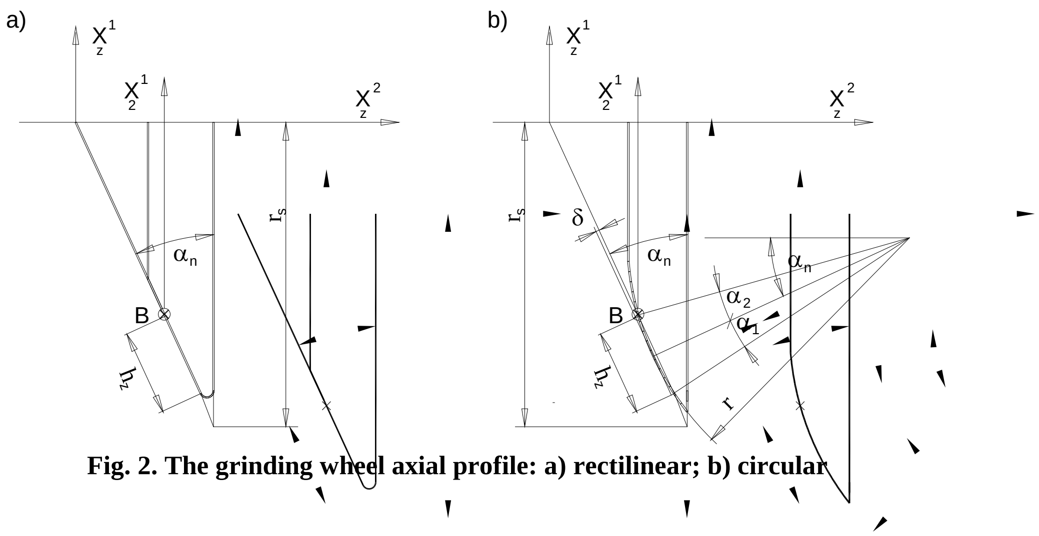

Fig. 2. The grinding wheel axial profile: a) rectilinear; b) circular

therefore, the grinding wheel action surface can be described by the following equation

$$\bar{\boldsymbol{r}}_s(u_n, \quad \varphi_n) = [2, \quad -\varphi_n]\bar{\boldsymbol{r}}_z \tag{3}$$

where:

φ_n - grinding wheel action surface parameter.

The grinding wheel positioning angle is equal to the lead angle of the hob rake surface on the analytical pitch diameter for the hob. After considering the relative helical motion of the grinding wheel and the hob, the equation for the grinding wheel action surface in the hob system is as follows – Fig. 3

$$\bar{\boldsymbol{r}}_n(u_{n,}\quad \varphi_n,\quad v_n) = [3,\quad -v_n+\xi][3,\quad -(\alpha_n+\gamma_{kn})]$$
$$\left([1,\quad -\varepsilon]\left(\bar{\boldsymbol{r}}_s + \left[r_n - \frac{d}{2}\frac{\cos\alpha_n}{\cos\gamma_{kn}},\quad -r_n tg\alpha_n + \frac{d}{2}\frac{\sin\alpha_n}{\cos\gamma_{kn}},\quad 0 \right]^T \right) + \right.$$
$$\left. + \frac{d}{2}\left[\frac{\cos\alpha_{nf}}{\cos\gamma_{kn}} - tg\gamma_{kn}\sin(\alpha_{nf}+\gamma_{kn}), - \frac{\sin\alpha_{nf}}{\cos\gamma_{kn}} - tg\gamma_{kn}\cos(\alpha_{nf}+\gamma_{kn})\quad ,\quad 0 \right]^T \right) +$$
$$+ [0,\quad 0,\quad p_n v_n]^T \tag{4}$$

where:

ξ - hob wear angle,
d - outer hob diameter,
ε - angle of grinding wheel twist in relation to the hob axis,
α_{nf} - angle of the grinding wheel profile in the analytical plane (in the hob face plane in the system of grinding wheel positioning relative to the hob),
m_n - hob module,
v_n - parameter of the relative helical motion of the grinding wheel and the hob,
p_n - reduced hob helical rake surface pitch,
γ_{kn} - angle of hob positioning on the grinder.

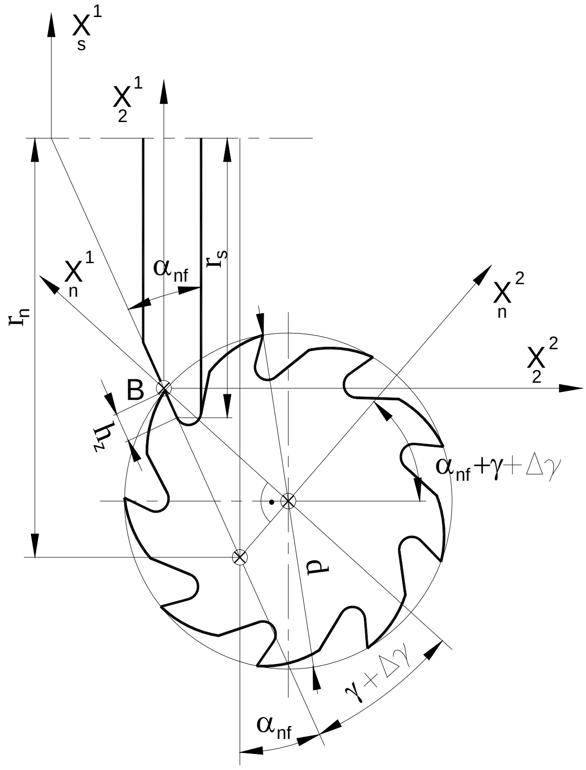

Fig. 3. Positioning of the grinding wheel in the grinding of the hob rake surface

In order to determine the hob rake surface, the envelope condition should be added to the equation for the grinding wheel family (3), which in general can be written in the form of the triple product of three vectors:

$$f_n(u_n, \quad \varphi_n) = \frac{\partial \bar{\boldsymbol{r}}_n}{\partial v_n} \frac{\partial \bar{\boldsymbol{r}}_n}{\partial u_n} \frac{\partial \bar{\boldsymbol{r}}_n}{\partial \varphi_n} = 0 \tag{5}$$

A characteristic feature of Equation (4) is that it does not include the parameter v_n of the relative motion of the grinding wheel and the hob. Thus, for the preset values of the parameter u_n, the corresponding values of the grinding wheel surface parameter φ_n can be determined from this equation by the method of successive approximations. The rake surface profile in the frontal section can be determined from condition below:

$$x_n^3(u_n, \quad \varphi_n, \quad v_n) = \bar{\boldsymbol{r}}_n[3] = 0 \tag{6}$$

So, for the preset values of the parameter u_n, and after determining the corresponding values of the parameter φ_n from Equation (5), the appropriate values of the parameter v_n can be determined from Equation (6). Substitution of the obtained values in Equation (4), which is equivalent to the system of three scalar equations, enables the determination of the successive points of the helical rake surface profile of the hob. The hob wear angle ξ defines the rotation of the rake surface around the hob axis, and for a new hob it is equal to zero. The grinding wheel positioning angle ε is theoretically equal to the lead angle of the rake surface on the analytical pitch diameter, and can be varied within a limited range. In practice, the grinding wheel axial profile angle α_n and the grinding wheel radius r_n have a decisive influence on the axial profile of the rake surface.

These parameters should be properly selected by the user, so that the calculated and measured rake surface profiles coincide with each other with the predetermined accuracy.

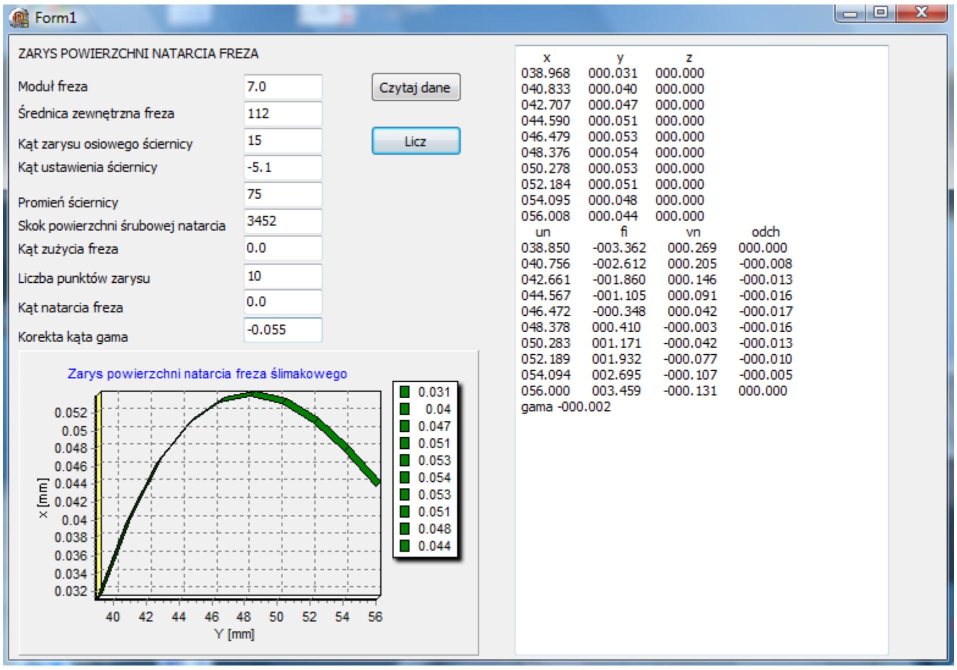

Fig. 4. The frontal profile of the hob rake surface

To obtain the preset hob rake angle, the hob should be positioned during its grinding with allowance being made for the correction of this angle

$$\gamma_{kn} = \gamma + \Delta\gamma \tag{7}$$

where:

γ - hob rake angle,

$\Delta\gamma$ - correction of hob rake angle.

The parameter u_n for consecutive points of the axial profile of the grinding wheel with a rectilinear profile in the axial section is determined from the relationship below:

$$u_n[i] = \frac{d}{2\cos\gamma} - h_z + h_z \frac{i-1}{n-1} \tag{8}$$

where:

h_z - hob profile height,

n - number of profile points,

i - profile point number.

In practice, grinding wheels with a circular profile in the axial section are also used - Fig. 2b. In this case, the following is assumed:

$$u_n[i] = \frac{\alpha_1 + \alpha_2}{n-1}(i-1) \tag{9}$$

where:

q_1, α_2 - angles defining the limits of the grinding wheel circular profile.

The axial circular profile of a grinding wheel can be described with the following equation:

$$\bar{\boldsymbol{r}}_s(u_n) = \begin{bmatrix} -r_n + \frac{d}{2}, \frac{\cos\alpha_n}{\cos\gamma} - h_z\cos\alpha_n + & r_n tg\alpha_n - \frac{d}{2}\frac{\sin\alpha_n}{\cos\gamma} + h_z\sin\alpha_n + & \\ +r\begin{pmatrix} \sin(\alpha_n + \alpha_1) - \\ -\sin(\alpha_n + \alpha_1 - u_n) \end{pmatrix}, & +r\begin{pmatrix} \cos(\alpha_n + \alpha_1) - \\ -\cos(\alpha_n + \alpha_1 - u_n) \end{pmatrix}, & 0 \end{bmatrix}^T \tag{10}$$

where: r - radius of the grinding wheel circular profile.

The radius of the grinding wheel circular profile can be determined in approximation from the following relationship:

$$\mathrm{r} = 0.72\frac{\mathrm{m}_\mathrm{n}^2}{\delta} \tag{11}$$

where:

δ - preset deviation from the straight line of the grinding wheel axial profile.

The parameter δ is assumed to be equal to the value of the maximum deviation from the straight line of the hob rake surface ground with the grinding wheel with a rectilinear profile in the axial section.

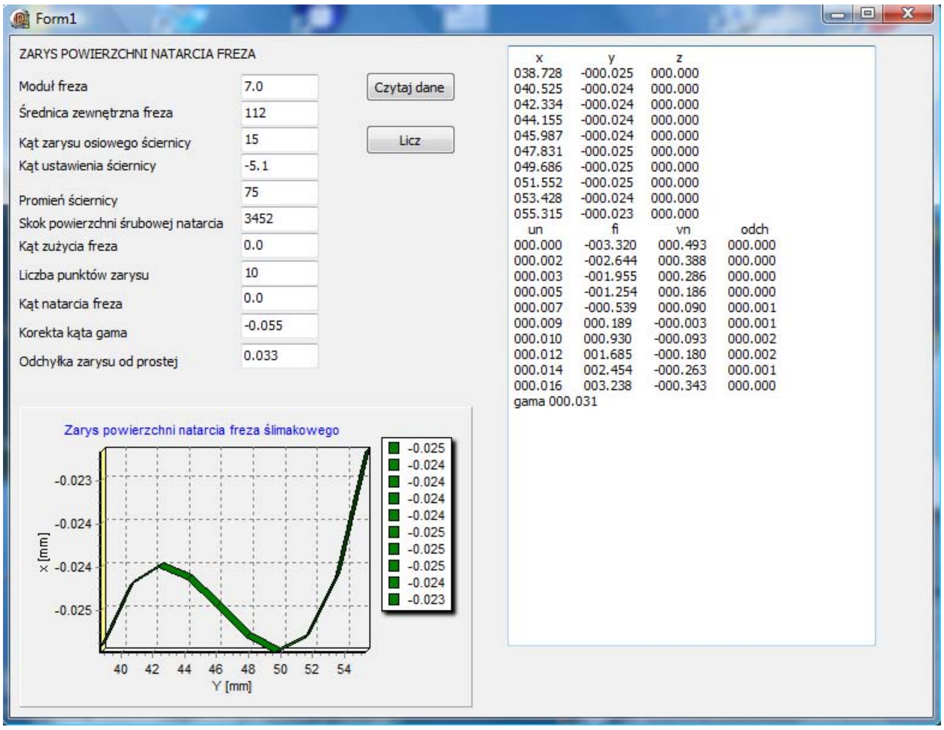

Fig. 5. The rake surface profile of the hob ground with the grinding wheel with a circular profile in the axial section

The discussion described above was illustrated on the example of a hob and a grinding wheel with the following specifications: $m_n = 7[mm]$, $d = 112[mm]$, $\alpha_n = 15[^\circ]$, $\varepsilon = 5.1[^\circ]$, $r_s = 75[mm]$, $S_r = 3452[mm]$, $\gamma = 0[^\circ]$, $\Delta\gamma = -0.055[^\circ]$. The deviation δ from the straight line of the frontal profile of the rake surface of the hob ground with the grinding wheel with a rectilinear profile in the axial section amounted to 0.033[mm], and the same result was yielded by measurements carried out - Fig. 4. While, the deviation from the straight line of the rake surface of the hob ground with the grinding wheel with a circular profile in the axial section, with a preset deviation from the straight line of 0.033[mm], amounted to 0.001[mm] – Fig. 5.

Summary

The measurement of the pitch and rake surface profile of a hob on a coordinate measuring machine is easy to accomplish.

The preset rake surface of a hob can be shaped with high accuracy using a unilaterally-tapered disc-type grinding wheel with a rectilinear profile in the axial section. The formation of the cone-derivative rake surface of a hob is technologically simple, which is of substantial importance to the correct operation of the hob.

By theoretical analysis, the appropriate axial profile angle of the grinding wheel and the its angle of positioning in the process of grinding the hob rake surface can be selected.

Grinding a hob with a grinding wheel with a circular profile in the axial profile will enable the ruled rake surface of the hob to be obtained with high accuracy.

The determination of the rake surface of the hob, as it wears, or its rotation after successive grinding operations, will make it possible to determine the blade cutting edge during the course of hob wear. The developed program is a module of the program designed for the examination of the accuracy of the cutting edge profile of hobs using an experimental and numerical method for determining the flank face of blades.

REFERENCES

1. *Nieszporek T.*: Podstawy konstrukcji narzędzi skrawających do obróbki walcowych uzębień zewnętrznych (Fundamentals of the construction of cutting tools for the machining of outer cylindrical toothing), Czestochowa University of Technology, Czestochowa 2004
2. *Gyenge C., Pethoe L., Mera M.*: Manufacturing of cylindrical gears with modified worm-hobs. Proceedimgs of the 10th International DAAAM Symposium, Vienna,Austria 1999, p. 177-8
3. *Nieszporek T., Legutko S.*: Automatyzacja projektowania zarysów frezów ślimakowych (Automation of the design of hob profiles). Wydawnictwo Poznańskiego Towarzystwa Przyjaciół Nauk, Poznan 1998
4. *Nieszporek T.*: Geometrical analysis of hobs. The 3rd International Conference Development of metal cutting DMC 2000, Kosice 2000, p. PL84-86
5. *Piotrowski A.*: Podwyższenie dokładności frezów ślimakowych modułowych (Enhancing the accuracy of modular hobs). A doctoral thesis, Czestochowa 2002

Identification of the rake surface of hobs

Abstract

The article describes the identification of the helical rake surface of the hob based on measurement made on a coordinate measuring machine. The rake surface can be ground with a unilaterally-tapered disc-type grinding wheel, as a cone-derivative helical surface. The hob rake surface can also be ground with high accuracy as a helical ruled surface using a disc-type grinding wheel with a circular axial profile.

Keywords: Hob, rake surface

Identyfikacja powierzchni natarcia frezów ślimakowych

Streszczenie

W artykule przedstawiono identyfikację śrubowej powierzchni natarcia freza ślimakowego na podstawie pomiaru na współrzędnościowej maszynie pomiarowej. Powierzchnia natarcia może być szlifowana ściernicą tarczową jednostronnie stożkową jako powierzchnia śrubowa stożkopochodna. Można też szlifować powierzchnię natarcia freza ślimakowego z dużą dokładnością jako powierzchnię śrubową prostokreślną za pomocą ściernicy tarczowej o zarysie osiowym kołowym.

Słowa kluczowe: frez ślimakowy, powierzchnia natarcia

Identyfikacja powierzchni natarcia frezów ślimakowych

TADEUSZ NIESZPOREK

Informacje o autorze

Dr hab. Inż. Tadeusz Nieszporek, prof. P.Cz.
Instytut Technologii Maszyn i Automatyzacji Produkcji
Wydział Inżynierii Mechanicznej i Informatyki
Politechnika Częstochowska
Ul. Armii Krajowej 21
42-200 Częstochowa
tel. 34 3250 509
e-mail: Tadek@itm.pcz.czest.pl

ANDRZEJ PIOTROWSKI

The use of the 1-wire network in drying room operation control systems

1. Introduction

One of Poland's predominant branches of industry is the processing of wood. Poland is a worldwide recognized manufacturer of different furniture products. One of the most important technological processes associated with the production furniture is the drying of wood. A classical wood drying room is a building furnished with equipment assuring the correct drying process, including: fans, heaters, flaps, and industrial automatics systems controlling the drying process. As standard, two types of solutions are used. The first of them, being older, involve computers furnished with special cards controlling the drying room equipment, most often through the RS-232C interface; and the second ones, more recent, use industrial PLC controllers. Both solutions are characterized by a high price and cause a number of problems during installation. In 2008, collaboration was established with a furniture manufacturer, who contended with the problem of an obsolete drying room operation control system, which was based on the first of the above-mentioned types. An innovative solution was proposed, which was based on the components of a very cost-effective industrial 1-wire network. The solutions, partially taken from the Internet, used for the construction of amateur weather stations, were modified and used for the control of drying room operation.

2. Description of the 1-wire network

The 1-wire is a kind of an electronic interface, as well as a communication protocol between devices. The name 1-wire comes from the fact that only a single data line is used for communication and data transmission. This is a semi-duplex, i.e. single-channel both-direction, type of transmission. The advantage of the 1-wire network is that the receiver (slave) can be power supplied directly from the data line through a pull-up resistor, using so called parasite power. The slave device is equipped with a 800 pF capacitor that takes energy from the data line, and then this energy is used for power supplying the receiver. The throughput of the data line ranges from 16 kb/s to 142 kb/s.

All 1-wire connections are digital connections via a two-core cable. The network is power supplied with constant voltage of 5V. The logic levels in 1-wire networks are compatible with the CMOS/TTL logic level standards.

A huge advantage over other solutions is the low price (ranging from a few to several dozen dollars per component). Each slave device has a unique 64-bit number assigned.

The 1-wire network consists of three main components: [3]

1. the 1-wire interface – a master device (managing controller),
2. secondary equipment – a slave device, and
3. electric connections between devices.

The operation of the 1-wire network resembles the structure of a telephone network (Fig. 1). When one of the devices wants to establish connection in order to transmit data, the master device sends a message to the network. The message is analyzed (commutated) by a MicroLan hub [9] which then sends a transmission start command to the device concerned (by sending the address of this device). All of the remaining devices will be informed of the occupancy of the network for the purposes of transmission. During transmission, the master device supervises the operation of the entire network and decides which slave devices can transmit data at a given time [3].

A data line called OWIO (One-Wire I/O) is used for transmitting signals. The actual flow of data bits is red out as a series of time-discretized events defined by the 1-wire protocol. Another line of the 1-wire network is a return line (mass line), commonly called OWRTN (One-Wire Return). There is only one earthing point in the 1-wire network, which is situated on the master device.

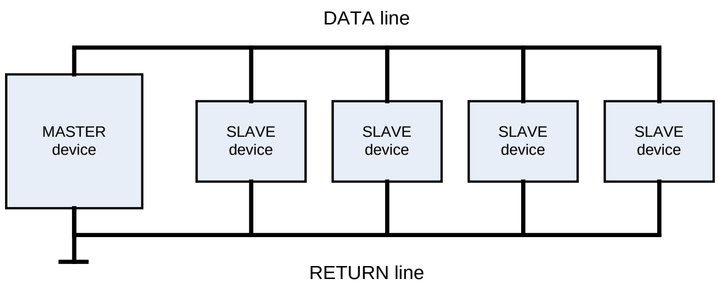

Fig. 1. A schematic diagram of the 1-wire network.

3. The 1-wire protocol

The basic 1-wire protocol consists of four principal sequences: initialization (zeroing the bus), sending (recording) the zero, sending (recording) the unity, and reading out the bits. In order to establish a connection with the slave device, initialization by a 480-960 µs-long zeroing pulse is required. Then the master device goes into a reception state, while the bus into a high state.

The slave device identifies the end of the zeroing pulse, then waits for 15-60 µs and then sends a presence pulse to the bus, whose duration is 60-240 µs. If the master device detects a “presence” pulse, it calls the slave device via its address.

In order to record data in the slave device, a series of pulses of an appropriate length is generated, which defines the logic states of either “0” or “1”. For a reading or recording sequence, a 60-120µs-long time slot is provided, which is initiated by the master device by forcing a low state on the bus. To assign the logic “0”, we generate a 60-120 µs-long pulse, after which we vacate the bus, and after a duration of minimum 1 µs we send a subsequent bit. The logic “1” is a pulse of a length of 1-15 µs; after that, we vacate the bus for a duration from 45 to 105µs. [3,6]

The readout of the value of the bit transmitted by slave device consists in generating a pulse with a duration of minimum 1 µs by the master device, and then vacating the data line and checking the logic state. The time allocated for this amounts to 15 µs from the start of the readout sequence. If the logic “0” is going to be transmitted by the slave device, then the pulse to be generated by the master device will be extended by a maximum of 14 µs. Before this time is out, the reading of the voltage state on the bus will attain the low level (“0”). If the logic “1” is going to be transmitted, the pulse generated by microcontroller will not be extended by the slave device and the high state (logic “1”) will be attained. [3,6]

4. The measurement of humidity

The system for measuring humidity within the drying room is built based on an HIH-3610 digital measuring sensor by Honeywell [1,14,17]. Its drawback is the lack of the 1-wire network interface. Therefore, an additional element of the humidity meter is a DS2438 system performing the function of a meter and a matching element. The HIH-3610 sensor generates linear voltage that is proportional to the relative humidity, RH. The consequence of this relationship is that any change in power supply voltage changes the output voltage on the measuring sensor. This introduces the necessity of measuring two voltages simultaneously. In addition, to compute the correct humidity, the ambient temperature must be known. The DS2438 meter lends itself perfectly for making the computation, as it contains a temperature sensor and two voltage converters. The analogue output signal from the HIH-3610 humidity sensor (Fig. 2) is connected to the main input of the ADC converter of the DS2438 meter. The humidity measurement starts with reading out the pin-connected DS2423 system’s power supply voltage that supplies also the humidity meter. After that, voltage fed from the HIH-3610 sensor to the input of the DS2438 system’s ADC converter is measured. At the end of the measurement process, the DS2438 meter checks its temperature, and from these three values the value of relative humidity, RH, is computed. In 2009, a new product of Maxim, DS1923, became available on the market, which is an integrated hygrometer of the iButton standard. This is a factory-calibrated system, so there is no need for its calibration. At the time of writing this paper it was not available on the Polish market yet, and therefore was not used in the project.

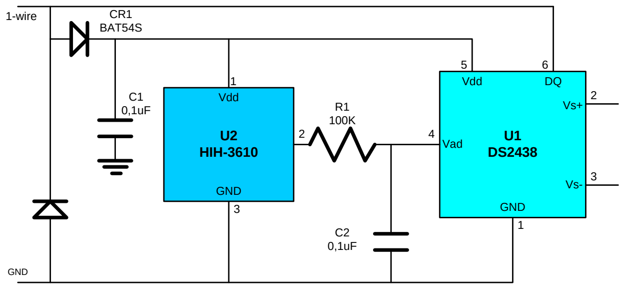

Fig. 2. The HIH-3610 humidity sensor with the DS2438 meter. [1]

5. Temperature measurement

A DS18B20 thermometer was used for the measurement of temperature [8]. This sensor measures temperature as the difference between two oscillators, where the temperature depends on one of them. The sensor operates within the temperature range from -55 °C to 125°C and assures an accuracy of ±0.5 °C in the range from 0°C do 70°. An added advantage of the sensor is its factory calibration, so no calibration by the user is required. The advantage of the DS18B20 systems if the possibility of placing numerous systems on the same 1-wire network wire along a cable of a maximum length of 200 m.

6. Pressure measurement

Similarly as in the case of the humidity meter, the pressure sensor [2] is radiometric, which requires both the output voltage as represented by atmospheric voltages and the supplied voltage to be known in order to accurately measure the barometric pressure. The diode BAT54S protects the circuit against interference, and the capacitor C1 provides a local power supply source. The digital pressure sensor MPXA4115 by Freescale Semiconductor [16] requires the current of 10mA at 5V, which means that an external power supply is required. It should be noted that the external power supply is also connected with the power pin of the DS2438 meter [11], thus enabling the circuit to measure the voltage fed to the pressure sensor. In the designed installation, the external power supply source does not present any problem, as the barometer is positioned within the room, near the power supply source.

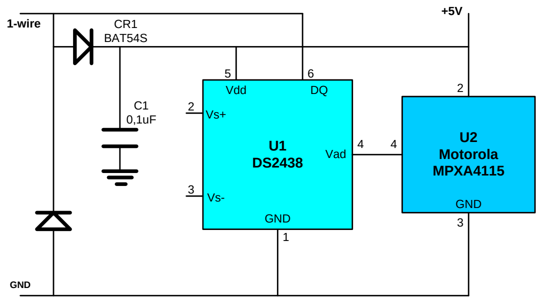

Fig. 3. A schematic diagram of the barometer with the MPXA4115 sensor. [2]

7. Control of the solenoid valves

For controlling the solenoid valves, a digital potentiometer, DS2890 [15], is used. It is manufactured in two types: with a 6-contact TSOC housing and a 3-contact TPO92 housing, respectively. The DS2890 is a linear 256-position potentiometer with a voltage range from 0 to 11V and a resistance of 100KΩ (Fig. 4). It is provided with a unique 64-bit address and can operate at the maximum 1-wire network overdrive speed of 142 kb.

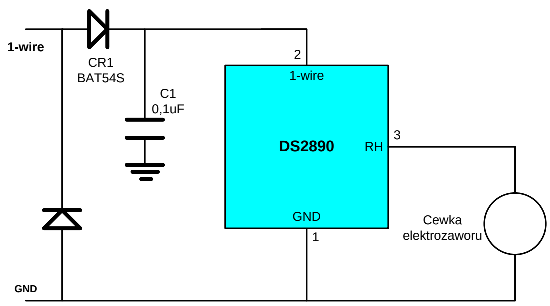

Fig. 4. A schematic diagram of the solenoid valves.

Similarly as for the other elements, the diode BAT54S protects the circuit against interference, and the capacitor C1 provides a local power supply source. The RH output is connected directly to the solenoid valve coil. The other coil input is connected to the ground (GND). By regulating the magnitude of resistance through the 1-wire network, we control the electromotive force generated by the coil. As a result, the solenoid valves controlling the operation of heaters, fans, flaps and the sprinkler are either opened or closed. In 2009, the Maxim Company ceased manufacturing the DS2890 systems and replaced them with a pair of the systems MAX 5400 and DS1805.

8. The software interface

Dallas-Maxim manufactures presently over 30 different 1-wire network devices, for which they develop an expand software libraries (API). All of the software libraries are free of charge (only systems are chargeable), and in the majority of instances they contain the full source code. [4,13].

The TMEX API interface is a set of language-independent 32-bit Windows libraries, which provide functionality for all 1-wire devices, including the limited 1-wire file structure that is used for communication with memories [4,13]. This interface is designed for operation with multi-processor and multi-strand applications that may compete for the same 1-wire port. The interface can support up to 16 different types of 1-wire adapters, each with sixteen separate ports. [13]

The 1-wire SDK for Microsoft Windows includes the TMEX API for the C, C++, C#, Pascal (Borland Delphi), Visual Basic, JScript (suitable for controlling the 1-wire network from the Web browser) and VBScript languages. [4,12,13]

In the wood drying room project, the application is being created in the Pascal language in the RAD Borland Delphi programming environment and using the TMEX API library. At the time of publication, the temperature, pressure and humidity measuring modules have already been created and tested, while the user-friendly interface is under creation.

9. The use of the 1-wire network for the control of the wood drying room

The process of drying wood is one of the most important stages of the production process of manufacturing wooden elements. Woods must be characterized by humidity at a level from 15 to 40%, depending on its species and purpose. In the case of too high humidity, warping of wooden elements, cracking of wood and, in extreme cases, destruction of the manufactured product could occur.

Wood humidity is expressed by the ratio of the mass of water contained in the wood to the mass of the dry wood, and it can exceed 300% in extreme cases. Under natural conditions, the drying process is long-lasting and, for hard species (such as oak or beech), it can take several years (and even up to 10-15 years). Therefore, for technological and economic reasons, it is accelerated, and in a correctly operating drying room it should not last more than 6-7 months for the hardest wood species. In the case of pinewood, the average drying time ranges from 3 weeks to 1.5 months.

The drying process takes advantage of one of the principal laws of physics, whereby any system tends to approach an equilibrium. By decreasing the humidity of the environment, we influence the evaporation of the wood water, which will tend to equalize the humidities. This is a very complex process, which requires constant monitoring of conditions prevailing in the drying room and responding to any changes occurring in the wood. It is dependent on many factors, the most important of them including:

- wood humidity level,
- wood species – hardness,
- springiness factor (from 1.5 to 3, depending on the wood species),
- temperature,
- relative humidity in the drying room.

The classical drying room is a building without windows, furnished with a suspended ceiling, a system of sprinklers and controllable roof flaps. Within the drying room there are special pallets, on which wood to be dried is laid. The fan system (consisting of one or several fans, depending on the room size) is positioned in front of the bank of thin-walled tubes, through which heating liquid flows. The cubage of the building allows wood in a volume ranging from a few to several dozen cubic metres to be dried.

The controlled parameters in the drying process include temperature, humidity and the flow of air through the wood being dried. Normally, heaters (water tubes) positioned in front of the two-way fan serve for changing the temperature. To assure the required measuring accuracy, 2 thermometers are provided in the room, which enable the temperature to be determined at two points (at the opposite ends of the drying room). This is one of the factors determining the decision on switching on the fan and choosing its rotation direction.

In the case of too high or non-uniform humidity within the room, fan rotation direction and speed and roof flap opening are controlled. If the humidity is too low, the wood is sprinkled with water from the sprinkler.

Two types of hygrometer are distinguished. The first of them, which are installed in the drying room, measure humidity within the room. Two HIH3610 hygrometer-based sensors are used in the project, which are installed at the opposite ends of the drying room. The second hygrometer type is special instruments for measuring the humidity of wood being dried. These are two mutually parallel metal spikes driven into the wood to a depth of several centimetres. By measuring the electric current flowing between those spikes, it is possible to accurately determine the wood humidity, since the higher water content, the lower resistance to the flowing current. A major drawback of this solution is the need for the calibration of the system. The calibration is most conveniently performed by putting a piece of damp blotting-paper between the contacts, allowing the blotting-paper humidity to equalize with the ambient humidity, and then comparing the system's calibration with another hygrometer. This is a long and laborious process, though once completed, it will not need to be repeated. For building wood hygrometers, the DS2438 system [11] was used. The measuring principle is very similar to that of the above-described system relying on the HIH3610 sensor [17].

The hygrometers placed in the wood play a very important role. By comparing the ambient humidity with the wood humidity, while allowing for the springiness factor and species of the wood, we are able to control the drying rate. With too a high rate, a situation may arise, where the humidity of the outer wood layers will decrease to such an extent that the wood pores will become closed and the water vapour contained in the core will not be able to escape. As a consequence, cracking of the wood may result. In that case, the drying process needs to be slowed down by lowering the temperature or by spraying water from the sprinkler installed above the ceiling. This will cause dampening of the outer wood structure and equalizing the humidity within the bulk of the wood.

For building drying rooms, industrial PLC controllers are used as standard, which are furnished with temperature and humidity sensors and outputs to control the fan, heaters and flaps. An additional element of the system are simple, several-row displays informing about the drying process status. The advantage of such a system is its unattended operation. The intervention of the operator is only needed to determine the wood species, springiness factor and target humidity when setting drying parameters. The drawback is the lack of capability to promptly respond to any failures, and the need for several controllers positioned at different points of the facility. A major problem is also the cost of the control equipment, which reaches the level of a dozen or so zlotys.

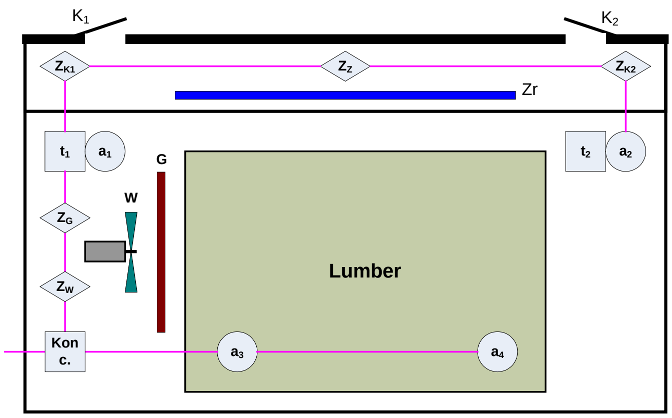

Fig. 5. The design of the drying room based on the 1-wire network.
G - heating elements, W – two-way fan, Zr – sprinkler, Konc. - 1-wire network hub, K_1 and K_2 – roof flaps, Z – solenoid valves controlled by the DS2890 system, t - DS18B20 digital thermometers, a - HIH-3610 hygrometer.

Therefore, it was proposed to build the drying room (Fig. 5) based on the 1-wire network and technologies proposed by DALLAS – MAXIM. The advantage of this solution is the possibility of controlling the wood drying process in several drying rooms on a single computer. The operator is able to control the drying process and respond to any problems on an ongoing basis. The maximum 1-wire bus length of 200 m could be easily extended by introducing additional hubs amplifying the signal. Another solution to the problem of bus length is the possibility of remote operation on a computer situated in the immediate vicinity of the drying room, virtually from any place in the world. A huge advantage is a very low installation cost of up to several hundred zlotys (about Zl 1000, including the costs of installation).

Works are ongoing on the construction of the first experimental drying room of a capacity of 5 m^3 of wood. Should this solution be successful, the construction of larger drying rooms could be started. The greatest unknown is the durability and reliability of the subassemblies used for building the network. Experiments carried out with the DS18B20 system-based temperature sensor [8] and the pressure sensor has so far showed a high resistance of the components. More than two years of operation of the outdoor sensors under different weather conditions have yielded very positive results. During the experiment, with measurements taken every 15 minutes, only two extreme measurement results deviated from the standard, and in four cases no results were red out – no sensor was found. More importantly, at the next readout, the system functioned correctly without any intervention by the operator. A decisive factor assuring high failure resistance is the reset (initialization) of the bust performed each time before the successive measurement.

10. Sub-atmospheric pressure drying rooms

Aside from the classical wood drying methods, as described above, sub-atmospheric pressure drying is also used in the furniture industry. Its huge advantage is the reduction of the drying process duration to two or three weeks (for the hardest wood species). For this purpose, pressure vessels of a capacity ranging from one to several or, in some instances, even dozen or so cubic metres are used. According to the laws of physics, the lower the pressure, the lower the boiling point of a liquid. The dependence of the boiling point on the pressure is expressed by the Cassius-Clapeyron formula which, as applied in approximation to the process where one of the states of aggregation is an ideal gas and the volume of the other is disregarded, gives rise to the following formula:

$$T_B = \left(\frac{R(\ln(P_B) - \ln(101.325kPA)}{\Delta H_{vap}} + \frac{1}{T_o} \right)^{-1}$$

where: T_B is the boiling point at the pressure P^0 (beyond the normal conditions),
R is the gas constant,
P_B is the pressure of saturated vapour at a given temperature,
T_0 is the boiling point at the normal pressure (101.325kPa),
ΔH_{vap} is the heat of vaporization of the substance.

At the pressure of 0.13 atm. (by approx. 85% lower than the atmospheric pressure), this temperature is equal to about 50°C.

For building a drying room, a vacuum pump is required to reduce the pressure and “sucking" out the water vapour from the vessel. When designing a control system for a drying room of this type (Fig. 9), a pressure measuring sensor and a solenoid valve to control vacuum pump operation should be provided in addition to the components used for the building of the classical drying room. This is a deviation from the control using classical PLC controllers. In this case, the pump is controlled by a time switch that switches it off for 4 hours’ period four times a day. The control using the 1-wire network is thus more accurate, as the switch-on time and the duration of vacuum pump operation is decided upon by the control program based on the conditions prevailing within the vessel.

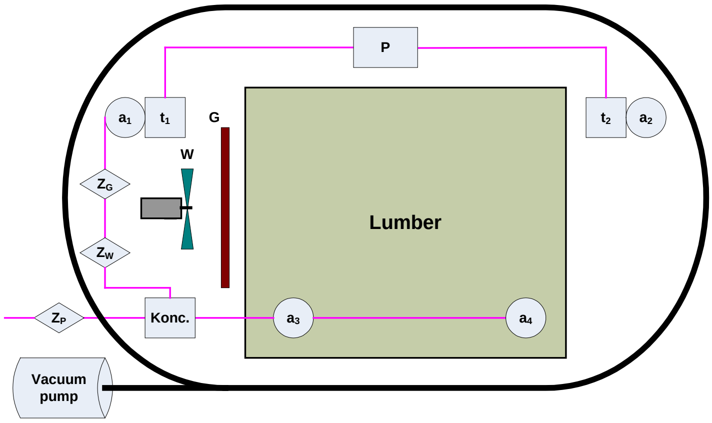

Fig. 8. The design of the sub-atmospheric pressure drying room.
G – heating elements, W – two-way fan, Konc. – 1-wire network hub, Z – solenoid valves controlled by the DS2890 system, t - DS18B20 digital thermometers, a - HIH-3610 hygrometers, p – MPXA4115 pressure gauges.

A serious problem in this case is the behaviour of the 1-wire network components under reduced pressure and high humidity conditions. At present, the installation is in the phase of testing the durability of the 1-wire components.

11. Summary

The 1-wire network was originally designed for collecting information from small devices, such as: digital thermometers, battery charging controllers, or iButton-type electronic locks. These devices are usually housed in a sturdy, weather-proof casing. For communication, a specially developed transmission protocol is used, which relies on the principle of querying slave devices by the master device, being known from other network solutions. The advantage is an each-time reset of the bus and the unique 64-bit address.

A great number of solutions using the 1-wire network can be found on the Internet. These include mainly any types of weather stations and data-colleting measuring systems. The very good programming interface and excellent operation with computers make it possible to build control systems similar to, or even superior to the industrial PLC controllers.

The designed industrial wood drying process control system, built wholly based on the 1-wire components, is evidence for the versatility of the 1-wire network. The modular structure allows the developed sensors and controllers to be used for other purposes. An example can be the supervision of a room, where measurements using a coordinate measuring machine are conducted. The system for the control of an air conditioner, temperature, vents and ventilators will provide a level of uniform measurement conditions much higher compared to the system integrated into the air conditioner, which will only respond to a change in temperature in the machine room. In recapitulation on the studies carried out on the use of the 1-wire network in industry, the reliability of the equipment, the simplicity of construction, and the low cost of installation should be emphasized. The presented solution is the beginning of the construction of more complex controllers and studies on the use of 1-wire network in other applications. It is very important to note that third-party devices using the 1-wire network for communication are appearing on the market.

REFERENCES

1. Awtrey D.: "1-wire Meteorological Station", Dallas Semiconductor, 2007
2. Bray D.W.: "1-wire barometer", http://davidbray.org/onewire/baro20.html, 2005
3. Dallas Maxim: "1-Wire Addressable Digital Instruments for Environmental Monitoring", Dallas Maxim 2001
4. Dallas Maxim: "1-Wire API for Java Software Development Kit", Dallas Maxim 2002.
5. Dallas Maxim: "1-Wire File Structure", Dallas Maxim 2000.
6. Dallas Maxim: "1-Wire Master Device Configuration", Dallas Maxim 2004
7. Dallas Maxim: "1-Wire Search Algorithm", Dallas Maxim 2002.
8. Dallas Maxim: "DS18B20 Programmable Resolution 1-Wire Digital Thermometer", Dallas Maxim 2006
9. Dallas Maxim: "DS2408 1-Wire 8-Channel Addressable Switch", Dallas Maxim 2004
10. Dallas Maxim: "DS2409 MicroLan Coupler", Dallas Maxim 2003
11. Dallas Maxim: "DS2438 Smart Battery Monitor", Dallas Maxim 2005
12. Dallas Maxim: "Guidelines for Reliable 1-Wire Networks", Dallas Maxim 2001
13. Dallas Maxim: "Software Resource Guide", Dallas Maxim 2002
14. Dallas Maxim: "The 1-Wire Weather Station", Dallas Maxim 2001
15. Dallas Maxim: “DS2890 1-Wire Digital Potentiometer”, Dallas-Maxim 2007.
16. Freescale Semiconductors: "MPX4115A", 2009
17. Honeywall: "HIH-3610 Series", 2007

Wykorzystanie sieci 1-wire w układach sterowania pracą suszarni

Streszczenie

Polska jest znanym na całym świecie producentem wyrobów meblarskich. Jednym z najważniejszych procesów przy produkcji drewna jest suszenie. Typowa suszarnia to budynek wyposażony w urządzenia zapewniające prawidłowy proces suszenia sterowane systemami automatyki przemysłowej. Najpopularniejsze systemy sterowania to komputer wyposażony w specjalizowana kartę lub sterowniki PLC. W artykule zaproponowano wykorzystanie sieci i komponentów 1-wire w procesie suszenia drewna. Takie rozwiązanie jest bardzo elastyczne i tanie oraz daje możliwość dokładniejszego nadzoru nad procesem suszenia.

Słowa kluczowe: drewno, sieć 1-wire, przemysłowe systemy sterowania

The use of the 1-wire network in drying room operation control systems

Abstract

Poland is a worldwide recognized manufacturer of different furniture products. One of the most important technological processes associated with the production furniture is the drying of wood. A classical wood drying room is a building furnished with equipment assuring the correct drying process, including: fans, heaters, flaps, and industrial automatics systems controlling the drying process. Mostly the industrial system, this is computers furnished with special cards controlling the drying room equipment or industrial PLC controllers. In this paper an innovative solution was proposed, which was based on the components of a very cost-effective industrial 1-wire network.

Keywords: wood, 1-wire, industrial automatics system

The use of the 1-wire network in drying room operation control systems

ANDRZEJ PIOTROWSKI

Informacja o autorze

Dr inż. Andrzej Piotrowski

Instytut Technologii Maszyn i Automatyzacji Produkcji

Wydział Inżynierii Mechanicznej i Informatyki

Politechnika Częstochowska

Al. Armii Krajowej 21

42-201 Częstochowa

tel. +48 34 3250509

e-mail: apiotr@itm.pcz.pl

VIKTOR MARCHUK
YURI LAPCHENKO
IRINA DEMJANOVA

Design of spectral descriptions of vibrations of roller bearings

A task is about vibroindignation which is generated the roller bearings with the technological errors of raceways of rings and rollers as a waviness in the conditions of axle-loading of bearing examined in [2]. The decision of task is determined by connection between the spectrums of waviness of rings and roller from one side, and by the spectrums of axial, radial and angular vibroindignation, that generated the roller bearings, from other. The proper dependences for radial vibroindignation (spectrum of the first approaching) are presented in a table. 1. On the basis of a number of the conducted experimental and theoretical researches it was set by us, that radial vibroindignations cause only the pair of accordions of waviness of rollers and accordion of waviness of paths woobling of rings, number of which differ from the multiple a number rollers of z values on ±1.

A task about dynamic properties of the roller bearings in composition the drive setting is examined in [3]. It is rotined that a vibration, which is registered a sensor, located on to the external ring of the roller bearing, is determined the vibrations of ring, as an absolutely solid and him by bendings vibrations on the first forms, thus the most expressed resonances, rings related to the bendings vibrations. Got and the following formula is experimentally tested for the eigenfrequencies of vibrations of the system:

$$v_m^2 = \frac{5(m^2-1)^2}{36(1+1/m^2)}\tilde{v}_2^2 + \frac{\lambda}{1+1/m}\cdot\frac{C_x}{4\pi^2 M}\text{, kHz}^2$$

where m is a number of form of vibrations (m=1 answers oscillation of ring, as an absolutely solid); M - vibrating mass, kg; λ=2 at $m \neq \frac{z}{2}q$; λ =0 and λ =4 at $m = \frac{z}{2}q$; q=1,2,3,...; $\tilde{v}_2$ - it is an eigenfrequency of the second forms of bendings vibrations of free ring which settles accounts after the following close formula:

$$\tilde{v}_2^2 = 5{,}06\cdot 10^3\frac{D-d}{(D+d)^2}\text{, kHz}^2$$

where D, d are external and internal diameters of external ring of bearing, mm;

Cx - is radial inflexibility of bearing which settles accounts on the following close formula:

$C_x = 3{,}75 z^{2/3} D_p^{1/3} \sin^{5/3} \pi ctg^2 \tau (0{,}1F_0)^{1/3}$, N/mkm

where D_p - is a middle diameter of rollers, mm;

F_0 - is an axle loading force, N.

TABLE 1. Dependences for determination of radial vibrations of roller bearings

Element which causes indignation	Number of accordion of error	Frequency of indignation	Amplitude of indignation
External ring	$\lambda = qz \pm 1$	$(\lambda \pm 1)\omega_1$	$C_x \alpha_\lambda$
Internal ring	$x = qz \pm 1$	$\xi\omega_3 \pm \omega_1$	$C_x \alpha_x$
Roller	$\xi = 2k$	$x\omega_2 \pm \omega_1$	$\frac{C_x}{\cos\tau}\sqrt{\frac{2}{\pi z}}\alpha_\xi$

In a table 1 λ, χ, ξ – number of accordions of waviness of raceway of external ring, internal ring and roller; α_λ, α_χ, α_ξ - amplitudes of the proper accordions; C_c - radial inflexibility of bearing; ω_1, ω_2, ω_3 - angulators of separator in relation to external, internal rings and roller about own axis.

Will consider the radial vibrations of external ring, as an absolutely solid (m=1). If to assume that amplitudes of vibrations are small in relation to geometrical axial pull (for this purpose the roller bearing is guilty to be loaded with large enough axial force of F_0), then the system can be considered near to linear, equalization of radial vibration of ring can be presented in a kind:

$$\ddot{\chi} + 2h\dot{\chi} + \omega_p^2 \chi = \sum_j F_j \sin(\omega_j t + \Psi_j)/M \,, \qquad (1)$$

where χ - the radial vibromoving of ring;

ω_p - an eigenfrequency, $\omega_p^2 = (2\pi v_{m1})^2 \cdot 10^6 = 10^6 K_\chi / M$ rad/s;

F_j, ω_j, ψ_j - amplitude, frequency and phase of j-ts accordion of vibroindignations, thus F_j and ω_j related to the waviness of raceways of rings and rollers dependences, presented in a table 1.

Vibromoving of external ring is the decision of equalization (1)

$$\chi = \sum_j F_j K_{\ddot{A}}(\omega_j)\sin(\omega_j t + \Psi'_j)\,, \qquad (2)$$

where K_D is a coefficient of dynamic:

$$K_{\ddot{A}}(\omega_j) = \frac{1}{M\sqrt{(\omega_p^2 - \omega_j^2)^2 + 4h\omega_j^2}}\,. \qquad (3)$$

Vehicle facilities for control of vibration are spectrum analyzers – arranged so that allow to control the root-mean-squares of vibromoving, vibrospeeds or vibroaccelerations. Taking into account min-square character of adding up of separate accordions, in place of (2) it is costed to use the following formulas:

$$\chi = \sqrt{\sum_j \left[F_j K_{\ddot{A}}(\omega_j)\right]^2}\ ;\ \chi = \sqrt{\sum_j \left[F_j K_{\ddot{A}}(\omega_j)\omega_j\right]^2}\ ;$$

$$\chi = \sqrt{\sum_j \left[F_j K_{\ddot{A}}(\omega_j)\omega_j\right]^2} \qquad (4)$$

where is adding up conducted after all j, for which ω_j take into in the considered range of frequencies.

Will consider the radial vibrations of external ring taking into account his bend. The root-mean-square of vibroacceleration of external ring will expect like (4):

$$\chi = \sqrt{\sum_j \left[F_j K_{\ddot{A}}(\omega_j)\omega_j\right]^2} \qquad (5)$$

where, however, the value of coefficient of dynamic of K_D (ω_j) will determine a not formula (3), but following semiempiric dependence:

$$\tilde{K}_{\ddot{A}}(\omega_j) = \sqrt{\sum_{m=1}^{l} \frac{1}{M_m^2\left[\left(\omega_m^2 - \omega_j^2\right)^2 + \left(2h_m\omega_j^2\right)\right]}}\,. \qquad (6)$$

Here ω_m it is an eigenfrequency of m-ts form of vibrations of external ring $\omega_m^2 = (2\pi\nu_m)^2 \cdot 10^6$;

M_m is a coefficient which characterizes inertia properties of ring ($M_{m=1}=M$ is mass of ring with the elements added to him);

h_m - a coefficient of damping of m-ts form of vibrations;

q - number of the considered forms of vibrations of ring.

In expressions for amplitudes of accordions of vibroindignations of F_j there is a permanent multiplier of K_X – radial inflexibility of the roller bearing. Will consider,

$$K_x / M_m = \omega_m^2\,,$$

that physically justified for m=1, and for all other values of m accepted hypothetically. Thus expression will look like for the root-mean-square of radial vibroacceleration of ring (5):

$$\chi = \sqrt{\sum_j A_j^2 \sum_{m=1}^{l} \frac{1}{\left[(\omega_m / \omega_j - 1)^2 + (2h_m\omega_j)^2\right]}} \qquad (7)$$

where $A_j = F_j / K_x$.

Does the design of peak spectrum of vibroaccelerations of the roller bearing consist in the calculation of values χ after a formula (7) for every frequency bar of spectrum, that in adding up for *j*-th amplitudes of accordions of vibroaccelerations, frequency ω_j what take in the proper bar of spectrum. Unknown coefficients of damping h_m it is costed to determine during a calculable experiment by comparison of results of design with the results of measurings and proper adjustment of values of h_m.

After a formula (7) determine the oscillation model of the roller bearing, linking between itself two types of spectrums. On the entrance of model are peak spectrums of technological errors of rings $\alpha_\lambda(\lambda)$, $\alpha_\chi(\chi)$ and rollers $\alpha_\xi(\xi)$. The vehicle mean of measuring of these spectrums is round ness as “Talirond-73” with the harmonious analysis of polar diagram.

The initial parameter of model is a peak spectrum of radial vibroaccelerations of external ring. Vehicle facilities of measuring of this spectrum are analyzers of spectrum of types 2033 or 2133 firms "Bryul' and K’er" (Denmark).

Basic difficulties which arises up at a design is determination of peak spectrums $\alpha_\lambda(\lambda)$, $\alpha_\chi(\chi)$ and $\alpha_\xi(\xi)$. For set these spectrums it is necessary to define amplitudes of a few ten of the first accordions of waviness of surfaces of rings and rollers, that appears practically problematic through the limited exactness of existent round ness (0,005 mkm) and slump of amplitudes of accordions of errors with growth of their numbers.

In this connection for the set spectrums of errors there is the possible use of regressive dependences of the following kind [4]:

$$\alpha_\lambda = \alpha_1 / \lambda^{\beta_1}; \quad \alpha_\chi = \alpha_2 / \chi^{\beta_2}; \; \alpha_\xi = \alpha_3 / \xi^{\beta_3} \tag{8}$$

Coefficients α and β this dependences determined as coefficients of regression by statistical treatment of results of measurings of types of parties of rings and rollers and their extrapolation on the high numbers of accordions, or on the basis of calculable experiment by comparison the results of design with the results of measurings of spectrums of vibration of the concrete roller bearings.

On the basis of such approach an algorithm and program of design of spectrum of radial vibroaccelerations of external ring of the roller bearing is developed in composition of the drive setting of “DVK” by an algorithmic language Basic. Example of results of design of spectrum of vibroaccelerations of bearing of type 7510 presented on pic. 1.a, and, on pic. 1,б is the experimentally set spectrum of vibroaccelerations of the that bearing, got by the analyzer of type 2131 at the tests of bearing in composition of the drive setting of DVK. Comparison of results of design with the results of measuring testifies to their closeness.

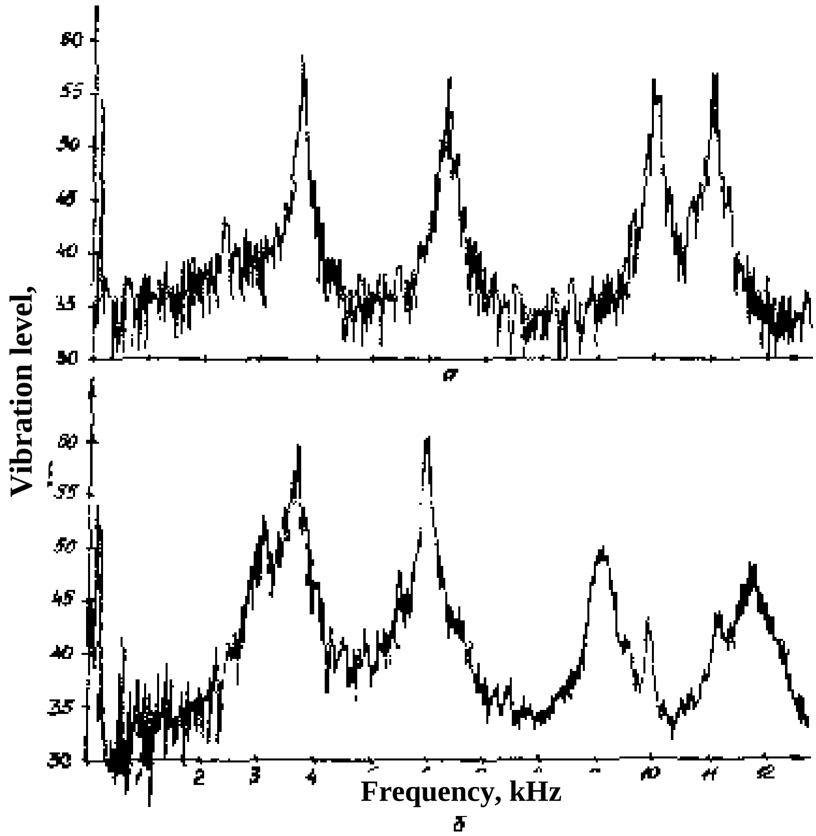

Pic. 1. Design of spectrum of vibroaccelerations of bearing type 7510

Numeral and experimental research of influence of frequency of rotation is conducted at the level of vibration of bearings of types 7505 and 7510 in the standard octave bars of frequencies and on the general level of vibration in the range of frequencies of 0-10 kHz. The design of spectrums of vibration in the octave bars of frequencies was conducted with the use of modification of the program “DVK”, measuring of spectrums of vibration in the octave bars of frequencies and general level of vibration, – on the improved driving setting of DVK, which provides possibility of adjusting of frequency of rotation within the limits of 600-3000 min^{-1}, with the use of analyzer of spectrum of type 2131.

Analysis of results of measuring of spectrums of vibroaccelerations of the roller bearings of types 7505 and 7510 allowed to get the following regressive dependence of level of vibration from frequency of rotation of internal ring:

$$A = A_0 \cdot N^{1,3}, \text{ m/s}^2 \qquad (9)$$

where A_0 is a coefficient which depends on a construction and bearing errors, m/s^2;

N is frequency of rotation, min^{-1}.

Do design results in a certain measure depend on the values of coefficients α and β (8), what approximates the spectrums of errors of rings and rollers. Direct determination of these coefficients as a result of harmonious analysis of polar diagrams appeared impossible in force of extraordinarily small values of amplitudes of high accordions of spectrums of errors of rings and rollers of the high-fidelity bearings. In that time did the analysis of theoretical model allow to set next dependence between the values of coefficients β dependences (8) and by the degree of dependence (9) of level of vibration from frequency of rotation of ring:

$$\delta = \beta - 0,5 .$$

In the total for δ=1,3 does have β =1,8.

Coefficients α_1, α_2 and α_3 got out on the basis of numeral experiment, coming from that even vibrations, conditioned the errors of external ring, internal ring and rollers, were approximately identical, and the general level of vibration of bearings, got as a result of design, answered the general level of vibration, which is registered at measurings.

For evidentness of comparison the results of measuring and design were approximated the different types of regressive dependences with the use of standard sub-program. The best coincidence with the results of experiments and design was got for regressive dependence of kind

$$y = a + b \ln x .$$

Coefficients of correlation of regressive dependence as a result of design, and also regressive dependence, as a result of measuring near to unit. Proper regressive dependences, and also these designs, and experiments on three octave bars of frequencies and presented the general level of vibration on pic. 2. On graphic arts by marks + marked results of design, and by marks 0 are results of measurings.

Comparison of presented calculation and testifies experimental dependences to their closeness, especially in the area of high-purity. In the area of LFS the results of design and measuring accord a bit worse, that is easily explained that the spectrum of vibration of the first approaching, which plays an important role in the area of LFS is not taken into account in the in-use program.

Thus, it is possible to establish as a result of the executed researches:

– the developed algorithm and program of design of spectrum of vibroaccelerations of external ring is taking into account bendings vibrations and different rejections of basic parameters of paths and bodies of woobling. Experimental researches were confirmed by results, got a calculation method;

– the experimentally tested formula of calculation of level of vibration at different frequencies of rotation of internal ring is got.

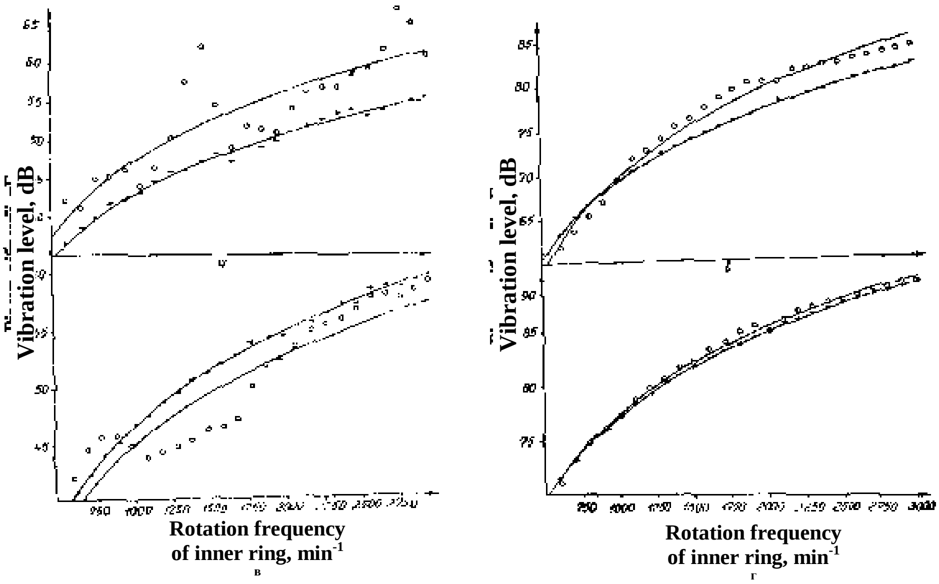

Pic. 2. Vibration spectrum of bearings (Hz): а – 250, б – 500, в – 1000, г - 2000

Practical realization of method of the automated spectrology is for the technical diagnostic of reasons of origin of technological vibrations

Development of theory of vibration of bearings is based on multilateral experimental and theoretical researches. The purpose of experiments is determination of coefficients or indexes of degree of various factors which influence on the vibration of bearings. The dependences and effects set as a result of experimental researches became the criterion of adequacy of theory and basis for development of method of the automated diagnosticating of vibroacoustic descriptions of bearings.

One of directions of experimental researches is influence of exactness and quality of making of working surfaces of rings and rollers on the vibration of bearings – becomes the object of the special attention of domestic and oversee authors. In particular, this question is examined in-process [2, 5], in which direct dependence of increase of level of vibration is rotined at the increase of waviness and roughness of details of ball-bearing. These facts are well known. Conducted complex of experimental researches, and also production experience important conclusions allowed to do in relation to intercommunications between the micro-geometry parameters of working surfaces and form and size of vibration of bearing.

Also sufficiently thoroughly investigational influence of structural parameters on the vibration of bearings. Difficult ambiguous connection is set them with a vibration. These parameters are also included in the existent models of vibration of bearings. The experimentally set influence is on the vibration of operating factors: contact tension on raceways, frequency of rotation and quality of greasing. The experimentally set dependence of vibration is certain in the type of approximating formula on an angulator. Experimental work is conducted from research of axial vibration at the different loadings. All these factors had a reflection in the models of vibration of bearings also.

Other important direction in experimental research of vibration of bearings is research of form of their vibrations. It is well-proven that a dominant role in the radial vibration of bearings in composition drive options in the range of frequencies of to 10 kHz is played by the bendings vibrations of rings of bearings. As most existent theories do not take into account this factor, then they can not adequately represent the oscillation processes of bearings. The necessary condition of the developed model is an account of all forms of vibrations of bearing, above all things bendings.

With the purpose of diagnosticating of reasons of origin of vibration of certain amplitude and frequency there was the developed model of resonance properties of the roller bearings, in it taken into account: inertia and hardness properties of external ring of bearing, Gertsevskiy contact between rollers and rings and mass of rollers.

Will consider the *m*-th form of vibrations for the roller bearing:

$$\omega = a \sin m\varphi \cos v_m t \,,$$

where a is amplitude of *m*-th form;

v_m - circular frequency;

t - time of contact the body of rotation with the elementary area of raceway;

m - number of form of vibrations ($m = 1$ answers oscillation of ring, as an absolutely solid);

φ - a corner of turn of mobile ring is in relation to a separator (roller)

Accepting, that displacement of *i*-th marble takes place after a law

$$s_i = \varepsilon a \sin m\varphi_i \cos v_m t \,,$$

two cases are possible.

In first cases number of semiwaves (2*m*) of bends of ring not multiple to the number of rollers of *z*. Formula of determination of frequency of *m*-th form of vibrations:

$$v_m^2 = \frac{\tilde{v}_m^2 + \dfrac{2}{1+1/m^2}\left[\varepsilon^2\omega_2^2 + (1-\varepsilon)^2\omega_1^2\right]}{1 + \dfrac{x}{1+1/m^2}\varepsilon^2} \,,$$

where

$$\omega_1 = \frac{z \cdot k_1}{2m_k}; \qquad \omega_1 = \frac{z \cdot k_2}{2m_k}; \qquad X = \frac{z \cdot m_{ï}}{m_k};$$

$\tilde{v}_m$ - circular frequency of vibrations of free ring, and ε it is determined from the condition of stationarity of eigenfrequencies

$$\frac{\partial v_m^2}{\partial \varepsilon} = 0,$$

what has the appearance of affected quadratic. In special case at K_1=K_2 (that characteristically for many types of bearings)

$$f_m^2 = \frac{\tilde{f}_m^2 + \frac{4}{1+1/m^2} f_1^2\left[\varepsilon^2 + 1(1-\varepsilon)^2\right]}{1 + \frac{x}{1+1/m^2}\varepsilon^2},$$

where ε it is from equalization

$$\frac{4x}{1+1/m^2}\varepsilon^2 + \left[\delta - x\left(\frac{\tilde{f}_m}{f_1}\right)^2 - 4\frac{x}{1+1/m^2}\right]\varepsilon - 4 = 0$$

In second cases at $2m = \ln(l = 1, 2, 3...)$ will have breaking up of frequencies, vibrations related to this form. One frequency will answer the location of bodies of woobling in the knots of vibrations. In this case frequency of f_m will coincide with frequency of vibrations of free ring, where fm is determined after the known formula:

$$\tilde{f}_m = \frac{1}{2\pi}\sqrt{\frac{E \cdot I \cdot m^2(m^2-1)^2}{\rho F r^4(1+m^2)}},$$

where F are areas of crossing;

ρ - a closeness;

r - a radius of central line of ring. Other frequency answers the location of bodies of rotation in antinodes rings, which bends. Proper eigenfrequency

$$f_m^2 = \frac{\tilde{f}_m^2 + \frac{8}{1+1/m^2} f_1\left[\varepsilon^2 + (1-\varepsilon)^2\right]}{1 + \frac{2x}{1+1/m^2}\varepsilon^2},$$

where ε - determined from equalization:

$$\frac{8x}{1+1/m^2}\varepsilon^2+\left[\delta-x\left(\frac{\tilde{f}_m}{f_1}\right)^2-\frac{8x}{1+1/m^2}\right]\varepsilon-4=0\,.$$

The calculation of eigenfrequencies on this formulas well conforms to the results, got in experiments [6, 7].

On the basis of calculation of resonances, coefficients of damping, the shown out formula of calculation of coefficient of dynamic (6) and got connection is between the spectrum of waviness and spectrum of vibration (see a formula 7), where adding up for j is determined frequencies of v_j, that fall in the proper bar of spectrum. Amplitudes and frequencies of indignations are presented in a table. 2.

TABLE 2. Dependences are for determination the parameters of vibrations of roller bearing

Bearing element	Number of accordion	Frequency ω_j	Amplitude A_j
External ring	λ =kz	$kz\omega_1$	α_λ
Internal ring	χ =kz	$kz\omega_2 \pm \omega_p$	α_χ
Rollers	ξ =2,4,6.	$\xi\,\omega_m \pm \omega_1$	$\sqrt{\frac{2}{\pi z}}\frac{1}{\cos\delta_0}\alpha_\xi$
Riznorozmirnist' of rollers	ξ =0	ω_1	$\frac{1}{3\sqrt{2z}\cos\delta_0}\Delta$

The however expounded theory based on determination of coefficient of dynamic and spectrum of vibrations is not complete, that is why the developed theory which takes into account all forms of oscillation of bearing and determines operating power indignations depending on the spectrum of waviness of bearing details.

It is built on the basis of decision of equalization of Lagrange vibrations of bearing ring, where as the generalized co-ordinates are used amplitudes of m-th form of vibrations of ring. Potential energy of the system is determined taking into account the spectrum of actual waviness. Basic equalization looks like for a m-th form:

$$\pi r\rho F(1+1/m^2)a_m+\left[\frac{\pi EI}{2r^3}(m^2-1)^2+\frac{k_x n}{2}(1-\mu_n^{2m}\cos 2m\omega_1 i)\right]a_m=$$

$$K_x\sum_{k=1}^{n}\rho_x(x)\cos my_k+K_x\sum_{k=1}^{n}\rho'(y_k)\cos my_k+K_x\sum_{k=1}^{n}\rho''(\Psi_k)\cos my_k+\mu_n^{2m}\frac{k_x n}{2}\delta$$

where a_m is amplitude of m-th form of vibrations;

ρ_k, ρ', ρ'' – waviness K-th rollers of external and internal rings;

$$\rho_k = \sum_{i=0}^{\infty} \omega_i^k \cos(i\chi + \tilde{\chi}_i^k); \quad \chi = 2\omega_ø t;$$

$$\rho' = \sum_{i=1}^{\infty} g_i \cos(i\varphi + \tilde{\varphi}_i); \ \ y_k = \omega_1 t + \frac{2\pi}{z} k;$$

$$\rho'' = \sum_{i=1}^{\infty} h_i \cos(i\psi + \tilde{\psi}_i); \ \psi_k = \omega_2 t + \frac{2\pi}{z} k$$

δ - axial tension

$$\mu_a^b = \begin{cases} 1; \ b \ \ divided \ \ on \ \ a \\ 0; \ b \ \ non \ \ divided \ \ on \ \ a \end{cases}$$

In particular, spectrum of indignations from defects on an external ring after the substitutions of expressions for the spectrum of defects values of corners looks like:

$$\frac{1}{2}\sum_{j=1}^{\infty}(g_{jn-m}\cos(jz\omega_1 t + \tilde{\varphi}_{jn-l}) + g_{jn+m}\cos(jz\omega_1 + \varphi_{jz+m}))$$

A main conclusion swims out from it: a vibration on the m-th form of vibrations of bearings is caused by inequalities of external ring with the numbers of accordions, levels, or multiple the number of rollers. The first forms of vibrations (m=1) answer a theory, expounded in [2] which describes oscillation of rings as absolutely solids. From a table 2 defects which cause a vibration have a number of accordion zk or qzk, where $q = 1, 2, 3...$. Thus, this theory is generalization of theory [60] of vibration of bearings taking into account the bendings vibrations of rings.

On the basis of this theory the developed program of calculation of vibration of roller bearings the executed verification of model adequacy.

On pic. 3 the rotined example of realization of method of determination of vibroactivity the surface of woobling of internal ring of roller bearing 7210 as informatively technological maps with the image of arctic diagram (polar diagram) and spectral description of the probed surface. On spectral description most amplitudes are for the proper accordions with numbers 2, 3, 21 shaded a dark background. In overhead right part of informative map the unsealed values of static (linear) rejections are in mkm and the proper values of amplitudes of speeds of vibrations (vibroactivity) for four accordions in mkm/s.

On pic. 4 example of identification map of values of amplitudes of speeds of vibrations in mkm/s for dangerous accordions with numbers even or multiple the number of bodies of woobling in bearing $Z = 19$. In addition in a table the given values of waviness for accordions with numbers $Z \pm 1$, $Z \pm 2$, $Z \pm 3$, $Z \pm 4$, $Z \pm 5$.

The spectrology of working surfaces after the method described higher is fixed in basis of the developed method of prognostication of vibroacoustic descriptions of bearings after the complex index of vibroactivity of rings and bodies of rotation.

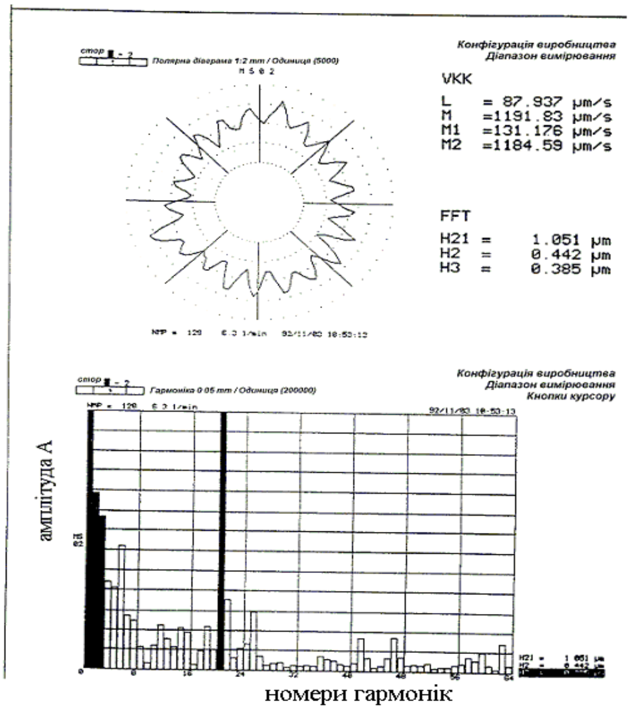

Pic 3. Polar diagram and spectral description the raceway of internal ring of bearing 7210

NUMERICAL RESULTS

Note:

Change MS with +/-

All Units in µm (/s)

Measuring range

MS01: NMP = 1024 4.965 rpm Inner Ring 02/25/04 11:23:42

Nr	Main Criteria	Sub Criteria	Exceeded Criteria	Lower Limit	Upper Limit	Measure Result	Comment
1	LSC	Δr	UPW	0.000	2.500	0.845	
2	MDi	WZ19	UPW	0.000	100.000	34.957	W95
3	MDi	W+-1	UPT	0.000	150.000	163.417	W20
4	MDi	W+-2	UPW	0.000	125.000	33.632	W59
5	MDi	W+-3	UPT	0.000	180.000	213.779	W22
6	MDi	W+-4	UPW	0.000	200.000	122.754	W72
7	MDi	W+-	UPW	0.000	250.000	225.298	W149

Filter	FL0	FL1	FL2	FL3	FL4	FL5	FL6	FL7	FL8	FL9
from	H 0	H 0	H 0	H 0	H 0	H 0	H 0	H 0	H 0	H 0
to	H 0	H 0	H 0	H 0	H 0	H 0	H 0	H 0	H 0	H 0

Exceeded Criteria	MS 01	MS 02	MS 03

Table - printout of all MS with P

Pic. 4. Identification table of values of vibro-speeds (to vibroactivity) of working surface of roller bearing 7210

The method of spectrology of working surfaces of rings became basis of the offered method of the selective drafting of roller bearing of high exactness of the special setting.

Conclusions

1. Developed method of the automated spectrology of vibration of bearing in comparison with the dynamic waviness of working surfaces allowed to find out important conformity to law, that the worst vibroacoustic descriptions of bearing arise up at coinciding of number of waves of *к*-th accordion on a raceway internal, and external ring with the number of bodies of rotation in bearing, or multiple this number, that $f_k = qz$, where f_k is a number of waves of basic *к*-th accordion on a raceway. The best results are marked, when $f_k = qz \pm 1$, $f_k = qz \pm 2$ et cetera, $q = 1, 2, 3...$. The method of spectrology opens a prospect for diagnosticating of reasons of appearance of technological defects. On the operations of form-making of racecourses of rings of roller bearing it is necessary to apply the technological methods of management a dynamic waviness (by vibroactivity of surface) with the receipt of accordions of waviness with numbers $Z \pm 1$, $Z \pm 2$, $Z \pm 3$, $Z \pm 4$, $Z \pm 5$. It is possible to attain by the management of form-making the modes, by inflexibility of the technological system, exception of casual vibroexcitations in the technological systems of machining, parameters and properties of toolpiece, by the features of correction diamond abrasive circles.

LITERATURE

1. Марчук В.І. Моделювання динамічної системи безцентрового врізного шліфування робочих поверхонь роликопідшипників // Наукові нотатки. Міжвузівський збірник (за напрямом “Інженерна механіка”), вип.14, серпень 2004. – Луцьк, 2004. – С. 187-198.
2. 60. Журавлев В.Ф., Бальмот В.Б. Механика шарикоподшипников гироскопов. – М.: Машиностроение, 1986. – 248 с.
3. 19. Бальмот В.Б., Самотин О.Н., Варламов Е.Б., Авдеев А.М. Вибрация и шум подшипников качения: Обзор. – М.: Цнинтэиавтопром, 1987. – 125 с.
4. 222. Струтинський В.Б. Математичне моделювання процесів та систем механіки: Підручник. – Житомир: ТІТІ, 2001. – 612с.
5. 197. Рагульскис К.М., Юркаускас А.Ю. Вибрации подшипников. / Под ред. К.М. Рагульскиса. – Л.: Машиностроение, ленинградское отделение, 1985, – 119 с.
6. 135. Марчук В.І., Матьошик В.О. Особливості моделювання зв’язків в технологічних системах штампування // Наукові нотатки: міжвузівський збірник (за напрямком “Інженерна механіка”) – Луцьк: Луцький державний технічний університет, – 2000. Вип.6. – С. 138-147.
7. 121. Марчук В.И., Кайдик О.Л. Забезпечення та стабілізація точності лімітуючого розміру в системі адаптивного шліфування кілець карданного роликопідшипника на бортикошліфувальному автоматі 280 СО // Труды 7-й международной научно-технической конференции «Физические и компьютерные технологии в народном хозяйстве», 27-28 мая 2003г. – Харьков: ХНПК “ФЕД”, 2003г. – С. 91-94.

Design of spectral descriptions of vibrations of roller bearings

Abstract
The design of vibration of any oscillating system is assumed by the decision of two basic questions: at first, about vibroindignation, that forces which causes a vibration; secondly, about dynamic properties of the oscillating system. Will consider the vibration of external ring of the roller bearing at his test on the drive setting of DVK [1].

Keywords: roller bearing, spectral analyze, polar diagram, vibroindignation, vibration, inner ring

Моделирование спектральных характеристик вибрации роликоподшипников

Вступление
Моделирование вибрации какой-нибудь колеблющейся системы допускает решение двух основных вопросов: во-первых, о вибровозбуждении, то есть силы, которая вызывает вибрации; во-вторых, о динамических свойствах колеблющейся системы. Рассмотрено вибрацию внешнего кольца роликового подшипника при его испытании на приводной установке DVK

Ключевые слова: роликоподшипник, спектральный анализ, круглограмма, виброскорость, вибрация, внешнее кольцо

Design of spectral descriptions of vibrations of roller bearings

VIKTOR MARCHUK
YURI LAPCHENKO
IRINA DEMJANOVA

Information about authors

Dr. Victor Marchuk
Device-building department
Lutsk national technical university
Lvivska st., 75
43018, Lutsk
Ph. 038-03322-6-49-43
E-mail: info@kptm.lutsk.ua

Dr. phd Yuri Lapchenko
Device-building department
Lutsk national technical university
Lvivska st., 75
43018, Lutsk
Ph. 038-03322-6-49-43
E-mail: info@kptm.lutsk.ua

Irina Demjanova
Device-building department
Lutsk national technical university
Lvivska st., 75
43018, Lutsk
Ph. 038-03322-6-49-43
E-mail: info@kptm.lutsk.ua

MARIUSZ WALCZAK
DANIEL GĄSKA
JOANNA SIDOR

Properties and application titanium and titanium alloys in aerospace systems

Introduction

Structures technology encompasses a wide range of component technologies from materials development to analysis, design, testing, production and maintenance. Materials and structures have largely been responsible for major performance improvements in many aerospace systems [1,2]. The maturation of computational structures technology and the development of advanced composite materials witnessed during the past 30 years have improved structural performance, reduced operational risk, and shortened development time. The design of future aerospace systems must meet additional demanding challenges [2,3]. For aircraft, these include affordability, safety and environmental compatibility [2,4]. For military aircraft, there will be a change in emphasis from best performance to low cost at acceptable performance. For space systems, new challenges are a result of a shift in strategy from long-term, complex, and expensive missions to those that are small, inexpensive and fast [2].

For example, aircraft that fly at higher speeds require higher temperature capability materials due to frictional heating. As a consequence, skin materials have progressed from wood and fabric used in the early aircraft to advanced alloys of aluminum, titanium, and polymer matrix composites containing high-strength carbon fibers [5].

In aerospace systems are used series of metal and non-metal materials. In the group of metallic materials are used: Al based alloys, ceramics, metal and polymer matrix composites, and titanium alloys. Nowadays, titanium and its alloys became the most popular materials. Titanium have very attractive properties, such as: corrosion resistance, low density and good mechanical properties. In aerospace systems from titanium are wide range manufactured fan turbine blade, tubes, missile fins, airframes for applications on advanced aircraft and spacecraft. In this article the characteristic of titanium and titanium alloys use in aerospace system were presented.

Properties of titanium and titanium alloys

Titanium was once considered a rare metal, but nowadays it is one of the most important metals in the industry. Chemically, titanium is one of the transition elements in group IV and period 4 of Mendeleef's periodic table. It has an atomic number of 22 and an atomic weight of 47.9. Being a transition element, titanium has an incompletely filled shell in its electronic structure [6,7]. Some basic physical properties of unalloyed titanium are summarized in Table 1. The incomplete shell enables titanium to form solid solutions with most substitution elements having a size factor within ±20%. In the elemental form, titanium has a high melting point (1668 °C) and possesses a hexagonal closely packed crystal structure (hcp) a up to a temperature of 882.5 °C. Titanium transforms into a body centered cubic structure (bcc) b above this temperature [6,8].

The mechanical properties of titanium and its alloys are summarized in table I . Titanium is very promising in orthopedics due to its high specific strength and low elastic modulus. However, titanium has low wear and abrasion resistance because of its low hardness.

TABLE I. Mechanical properties of a typical titanium and its alloys [9]

Grade	Tensile strength Rm=MPa	0,2% yield strength Rp 0.2=MPa	Elongation A5=% min.
Grade 1	min. 240	170-310	24
Grade 2	min. 345	275-450	20
Grade 3	min. 450	380-550	18
Grade 4	min. 550	483-655	15
Grade 5 6Al-4V	min. 895	Min. 825	10
Grade 7 + Pd	min. 345	275-450	20
Grade 11 +Pd	min. 240	170-310	24

Materials and structures

Titanium alloys may be classified as a, near-α, α + β, metastable β, or stable β depending upon the room temperature microstructure [6,10]. In this regard, alloying elements for titanium fall into three categories [6]:

(1) α - stabilizers, such as Al, O, N, C;
(2) β - stabilizers, such as Mo, V, Nb, Ta (isomorphous), Fe, W, Cr, Si, Co, Mn, H (eutectoid);
(3) neutrals, such as Zr and Sn.

The α and near-α titanium alloys exhibit superior corrosion resistance but have limited low temperature strength. In contrast, the α + β alloys exhibit higher strength due to the presence of both the a and b phases. The properties of the materials depend on the composition, relative proportions of the α and β phases, thermal treatment, and thermo–mechanical processing conditions. The β alloys also offer the unique characteristic of low elastic modulus and superior corrosion resistance [6,11,12]. In the picture fig. 1 very popular microstructure of Ti commercially pure and Ti-6Al-4V alloy were presented.

a)

b)

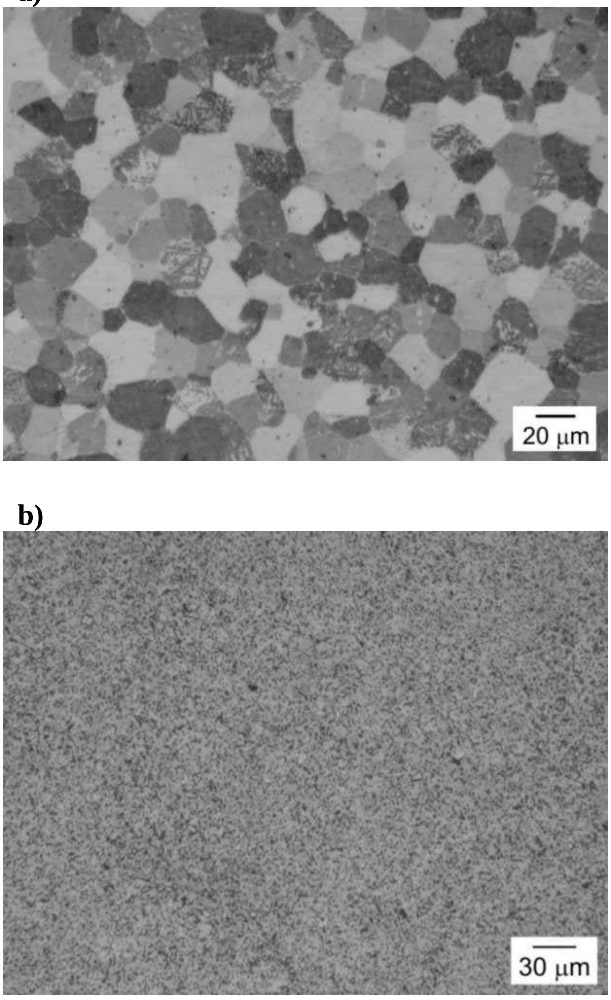

Fig. 1. Microstructure of materials: (a) Ti commercially pure (ASTM - grade 2) – α microstructure and (b) Ti6Al4V alloy (ASTM – grade 5) – α + β microstructure

Corrosion resistance

The excellent corrosion resistance of titanium alloys results from the formation of very stable, continuous, highly adherent, and protective oxide films on metal surfaces. Because titanium metal is highly reactive and has an extremely high affinity for oxygen, these beneficial surface oxide films form spontaneously and instantly when fresh metal surfaces are exposed to air and moisture. In fact, a damaged oxide film can generally reheat itself instantaneously if at least traces of oxygen or water are present in the environment. However, anhydrous conditions in the absence of a source of oxygen may result in titanium corrosion, because the protective film may not be regenerated if damaged [13].

The nature, composition, and thickness of the protective surface oxides that form on titanium alloys depend on environmental conditions. In most aqueous environments, the oxide is typically TiO_2, but may consist of mixtures of other titanium oxides, including TiO_2, Ti_2O_3 and TiO. High-temperature oxidation tends to promote the formation of the chemically resistant, highly crystalline form of TiO, known as rutile, whereas lower temperatures often generate the more amorphous form of TiO, anatase, or a mixture of rutile and anatase [6,13].

According to literature data [14,15], spontaneous (after time already 10^{-9}s) form coating titanium oxide on titanium substrate about $1,5 \div 5$ nm thickness.

Although these naturally formed films are typically less than 10 nm thick and are invisible to the eye, the TiO; oxide is highly chemically resistant and is attacked by very few substances, including hot, concentrated HCl, H_2SO_4, NaOH and (most notably) HF. This thin surface oxide is also a highly effective barrier to hydrogen [6,13].

The methods of expanding the corrosion resistance of titanium into reducing environments include [13]:

- Increasing the surface oxide film thickness by anodizing or thermal oxidation;
- Anodic polarizing the alloy (anodic protection) by impressed anodic current or galvanic coupling with a more noble metal in order to maintain the surface oxide film;
- Applying precious metal (or certain metal oxides) surface coatings;
- Alloying titanium with certain elements;
- Adding oxidizing species (inhibitors) to the reducing environment to permit oxide film stabilization.

Titanium alloys, like other metals, are subject to corrosion in certain environments. The primary forms of corrosion that have been observed on these alloys include general corrosion, crevice corrosion, anodic pitting, hydrogen damage, and stress-corrosion cracking.

In any contemplated application of titanium, its susceptibility to degradation by any of these forms of corrosion should be considered. In order to understand the advantages and limitations of titanium alloys, each of these forms of corrosion will be explained. Although they are not common limitations to titanium alloy performance, galvanic corrosion, corrosion fatigue, and erosion-corrosion are included in the interest of completeness [13].

Corrosion is characterized by a relatively uniform attack over the exposed surface of the metal. At times, general corrosion in aqueous media may take the form of mottled, severely roughened metal surfaces that resemble localized attack. This often results from variations in the corrosion rates of localized surface patches due to localized masking of metal surfaces by process scales, corrosion products, or gas bubbles; such localized masking can prevent true uniform surface attack.

Titanium alloys may be subject to localized attack in tight crevices exposed to hot (>70 ^{o}C) chloride, bromide, iodide, fluoride, or sulfate-containing solutions. Crevices can stem from adhering process stream deposits or scales, metal-to-metal joints (for example, poor weld joint design or tube-to-tubesheet joints), and gasket-to-metal flange and other seal joints [6,13].

Pitting is defined as localized corrosion attack occurring on openly exposed metal surfaces in the absence of any apparent crevices. This pitting occurs when the potential of the metal exceeds the anodic breakdown potential of the metal oxide film in a given environment. When the anodic breakdown potential of the metal is equal to or less than the corrosion potential under a given set of conditions, spontaneous pitting can be expected.

Titanium alloys are widely used in hydrogen containing environments and under conditions in which galvanic couples or cathodic charging causes hydrogen to be evolved on metal surfaces. Although excellent performance is revealed for these alloys in most cases, hydrogen embitterment has been observed.

The surface oxide film of titanium is a highly effective barrier to hydrogen penetration. Traces of moisture or oxygen in hydrogen-containing environments very effectively maintain this protective film, thus avoiding or limiting hydrogen uptake. On the other hand, anhydrous hydrogen gas atmospheres may lead to absorption, particularly as temperatures and pressures increase.

Stress-corrosion cracking is a fracture, or cracking, phenomenon caused by the combined action of tensile stress, a susceptible alloy, and a corrosive environment. The metal normally shows no evidence of general corrosion attack, although slight localized attack in the form of pitting may be visible. Usually, only specific combinations of metallurgical and environmental conditions cause stress-corrosion cracking. This is important because it is often possible to eliminate or reduce stress-corrosion cracking sensitivity by modifying either the metallurgical characteristics of the metal or the makeup of the environment.

Another important characteristic of stress-corrosion cracking is the requirement that tensile stress is present. These stresses may be provided by cold work, residual stresses from fabrication, or externally applied loads.
The key to understanding stress-corrosion cracking of titanium alloys is the observation that no apparent corrosion, either uniform or localized, usually precedes the cracking process. As a result, it can sometimes be difficult to initiate cracking in laboratory tests by using conventional test techniques.

It is also important to distinguish between the two classes of titanium alloys. The first class, which includes ASTM grades 1, 2, 7, 11 and 12, is immune to stress-corrosion cracking except in a few specific environments. These specific environments include anhydrous methanol/halide solutions, nitrogen tetroxide (N_2O_4) and liquid or solid cadmium. The second class of titanium alloys, including the aerospace titanium alloys, has been found to be susceptible to several additional environments, most notably aqueous chloride solutions [6,8,13].

The coupling of titanium with dissimilar metals usually does not accelerate the corrosion of titanium. The exception is in strongly reducing environments in which titanium is severely corroding and not readily oxidizable. In this uncommon situation, accelerated corrosion may occur when titanium is coupled to more noble metals. In its normal passive condition, materials that exhibit more noble corrosion potentials beneficially influence titanium.

The general corrosion resistance of titanium can be improved or expanded by one or a combination of the following strategies: alloying, inhibitor additions to the environment, precious metal surface treatments, thermal oxidation and anodic protection.

Perhaps the most effective and preferred means of extending resistance to general corrosion in reducing environments has been by alloying titanium with certain elements. Beneficial alloying elements include precious metals (>0.05 wt% Pd), nickel (>= 0.5 wt%), and/or molybdenum (>= 4 wt%). These additions facilitate cathodic depolarization by providing sites of low hydrogen overvoltage, which shifts alloy potential in the noble direction where oxide film passivation is possible. Relatively small concentrations of certain precious metals (of the order of 0.1 wt%) are sufficient to expand significantly the corrosion resistance of titanium in reducing acid media [6,13].
These beneficial alloying additions have been incorporated into several commercially available titanium alloys, including the titanium-palladium alloys (grades 7 and 11), Ti-0.3Mo-0.8Ni (grade 12), Ti-3Al-8V-6Cr-4Zr-4Mo, Ti-15Mo-5Zr, and Ti-6Al-2Sn-4Zr-6Mo. These alloys all offer expanded application into hotter and/or stronger HCl, H_2SO_4, H_3PO_4, and other reducing acids as compared to unalloyed titanium. The high-molybdenum alloys offer a unique combination of high strength, low density, and superior corrosion resistance [13].

Titanium Matrix Composites

This demand for increased performances continues to drive material development efforts to explore new concept such as Titanium Matrix Composites (TMC), which involve the reinforcement of the titanium or titanium alloys. The main advantages of TMCs are the increased mechanical and physical properties, i.e. strength, stiffness, hardness etc. The direction of the reinforcements dictates the properties, providing the option to tailor specific properties in specifics directions. It is important to distinguish between continuously reinforced and discontinuously reinforced TMCs. Although they share some common features they also display different ones, for example the isotropy or anisotropy of properties [16,17].

For over 30 years, TMCs continuously reinforced with silicon carbide (SiC) monofilaments have been highly regarded and reached maturity through huge development efforts. The benefits of this kind of TMCs, that can match the strength and stiffness of steel at roughly half the weight, have been recognized mainly by airframe and turbine engine manufacturers. Nevertheless, some drawbacks, such as the prohibitive cost of SiC monofilaments, the manufacturing cost and complexity, the chemical instability between the fibre and the matrix and their coefficient of thermal expansion mismatch together with highly anisotropic properties of these composites, have restricted their use to the mentioned highly specialized applications [16]. Typical composition of TMCs are shown in Fig. 2.

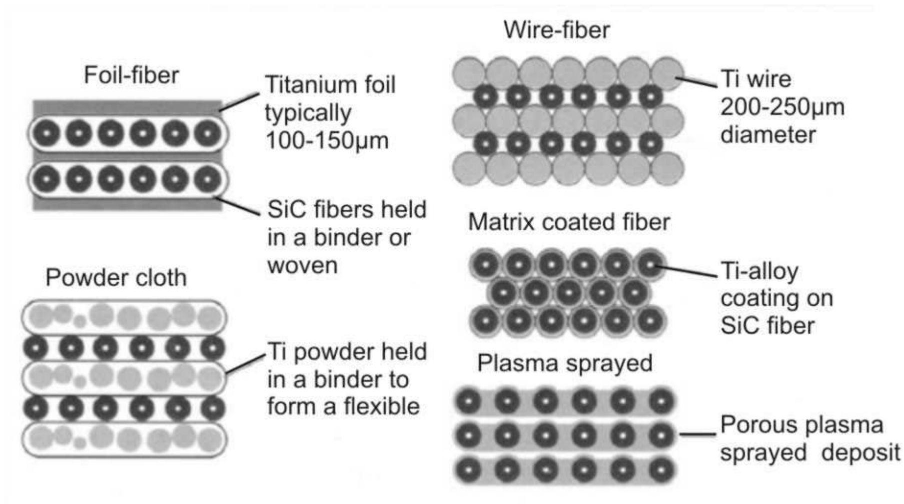

Fig. 2. Titanium Matrix Composites – most cost fabrication route [18]

The need to develop new high-performance and low-cost TMCs arose due to these limitations. Their research and development will lead to gain not only for the aerospace industry, but other weight-sensitive and mass-production industries such as automotive, medical, sport, etc [16-18]. Selected properties of the major constituents of a typical TMCs system are given in table II.

From the technical point of view, the ideal reinforcement for titanium alloys should meet the following criteria: superiority in physical and mechanical properties (stiffness, strength, hardness, etc.), thermo dynamical stability and minimum difference in thermal expansion between the two constituents. Another interesting feature is the possibility to reinforce the material in the required direction, or in all directions, to obtain isotropic properties.

TABLE II. Properties of a typical TMC comprised of SiC monofilaments and a titanium matrix [17]

Property	Dimension	Matrix		Fiber	
		20◦C	300◦C	20◦C	300◦C
Young’s modulus	GPa	110	96	400	394
Poisson’s ratio	1	0,3	0,3	0,25	0,25
Initial yield strength	MPa	770	560	–	–
Ultimate tensile strength	MPa	1050	780	4000	3980
Density	g/cm^3	4,5	–	3	–
Coefficient of thermal expansion	Ppm/k	10,36	10,70	1,61	3,90
Thermal conductivity	W/mK	10	–	25	–
Specific heat capacity	J/kgK	550	–	670	–

Previous studies have proved that the titanium boride (TiB) meets all the above mentioned requirements. The TiB can be obtained by means of *in-situ* techniques. These techniques involve a chemical reaction resulting in the formation of thermodynamically stable reinforcing phase within the metal matrix. Unlike reinforcements added from external sources, *in-situ* formed ones consist of contaminant-free interfaces and the composites obtained present isotropic properties [16].

Titanium aluminide alloys

Titanium aluminide alloys are based on the intermetallic compounds Ti_3Al (α_2) and TiAl(γ) in the Ti-Al system. the primary advantages of titanium aluminide alloys are low density, high strength-to weight ratio, high stiffness and strength at elevated temperature compared to conventional titanium alloys and good oxidation resistance. As such, they are being considered as replacements for nickel based superalloys in aircraft turbine engines, missile fins, airframes and automotive engines. Turbine engine applications include both static and roating components in the high-pressure compressor, combustor, low–pressure turbine and nozzle [19]. The γ-alloys are more attractive than pure α-alloys because of the higher temperature capability as well as the lower density and higher modulus.

In grup α_2 – titanium alloys is very popular: Ti-25Al, Ti-48Al, Ti-25Al-5Nb, Ti-24Al-11Nb, Ti-25Al-10Nb-3V-1Mo and Ti-24.5Al-12.5Nb-1.5Mo. Whereas typical γ-alloys are: Ti-48Al-1V, Ti-48Al-2Mn and Ti-48Al-2Cr-2Nb [19,20].

Applications of titanium and its alloys

Ti alloys have been used for special purpose applications in both military and commercial aircraft for several decades. In addition to the high speed military airplane, the SR-71, described earlier, there are a number of applications of Ti alloys for heavily loaded structure such as bulkheads in fighter aircraft, the wingbox on the B1-B bomberand the landing gear beam in the Boeing 747 [5,21].

In each of these cases, Ti alloys were chosen because, compared to Al alloys, they have equal or better density corrected strength, good damage tolerance and excellent corrosion resistance. The alloys chosen for each of these three applications is the old, but still widely used $\alpha + \beta$ alloy, Ti-6Al-4V. Higher strength $\alpha + \beta$ and β Ti alloys are available, but the damage tolerance, both toughness and crack growth, typically decreases in the higher strength alloys. Thus incorporation of higher strength alloys without a commensurate increase in toughness increases the risk of catastrophic failure which is generally unacceptable. In addition to the intrinsic mechanical properties of Ti alloys, the corrosion resistance makes them attractive, especially for components that are embedded in the aircraft and, as a consequence, are very difficult to inspect for corrosion attack. The better resistance to general corrosion and essential immunity to exfoliation corrosion compared to high strength Al alloys is an advantage for Ti alloys. Ti alloys are also used in circumstances where their higher strength allows the same load to be carried by a physically smaller structural member, even though there is no weight advantage because of the higher density of Ti alloys [5, 22].

Ti alloys are also a very good alternative to high strength steel, even though at the highest strength levels, the structural efficiency achievable with steel is considerably higher. The issue here is that the susceptibility of steel to hydrogen embrittlement becomes much higher at strength levels 1250 MPa. Using steel at strengths higher than this requires use of a protective coating such as paint or plating with Cd or Cr. The former of these approaches requires periodic maintenance to repair scratches and chips and the latter of these is being phased out for environmental and health hazard reasons. The landing gear of most commercial aircraft has traditionally been made of high strength steel such as AISI 4340 heat treated to strengths of 1800–1900 MPa. Service history has shown that numerous hydrogen embrittlement failures have been experienced, despite the use of stringent maintenance procedures. Recently, a high strength β alloy, Ti-10V-2Fe-3Al, has been selected for the landing gear of the Boeing 777. For this application, Ti-10V-2Fe-3Al is heat treated to the 1250 MPa strength level. The decision to use Ti-10V-2Fe-3Al is driven by the ability to achieve weight reduction and eliminate the risk of hydrogen embrittlement failure, albeit at an increase in cost [5,21,22].

Titanium alloys have been employed for high temperature applications in the F16 [23,24]. In this military aircraft from titanium are manufactured engine nozzle seal (Fig. 3a) [23]. Moreover are installed from TMC lower drag braces in F16 main landing gear (Fig. 3b) [24].

a)

b)

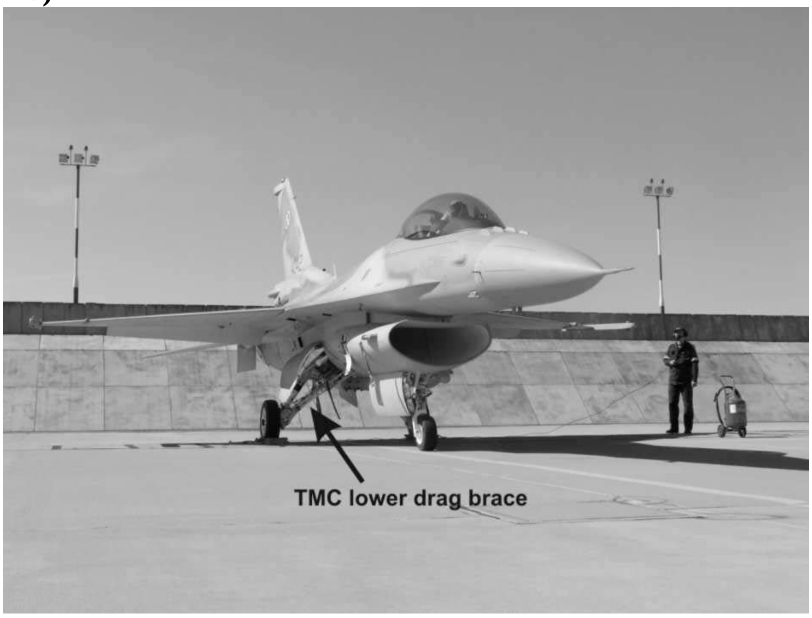

Fig. 3. Application of titanium materials in the F16: a) installation of the TMC lower drag brace in main gear; b) engine nozzle seal.

Fig. 4 show the history of titanium use on military aircraft. As this figure illustrates, titanium use shows no consistent trend over time. However, it does tend to be higher in dedicated air superiority fighters, which are characterized by stringent temperature and other performance requirements [23].

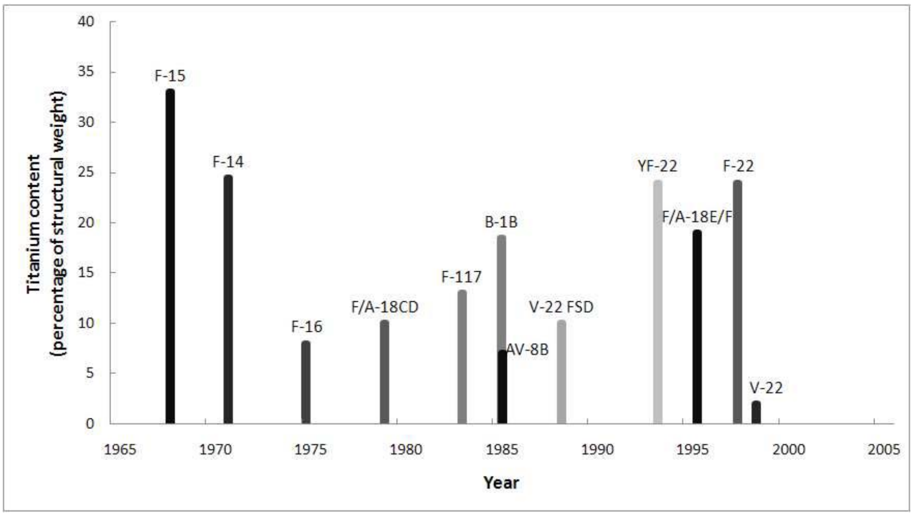

Fig. 4. History of titanium use on military aircraft, according to literature data [23]

Gamma titanium aluminide sheet is being developed for applications on advanced aircraft and spacecraft. Potential automotive applications include turbo-charger rotors and exhaust valves. Moreover, the specific strength of titanium aluminide alloys exceeds that of common titanium alloys and matches some nickel base superalloys. In sheet form, gamma titanium aluminide is being considered for aerospace applications such as hot skin, control surfaces, heat shields and exhaust ducts Space applications include the X-33 single-stage-to-orbit vehicle, the X37 Future X and X-38 crew return vehicle [19,25].

Summary

Titanium and titanium alloys are very attractive materials because of their excellent combination of properties that give them the possibility to be used in aerospace system. Titanium has excellent heat and corrosion resistance and is stronger than aluminum. its primary drawback is cost; the raw metal it self is five to seven times as expensive as aluminum. Titanium is used extensively in military and civil airframe aft fuselages by virtue of the need to withstand engine exhaust temperatures, and it is also used where strength is a key property.

In summary, the manuscript briefly reviewed the competitiveness of titanium alloys and a few other titanium aluminides within selected properties–use relationships, or materials selection aspects of structural materials. The brief survey of properties illustrates new capabilities available materials with titanium.

REFERENCES

1. *Noor A.K. editor.*: Structures technology - Historical perspective and evolution. Reston, VA: AIAA, 1998.
2. *Noor A.K., Venneri S.L., Paul D.B., Hopkins M.A.:* Structures technology for future aerospace system. Computers and Structures. 74 (2000) pp. 507-519.
3. *Noor A.K., Venneri S.L.:* Future aeronautical and space systems. In: Progress in astronautics and aeronautics, vol. 172. Reston, VA: AIAA, 1997.
4. *Davies G.A.O.:* Aircraft structures. The Aeronautical Journal. 100 (1996) pp. 523- 529.
5. *Williams J.C., Starke E.A.Jr.*: Progress in structural materials for aerospace systems. Acta Materialia. 51 (2003) pp. 5775-5799.
6. *Liu X., Chu P.K.,Ding Ch.*: Surface modification of titanium, titanium alloys, and related materials for biomedical applications. Materials Science and Engineering. R 47 (2004) pp. 49-121.
7. *Ogden H.R.. in Clifford A.H. (Ed.):* Rare Metals Handbook, Rinhdd Publishing corporation. Chapman & Hall Ltd., London, 1961 pp. 559-579.
8. *Collings E.W.:* The physical metallurgy of titanium alloys, in Gegel (Ed.), ASM Series in Metal Processing. Edward Amold Publications. Clevland. Metals Park, OH 1984.
9. Commercial Catalog Bibus Metal Sp. z o. o. Tytan i stopy tytanu. Nikiel i stopy niklu. Odlewy odśrodkowe i piaskowe. (Publishing Poland) www.bibus.metals.com.pl, 2002.

10. *Polmear J.J.*: Titanium alloys, in: Light Alloys, Edward Arnold Publications. London 1981.
11. *Bania P.J. in: Eylon D., Boyer R.R., Koss D.A. (Eds.)*: Titanium Alloys in the 1990's, The Mineral. Metals & Materials Society, Warrendale, PA, 1993 pp. 3-14.
12. *Schutz R. W., in Eylon D., Boyer R.R., Koss D.A. (Eds.)*: Beta Titanium Alloys in the 1990's, The Mineral. Metals & Materials Society, Warrendale, PA, 1993 pp. 75-91.
13. *Schutz R.W.:* Corrosion of Titanium and Titanium Alloys. ASM Handbook Vol. 13B. corrosion Materials. 2005 pp. 252-299.
14. *Walczak M.*: The study of multilayered system metal-ceramics-ceramics in dental prosthetics applications. Doctor's thesis. Lublin 2006. (Poland)
15. *Marciniak J.*: Biomateriały metaliczne, w Błażewicz S., Stoch L.: Biomateriały. Tom 4, Akademicka Oficyna Wyd. Exit, Warszawa 2003. (Poland)
16. *Garrcia de Cortázar M.*: Development of a new reinforced titanium alloy: Basic research and technological transfer for the Ti-6Al-4V/TiB material. Doctor's thesis. Barcelone 2006.
17. *Larsen J.M., Russ S.M., Jones J.W.*: An Evaluation of Fiber-Reinforced Titanium Matrix Composites for Advanced High-Temperature Aerospace Applications. Metallurgical and Materials Transactions. 26A (1995) pp 3203-3211.
18. *Marsh G.*: Metals shed weight to compete. Materials Today. 4 (2001) pp.25-29.
19. *Moll J.H., McTiernan B.J.*: PM TiAl alloys: the sky's the limit. Metal Powder Report. 55 (2000) pp.18-22.
20. *Koster J.*: Titanium alloys. ASEN 4012, JOM July 1994 pp.30-39.
21. *Starke Jr. E. A.*: Aerospace materials for future technologies. Journal of the Japan Institute of Light Metals. 51 (2001) pp. 77–85.
22. *Lütjering G., Williams J.C.*: Titanium. Berlin: Springer-Verlag, 2003.
23. *Younossi O., Kennedy M., Graser J.C.*: The Cost of Future Military Aircraft: Historical Cost Estimating Relationships and Cost Reduction Initiatives. Published 2001 by RAND, 168 pp.
24. SP aerospace and vehicle sysytem "F16 Metal Matrix Drag Brace" June 2003 pp. 1-3
25. *Cotton J.D., Will J.D., Rhodes C.G., Berbon P.B.*: Assessment of Gamma-TiAl Sheet Alloys for Aerospace Applications. Presented at AeroMat '99, 10th Annual Advanced Aerospace Materials & Processes Conference, Dayton, OH, June 1999.

Properties and application titanium and titanium alloys in aerospace systems

Abstract
In this paper presented properties of materials basic on titanium in aerospace system applications. Chief among these properties are strength and stiffness, especially in relation to weight. Other important material properties, such as corrosion resistance, microstructure and service temperature, are also briefly discussed. Moreover, described numerously examples properties the major of typical titanium alloys and titanium matrix composites in air force and civil aviation.
Keywords: titanium, titanium alloys, titanium matrix composite, aerospace system, aircraft, aviation.

Właściwości i zastosowanie tytanu i stopów tytanu w systemach przestrzeni powietrznej

Streszczenie
W artykule przedstawiono właściwości materiałów na bazie tytan stosowanych w systemach przestrzeni powietrznej. Analizowano właściwości mechaniczne, sztywność i ciężar oraz właściwości związane z mikrostrukturą, odpornością na korozję i temperaturą użytkową opisywanych materiałów. Ponadto opisano liczne przykłady zastosowań w lotnictwie wojskowych i cywilnym typowych stopów tytanu i tytanowych materiałów kompozytowych.

Słowa kluczowe: tytan, stopy tytanu, kompozytowe materiały o osnowie ceramicznej, systemy przestrzeni powietrznej, samoloty, lotnictwo.

Properties and application titanium and titanium alloys in aerospace systems

MARIUSZ WALCZAK
DANIEL GĄSKA
JOANNA SIDOR

Informacje o autorach

Dr inż. Mariusz Walczak
Instytut Technologicznych Systemów Informacyjnych
Wydział Mechaniczny
Politechnika Lubelska
ul. Nadbystrzycka 36
20-618 Lublin
tel. (0-81) 53-84-535
e-mail: m.walczak@pollub.pl

Mgr inż. Daniel Gąska
Instytut Technologicznych Systemów Informacyjnych
Wydział Mechaniczny
Politechnika Lubelska
ul. Nadbystrzycka 36
20-618 Lublin
tel. (0-81) 53-84-582
e-mail: d.gaska@pollub.pl

Mgr Joanna Sidor
Wyższa Szkoła Ekonomii i Innowacji
ul. Mełgiewska 7/9
20-209 Lublin
tel. (0-81) 74-93-243
e-mail: joanna.sidor@wsei.lublin.pl

VLADIMÍR BALÁŽ
IVAN IGNÁTH
DOMINIKA PALAŠČÁKOVÁ

Robotized training workstations on Department of production systems and robotics

1. Introduction

While before certain era acquired technical education was enough almost for one's life, nowadays we are witness of unprecedented transformation of classic skills to newones. Orientation on fastness of customer's satisfaction is demanding high qualification and fine flexibility of all persimmons. Persimmons are given variant responsibilities in the working team, they negotiate from one working system to another and they use their working time very flexibly. Acquirement and retaining of advantages before competitors became basic priority of industry and individuals, to success. Today is not enough to hold powerful technology and modern computer technology, but also know-how its utilizing as necessary condition of success. Fast advances in technology and production organization with utilizing of informative technology touches all enterprises staff. Enterprise, which recognize a possibility of achievement competitive advantage with knowledge of it's workers, forces it's staff to continual cycle of education.

2. Reasons of e-learning trainings

All high developed countries accentuates on building of computer society and on utilizing of modern informatics technologies. Nowadays are many companies forced to make their production more flexible to comply market requirements and not only to boost productivity a quality. Current economic environment could be specified by enormous growth of competition, fast introducing of new products, expand of product's function, shorten product's lifecycle. It is not only due to customer's requirement, but also progress of technology and in today's wide implementation of computer technology in process of arrangements and management of production. This process requires continuing acquisition of new attainments. Classic way of training has a several limitations in this case. There are training in certain time period, sometimes after several year and they are „ one-shot" and last few days. Orientation of training on e-learning allows workers to study by own time schedule without binding to school and to teacher.

3. The structure of lessons

The "Integrated Set of vocational trainings in the field: most advanced solutions in technology, organization and safety in Automated and Robotized manufacturing (A&RM) systems" (ISAR) project is funded under the EU Leonardo Da Vinci Programme for a duration of two years. ISAR addresses vocational training systems and content in an integrated manner that facilitates the advancement of methods and technologies in the field of e-learning. The innovative trainings (knowledge, methodology, tools, services) will be interactively composed and based on the e-learning state-of-the-art solutions in a combination with learning groups and transnational virtual study circles in order to motivate the users to improve and advance their abilities to introduce advanced solutions in technology, organization and work safety in A&RM systems, especially in SMEs.

Main topics of lessons are:

- Introduction to A&RM
- Problems by selection, introduction and application of A&RM systems in SMEs
- Specification of A&RM system integration in existing SW environment
- Programming of robot and NC systems.
- Maintenance of A&RM systems and diagnostic
- Operational aspects of A&RM systems

The lessons for students will be placed on the web site so they can study from them. After studying the lessons students can practice their theoretical knowledge at our workplaces (laboratories). Practice lessons will sweep under the supervision of the lectors.

Each lesson must include:

- An explanation of the method – textual/graphical
- An example (practical example)
- An exercise – practice (set of multiple-choice questions, tasks etc.)

All example and exercise must be related to real industry A&R solutions. Currently each example follows the same case study:

- Introduction to the lesson
- Aims of the lesson
- Instructions
- Example
- Exam

Target groups addressed by the project are:

- Management from industrial SMEs,
- Technical staff,
- Less qualified workers and unemployed workers,

- Trainers and Consultants,
- Students of technical schools and unemployed highly qualified people (engineers).

4. Robotized cell with robot KUKA for spot welding

The structure of the cell is made by the KUKA robot, type KR 125 with the articulatory kinematics and the load capacity to 125 kg., fig.1.

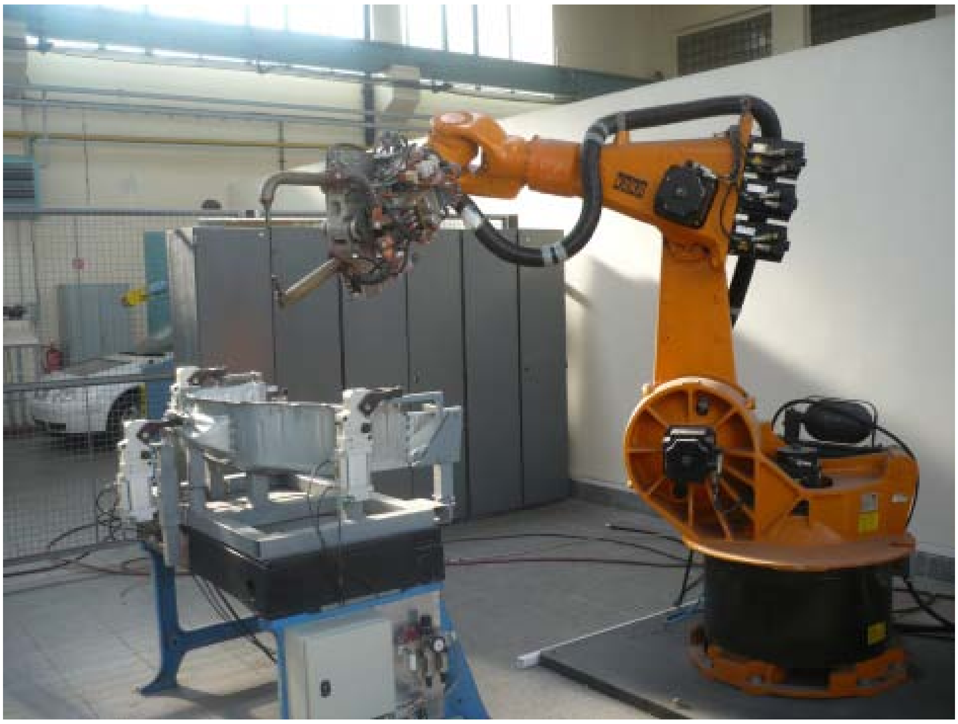

Fig. 1 Robotized cell with KUKA

KUKA robots with present kinematics are used mostly in manufacturing automobiles using spot welding in all types of VW automobile. The Robot is equipped with the welding jaws for the spot welding of Nimak type and with welding aggregate FASE Kompakt. The workstation is implemented with the modular system of future for welding of special parts of an automobile.

Functional components are equipped with the sensors for monitoring of choose parameters of the workstation and for the visualization of the operating process. Scanned parameters are used for direct control and also for statistic manipulation of the duration of the operating process with the possibility of presentation on the internet.

5. Robotized cell with robot OTC Daihen for arc welding

Arc welding cell is equipped with OTC Almega AX-V6 robot with six laxity levels and carrying capacity of 6kg at the flange. Robot is operated by AX-C system, which enables to achieve repeatable accuracy 0,08 mm. Operating system works with Windows NT4 disc operating system and RTX upgrade, which enables to operate the robot in real-time mode. Robot is offset with effector for manipulation with components. Fig.2. depicts robotic cell with robot OTC .

Fig. 2. Robotic cell with robot OTC Almega AX-V6

6. Robotized cell with robot Scara for palletization

Palletization cell is equipped with robot Yamaha YK400X with four degree of freedom and carrying capacity of 3kg at the flange. Robot is operated by RCX142 system, which enables to achieve repeatable accuracy 0,01 mm. Robot is equipped with effector for manipulation with components. Effector is constructed in such a way, that it can a) transmit the components by the help of a couple of suckers and b) manipulate with the second part with components by means of two-finger tentacle. Effector was designed and constructed at our department. Schema of the transmission of information in palletizational cell is in the fig.1. Components are transported to the robot on a conveyor, which is operated by its own operating system. Programme is intelligent contactor and we can by means of analogue module operate frequency changer. That enables us to change the speed of engine rotation and by that to change also the shift of the conveyor according to robot´s operating system´s requirements. Components are laid on the conveyor at random and the robot´s task is to identify them by the help of camera. For the purpose of identification we used the camera MINTROM AVT Marlin F-033B. Camera je connected to PC via usb port. Resolution of this camera can be adjusted from 160x120 to 640x480 by 74 snapshots per second. Robotic cell with robot Scara is on fig.3.

Fig.3. Robotic cell with robot Scara - Yamaha YK400X

7. Conclusion

Once these lesson parts area created they can then be used interchangeably to suite the individual learner. For example the business student and the owner manager may have the same lesson regarding the overview of the project as well as the detail of the analysis and conception phase. Also both groups will also share the smaller detail of the selection and specification phase. By creating these lesson objects the developers of the courseware for the methodology can create interchangeable and reusable lesson parts hence reducing the overall development effort required. Lessons for these groups shall be prepared very carefully to ensure that their content will be up to date and include latest advances in A&RM systems and also focus on practical issues and applications and provide real world case studies. That is because the most important topics for trainers and consultants as well as for other target groups are those related to application of A&RM systems in SME and their effect on a financial and strategic basis, and what is more important for SME employees – they may loose interest if theoretical knowledge is not linked to the area of world situations.

REFERENCES

1. Hajduk M., Baláž V., Ignáth I., Palaščáková D., Special education in field automation and robotic on base eLearning, Virtual university, Bratislava, 2006
2. Hajduk M., Ignáth I., Šidlovská Ľ., Pilotný projekt ISAR, Acta Mechanica Slovaca, Košice, 2006
3. Huba M. a kol., www a vzdelávanie, STU Bratislava, 2003
4. Huba M., Orbanová I.: Pružné vzdelávanie, STUBratislava, 2000
5. Kirchohoff U., Ch. Wolf.:AmI-Ambient Inteligence. In. Systém requirement specification and ISAR System Model. ISAR Project, 2006
6. Klimasara W., Pilat Z., Sawwa R., Slowikovski m., Zielinski J.: Application of e-Learning Improve the Efficiency of Vocational training in Automation and Robotíce. Acta Mechanica Slovaca, Košice, 2006
7. Kočíková E.: Počítačová podpora vzdelávania pri získavaní ECDL a možnosti využívania IT pri celoživotnom vzdelávaní, AT&P journal 4/2006
8. Králiková R., - Anna V.: Environmental information as tools for environmnetal management In: Proceedings of the 12th International Conference on Tools ICT- 2007 : September 6-8, 2007, Miskolc, Hungary. Miskolc : University of Miskolc, 2007. p. 175-179.
9. Pokorný, Peter - Peterka, Jozef: Technological postprocessor design for copy milling. In: Vedecké práce MtF STU v Bratislave so sídlom v Trnave. - ISSN 1336-1589. - Vol. 12 (2002), s. 113-117
10. Setchi R., Lagos N.: E-Learning and e-trianing – ontologies. ISAR Project, 2006
11. TOMAGOVÁ, Mária: Všeobecné tolerancie pre zvárané konštrukcie - STN EN ISO 13920 (050235). In: Nové trendy v konštruovaní a v tvorbe technickej dokumentácie 2004 : Zborník z medzinárodnej vedeckej konferencie poriadaný počas konania 11. Medzinárodného strojárs-keho veľtrhu v Nitre, 27. máj 2004. Nitra : SPU, 2004. s. 173-176. ISBN 80-8069-362-

Robotized training workstations on Department of production systems and robotics

Abstract

This contribution describes needs of another education for worker in field of automated production. Current development of production systems is based on implementation of new computer technologies. Production management and workers, who use "classic production" are coming a brake of development of modern production systems bases on flexible NC machines, robots and computer based controll systems. Specially for this field is within the project „Leonardo Da Vinci Programme" prepared integrated set of vocational trainings based on e-learning technologies. Project participants are PIAP Varsava (Poland), ATB Bremen (Germany), CU Cardiff (Great Britain) and TU Kosice (Slovakia). Importance of education for field of robotics is particularly important to the Slovak republic because of orientation of Slovak’s machina industry on automobile industry. This industry binds wide range of subcontractor on itself from sector of small and medium enterprises - SMEs, for which is not easy to recruit qualified workers.

Keywords: ISAR, e-learning

Robotized training workstations on Department of production systems and robotics

VLADIMÍR BALÁŽ
IVAN IGNÁTH
DOMINIKA PALAŠČÁKOVÁ

Ing. Vladimír Baláž, PhD
Technical university
Faculty of Mechanical Engineering
Department of Production systems and robotics
Boženy Nemcovej 32
041 00 Košice
Slovakia
e-mail:vladimir.balaz@tuke.sk

Ing. Ivan Ignáth
Technical university
Faculty of Mechanical Engineering
Department of Production systems and robotics
Boženy Nemcovej 32
041 00 Košice
Slovakia
e-mail:ivan.ignat@tuke.sk

Ing. Dominika Palaščáková
Technical university
Faculty of Mechanical Engineering
Department of Production systems and robotics
Boženy Nemcovej 32
041 00 Košice
Slovakia
e-mail:dominika.palascakova@tuke.sk

MIKULÁŠ HAJDUK
MAREK VAGAŠ
MATEJ ČIRIP

PROPOSAL KINEMATICS AND PRINCIPLE OF HUMANOID ROBOT GAIT

Introduction

One of the most developed area of humanoid robots, where is many times presented an actual implementation of proposals in technical solutions is robosoccer. Robosoccer became a scientifically base for solve problems in this event in recent years.

Match in robosoccer is similar to normal football match with rules adapted to requirements for robosoccer. For regularity of game is supervising a referee – man. There are a many kinds of competitions in category of MiroSot, NaroSot, HuroSot, RoboSot and SimuroSot in the world.

Humanoid robot is conceived on biological model of human base. The movement of robot is going on with the aid of two legs to replicate a walking gait of human body. Humanoid robots must be able to determine their own position in environment, perceive the surrounding, identify and obstacle avoidance. Robot uses a torso and two upper limb anthropomorphic types. It has an artificial eyes used for remote visual receptor, recognize and understood of human speech.

Design approach to built a humanoid robot

In the analysis of design approaches to building humanoid robot is taken as an example of building the human body, its degrees of freedom and movement. As the most common presentation for building a humanoid robot takes scheme under Fig.1.

In design it is necessary to ensure not only on the order of arrangement of kinematics pairs, which has a large impact on the functionality of the system, but also on their mutual distribution so that the same proportion to the human body. The correct arrangement relative position of each joints ensure an accurate similarity of human limbs kinematics and facilitate the calculations the positions of individual joints and the creating of a mathematical model of walking gait using inverse kinematics.

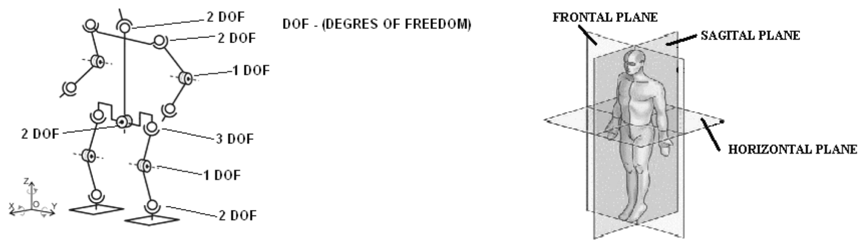

Fig. 1. kinematics arrangement

The proposed number of degrees of freedom (DOF) is divided so that 3 DOF be hip, then it is a spherical joint. Knee-joint with 1 DOF of movement in the sagital plane and ankle joint with 2 DOF, which perform tilts in sagital and frontal plane of the body mechanism.

Right and left foot of robot is in place of pelvis associated with flexible coupling, which allows slight movements of the mechanism and takes their correct position. This system partially absorb the inertial damping energy of moving limbs in the transmission phases and reduce the vibration transmitted from one limb to another one and thus increases the stability of the robot in walking.

The joints of torso part are catered by 2 DOF of movement, rotation of the upper torso structure from side to side in the frontal plane and tilts forward or the rear upper part of the sagital plane which axes of rotation intersect at a common point. Shoulder joint is designed with 2 DOF of movement and can move the arms in the sagital and frontal plane, the axes of rotation also intersect at a common point. The joint of head also has a 2DOF of movement, where it is realized a turning head let as say the camera system around the vertical axis in the horizontal plane and tilt forward and backward in the sagital plane. The elbow joint is carried out with 1 DOF of movement in the sagital plane of the body.

Structure design of humanoid robot gait

Human gait is a complex sequence movement of lower limb, which are consecutive and periodically repeat. Minimally one leg is still in contact with ground during the walking while the other leg performed a transmission phase and so change its position without contact with ground. The structure of step design on humanoid robot is applied to a kinematical chain (previously Fig.1) contains from 13-th phases which have static stability movement Fig.2.

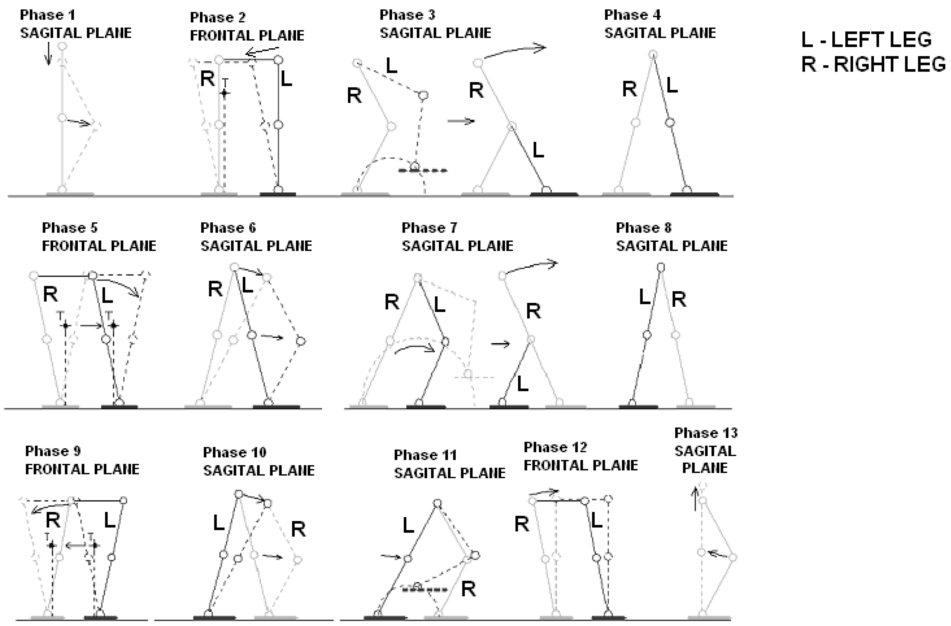

Fig. 2. Phases of robot step

The main aim of human robot designing gait is necessary take to account that the model for every movement is human gait. I want to say that in some phases of movement isn't center of gravity upright over the supporting foot which means a dynamical stability movement. System of dynamic stability uses a force of inertia potential body and its parts so, that to avoid uncontrolled position (collapse). Here is used transmission balance principle and working of inertia moments, for example opposing pitching arms with opposite leg.

To achieve a dynamic stability of humanoid walking robot is technically very complicated problem, therefore is the first walking principle verification of designing humanoid robot performed on the model with static stability. This means that the center of gravity (CoG) is still upright over the supporting foot Fig.3.

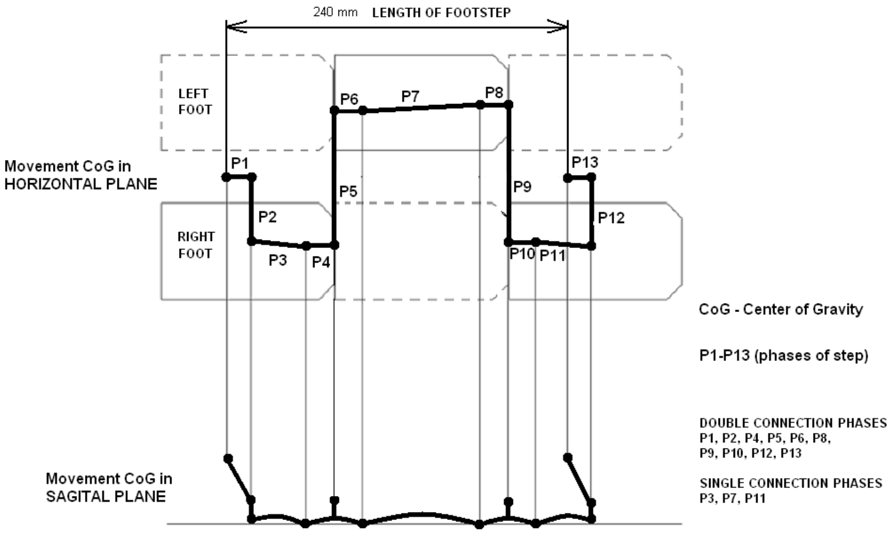

Fig. 3. The trajectory of center of gravity (CoG) movement in designing phases of robot step

For calculating of individual robot movements in scope we used calculation of inverse kinematics i.e. we know a trajectory of end – point kinematics chain, for example joint of ankle and so we backward calculate angular positions of other depending joints. For these calculations we used a simpler method by goniometrical functions and cosinus sentence which suffice for designing model of robot step.

It also considerably simpler a calculation of inverse kinematics and movement control. Structure design of humanoid robot gait is determined for transmission balance principle from one leg to another one, which we can influence also movements of upper limb and trunk of robot. Each movements include upper parts of body will be embedded to overall mathematical model of robot step. It will facilitate to reach a better stability of two legged walking system.

Conclusions

The positive trends of previous development humanoid robots have contributed to developing new design components and motion systems. There is no doubt that in the coming period will be knowledge oriented on the design of structures humanoid robot will continue to improve.

It can therefore be assumed that the need for the creation of new knowledge will help find solutions that will become particularly important for further development. This leads, in real terms to a suitable methodological progress to be used for design of construction humanoid robot.

The necessary prerequisite for building such systems is a further revision of existing design methodologies and their closer connection with the systematic base of accumulated knowledge in this discipline.

Abstract

This contribution describes a problematic of kinematics design on humanoid robot and offers a principal design of humanoid robot gait according to human base. Also contains a problematic of center of gravity (CoG) movement during walking of robot.

REFERENCES

1. HAJDUK, M.: Present status and evolution trend of service and humanoid robotics. In. Service and Humanoid Robotics, Košice, 2007
2. SCHRAFT R. D., HÄGELE M., WEGENER K.: Service roboter visionen, Hanser,ISBN3-446-22840-3
3. SMRČEK, J., PALKO, A., JURČIŠIN, J.: Problematika servisných robotov, štúdia princípov a metodík ich aplikácieI., II.Strojárstvo, č.4-5/99, s. 20, 72-74
4. http://world.honda.com/ASIMO/new

PROPOSAL KINEMATICS AND PRINCIPLE OF HUMANOID ROBOT GAIT

MIKULÁŠ HAJDUK
MAREK VAGAŠ
MATEJ ČIRIP

Informacja o autorach

Technical University of Kosice /Slovakia/
Department of production systems and robotics,
Faculty of Mechanical engineering